Molecular Mechanisms of Autophagy Induction and Mitochondrial Degradation in the Yeast *Saccharomyces cerevisiae*

by
Kai Mao

A dissertation submitted in partial fulfillment
of the requirements for the degree of
Doctor of Philosophy
(Molecular Cellular and Developmental Biology)
in The University of Michigan
2014

Doctoral Committee:
Professor Daniel J. Klionsky, Chair
Professor Laura J. Olsen
Professor Lois Weisman
Associate Professor Haoxing Xu

To My Daughter

Acknowledgments

I must give my greatest gratitude to my advisor Dr. Daniel J. Klionsky for completely changing my life. I could never imagine being where I am without obtaining the privilege joining his laboratory. As a scientist, his outstanding scientific expertise and enormous passion to science have been encouraging me to learn, to discover, and to explore all the time. As an advisor, he has been giving endless support and guidance to my research, and his dedication to my scientific study has made an indelible mark on me, the “Klionsky” brand. I have learned and will continue learning the remarkable lessons from him, which is my invaluable treasure throughout my life.

I would like to thank my outstanding thesis committee members, Dr. Lois Weisman, Dr. Laura J. Olsen, and Dr. Haoxing Xu for their insightful suggestions and criticisms for my project. Additionaly, I am grateful to Dr. Haoxing Xu for his indispensable support to my recruitment to the University of Michigan; to Dr. Laura J. Olsen for her generous help at the beginning of my Ph.D. study; to Dr. Lois Weisman for her strong recommendation during my post-doctoral application.

I would like to thank my parents, my parents in law and my wife for their gratuitous love and support. Especially, I am extremely grateful to my wife Donglin Li, who made my monochrome life become colorful. Donglin not only gave me a brilliant marriage and a lovely daughter, but also sacrificed for me during my graduate study for many years. I could never imagine what my life would be without her.

I would like to thank my colleagues and intimate friends, Dr. Tao Xu and Dr. Jiefei Geng for discussing scientific questions with me. Their creative ideas and critical thinking helped me dramatically improve my scientific knowledge and skills. It also has been wonderful to work together with members of the

Klionsky laboratory. This thesis would not have been possible without the hard work of my colleagues Dr. Yuko Inoue-Aono, Dr. Heesun Cheong, Xu Liu, Ke Wang, Dr. Usha Nair, Mantong Zhao, and Dr. Hana Popelka. I would also like to thank Dr. Yang Cao for technical training during my rotation, Meiyan Jin for teaching me generating yeast spheroplast, and Dr. Steven Backues for teaching me protease protection assay. I also received lots of help from Dr. Zhiping Xie, Dr. Wei-lien Yen, Dr. Midori Umekawa, Dr. Amelie Bernard, Katie Parzych, Yuchen Feng, Ding He, and Zhiyuan Yao. Everyone from Klionsky laboratory is kind and willing to help each one, and all of you made my past five years very enjoyable.

My sincere thanks will also go to Dr. John Kim and Dr. Ting Han from University of Michigan, Dr. Brenda A. Schulman and Dr. Stephen E. Kaiser from St. Jude children's research hospital, and Dr. Calvin K. Yip and Leon H. Chew from University of British Columbia. They generously shared their expertise and experience and help me complete the projects and pursue postdoctoral position.

At last, I am grateful for the people in the MCDB departmental office, in particular Ms. Mary Carr and Ms. Diane Durfy, for their constant assistance.

Preface

This thesis comprises the research I conducted in Prof. Daniel J. Klionsky's lab starting from April 2009. The objective was to better understand the molecular mechanisms of proper autophagy induction and how autophagy mediates mitochondrial degradation.

Chapters 2, 3, and 4 were published in *Journal of Cell Biology* (2011; 193(4):755-67), *Developmental Cell* (2013; 16(1):9-18), and *PNAS* (2013; 110(31):E2875-84), respectively. Chapter 5 is currently under revision at *Autophagy* and will be submitted by December 2013.

Chapter 2 describes the identification of two conserved mitogen-activated protein kinases, Slt2 and Hog1, which are required for mitophagy. These two pathways are important for regulating proper degradation of excessive or damaged mitochondria. I initiated this project and performed most of the experiments; Ke Wang helped design the experiments; Mantong Zhao performed the experiments in Figure 2.5 A and B; Tao Xu constructed the plasmids.

Chapter 3 describes the direct link between the mitochondrial fission complex and the mitophagy machinery, suggesting that mitochondrial fission facilitates mitophagy. I initiated this project and performed most of the experiments; Ke Wang helped design the experiments; Xu Liu made several yeast strains.

Chapter 4 describes the molecular and structural analysis and the Atg17-Atg31-Atg29 protein complex and the function of Atg29 phosphorylation during autophagy induction. This project was initiated by two former members from Klionsky lab, Heesun Cheong and Yuko Inoue-Aono, and was finished by me. I performed most of the experiments described in the publication: Leon H. Chew contributed the single particle electron microscopy; Usha Nair made the

Atg1 mutant which lost the interaction to Atg11; Hana Popelka made the computational analysis of Atg29.

Chapter 5 describes the role of peroxisomal fission during peroxisomal degradation. This project, together with the one in Chapter 3 reveals a novel mechanism that is generally applicable to the fission and degradation of some organelles, such as peroxisomes, mitochondria and probably chloroplasts. Xu Liu and I contributed equally to this work. I initiated the project, made the original observations and designed all of the eperiments. Xu performed many of the experiments, observed many novel phenomena, and generated many results.

Table of Contents

List of Tables

List of Figures

Abstract

Eukaryotic cells rely on autophagy to degrade damaged or excess proteins and organelles. In autophagy, cytoplasmic components or organelles are engulfed by the sequestering compartment, the phagophore. The membrane expansion of the phagophore results in the formation of the autophagosome. This event begins with the organization of the phagophore assembly site (PAS), where most of the autophagy-related (Atg) proteins are at least transiently localized and mediate autophagosome formation. Autophagy can occur in either nonselective or selective modes. Nonselective autophagy sequesters bulk cytoplasm; in contrast, selective autophagy targets specific proteins or organelles as cargos, such as mitochondria (mitophagy) and peroxisomes (pexophagy).

My doctoral thesis has focused on the molecular mechanisms of autophagy and mitophagy in *S. cerevisiae*. These studies comprise three major findings:

1. Mitophagy plays an essential role in the maintenance and quality control of mitochondria. Little was known regarding how upstream signaling pathways control this process. I identified two mitogen-activated protein kinases (MAPKs), Slt2 and Hog1, which are required for mitophagy in *S. cerevisiae*. Wsc1 and Sln1, two plasma membrane sensors receive the signals and transmit them to Slt2 and Hog1, respectively. Upon activation, Slt2 and Hog1 remain in the cytosol and phosphorylate currently unknown targets to promote mitophagy. Slt2, but not Hog1, affects the recruitment of mitochondria to the PAS, a critical step in the packaging of cargo for selective degradation. This work presents the first identified upstream signaling pathways regulating mitophagy and is published in *The Journal of Cell Biology* (2011; 193(4):755-67).

2. Both mitochondrial degradation and division are significant for

maintaining the proper quality and quantity of this organelle. Mitochondrial division is controlled by a fission complex containing Fis1, Dnm1, Mdv1, and Caf4. The role of mitochondrial fission during mitophagy has been unclear. My work showed that mitochondrial fission is important for the progression of mitophagy. The bimolecular fluorescence complementation (BiFC) assay was used to generate a proper marker for the superfluous mitochondria destined for degradation. When mitophagy is induced, the fission complex is recruited to these mitochondria through an interaction between Dnm1 and Atg11, a scaffold protein essential for selective autophagy. After recruitment, the fission complex drives the separation of a fragment of the mitochondria from the remaining reticulum. These isolated fragments of mitochondria will then be targeted by autophagy for degradation. Interfering with the interaction between Dnm1 and Atg11 severely blocks mitophagy. These data establish a paradigm for selective organelle degradation, and the results have been published in *Developmental Cell* (2013; 16(1):9-18).

3. Autophagy occurs at a basal level, and can be induced by various types of stress; the process must be tightly regulated because insufficient or excessive autophagy can be deleterious. Autophagy begins with the organization of the phagophore assembly site, and a complex composed of Atg17-Atg31-Atg29 is vital for PAS organization and autophagy induction, implying a significant role in autophagy regulation. My work demonstrates that Atg29 is a phosphorylated protein and that this modification is critical to its function. *In vivo* data show that the Atg17-Atg31-Atg29 complex interacts with Atg11, and these four proteins constitute the minimal components as the platform that recruits other Atg proteins to the PAS. Alanine substitution of the phosphorylation sites of Atg29 blocks its interaction with Atg11, and its ability to facilitate assembly of the PAS. Atg29 has the characteristics of an intrinsically disordered protein, suggesting that it undergoes dynamic conformational changes upon interaction with a binding partner(s). Single-particle electron microscopy analysis of the Atg17-Atg31-Atg29 complex reveals an elongated

“S” structure with Atg29 located at the opposing ends. This work reveals the mechanisms of how Atg17-Atg31-Atg29 is activated and mediates PAS organization and has been published in *Proceedings of the National Academy of Sciences USA* (2013; 110(31):E2875-84).

Together, these studies advance our understanding of the regulation and mechanism of selective autophagy, a process that is conserved from yeast to human, and that plays a critical role in cell physiology and disease.

Chapter 1
Introduction

In eukaryotic cells, autophagy is a potent lysosome/vacuole-dependent mechanism that serves for the elimination of damaged or excess proteins and organelles under nutrient starvation or specific developmental, physiological and pathophysiological conditions. Autophagy plays significant roles in development, immune defense, programmed cell death, tumor suppression, and prevention of neuron degeneration (1-3).

Up until now, three primary forms of autophagy have been observed, including macroautophagy, microautophagy, and chaperone-mediated autophagy. In this dissertation, I will focus on macroautophagy (hereafter referred to as autophagy), which is the most widely studied one. During autophagy, an expanding membrane structure termed the phagophore enwraps portions of the cytoplasm, which leads to the formation of a double-membrane sequestering vesicle, termed the autophagosome. Autophagosomes subsequently fuse with lysosomes/vacuoles, releasing their inner compartment to the lysosomal/vacuolar lumen. The inner membrane part of the autophagosome, together with the enclosed cargo, is degraded, and the resulting macromolecules are released into the cytosol through lysosomal/vacuolar membrane permeases for recycling (Figure 1.1).

During the past two decades, genetic screens in *Saccharomyces cerevisiae* and other fungi have identified 38 AuTophaGy-related (*ATG*) genes, which are involved in various types of autophagy. Furthermore, orthologs of many yeast *ATG* genes have been identified in higher eukaryotes. The characterization of these gene products (Atg proteins) have largely expanded our knowledge of this process, and provided us with genetic and biochemical tools for exploring the diverse functions of autophagy and further revealing the

molecular mechanisms of autophagy.

The proposed site of autophagosome formation is the phagophore assembly site (PAS). Atg proteins accumulate, at least transiently, at the PAS and initiate phagophore formation. In *Saccharomyces cerevisiae*, the PAS is observed at the vacuolar periphery (4, 5); and in mammalian cells, the autophagosomes are formed at the ER-mitochondria contact sites, which suggested that the PAS may also localize at the ER-mitochondria contact sites (6).

1.1 Core molecular machinery of autophagy

Among the identified *ATG* genes, a subset of genes is required for autophagosome formation in all types of autophagy. The corresponding gene products were referred to as the "core" molecular machinery of autophagosome formation. The core machinery is composed of four major groups based on their functions in different aspects of autophagy: (1) the Atg1 kinase complex; (2) the phosphatidylinositol 3-kinase (PtdIns3K) complex; (3) the ubiquitin-like protein (Ubl) system; and (4) the Atg9 cycling system.

1.1.1 The Atg1 kinase complex

The Atg1 kinase complex includes Atg1, Atg11, Atg13, Atg17, Atg29, and Atg31 (Figure 1.2). Among the 38 known Atg proteins, Atg1 is the only kinase, and plays a particularly essential role in autophagy induction by controlling the trafficking of other Atg proteins including Atg9 and Atg23 (7), and in the proper organization of the PAS (8, 9). Atg1 has several (direct) binding partners, including Atg13 (which interacts with Atg17) and Atg11; the kinase activity of Atg1 is regulated in part by its binding partners (10, 11).

The Atg17-Atg31-Atg29 complex is constitutively formed in both growing and nitrogen starvation conditions (12). Atg31 directly interacts with Atg17 and Atg29 to bridge these two proteins (13), hence the order of the components is written "Atg17-Atg31-Atg29" to signify these interactions. Atg17 interacts with

Atg1 via Atg13 (14). When autophagy is initiated, the Atg17-Atg31-Atg29 complex is first targeted to the PAS and recruits other Atg proteins, including Atg1 and Atg13, highlighting the significance of this ternary complex (15, 16).

In Chapter 2, I provide new evidence showing that Atg11 is also able to connect the Atg17-Atg31-Atg29 complex to Atg1, through direct interaction with Atg1 and Atg29 (Figure 1.2).

1.1.2 The PtdIns3K complex

The PtdIns3K complex contains vacuolar protein sorting (Vps)34, Vps15, Vps30/Atg6 and Atg14. Vps34 is a class III PtdIns3K, generating PtdIns3P, and participates in multiple vesicular trafficking pathways, including endocytosis and autophagy (17). Vps15, a protein kinase interacting with Vps34, is required for the membrane association of Vps34 (18, 19). In *Saccharomyces cerevisiae*, Vps15, Vps34, Vps30, and Vps38 form a complex (PtdIns3K complex II) involved in the trafficking of a subset of vacuolar proteins through the Vps pathway; however, Vps15, Vps34, Vps30, and Atg14 form another complex (PtdIns3K complex I), localizing at the PAS and recruiting PtdIns3P-binding proteins such as Atg18 (20-22). In mammals, BECN1 is the homolog of Atg6; however, BECN1 is primarily involved in autophagy, rather than endocytosis (23-25)

1.1.3 The ubiquitin-like protein system

Atg8 and Atg12 are the two Ubls (26, 27). The crystal structures of Atg8 and Atg12 show that each has a ubiquitin fold at the C terminus, although their primary sequences do not display clear homology to ubiquitin (28, 29). The C-terminal glycine of Atg12 is attached to an internal lysine in Atg5, whereas the C-terminal glycine of Atg8 is attached to phosphatidylethanolamine (PE) (30, 31). Specifically, the C terminus of Atg8 is first processed by a cysteine protease, Atg4, to expose the glycine residue before conjugation (32, 33). Atg7 is the E1-like activating enzyme for both Atg8 and Atg12, and Atg3 and Atg10

are the E2-like conjugating enzymes for Atg8 and Atg12, respectively (34-38). The Ubls are suggested to regulate phagophore expansion, and their PAS localization depends on Atg9 and the autophagy-specific PtdIns3K complex (4).

1.1.4 The Atg9 cycling system

Atg9 is the only transmembrane Atg protein that is absolutely required for autophagosome formation, and it has six transmembrane domains with its amino and carboxyl termini exposed in the cytosol (39, 40). In *Saccharomyces cerevisiae*, Atg9 self-interacts and shuttles between the PAS and the mitochondrial periphery; and this shuttling is proposed to be involved in the process in which membrane is contributed to the PAS (7, 41). In mammals, Atg9 homologs localize to the *trans*-Golgi network and late endosomes (40).

The anterograde transport of yeast Atg9 to the PAS requires Atg23 and Atg27 (42, 43), whereas the retrieval of Atg9 from the PAS depends on the Atg1 kinase complex, Atg2 and Atg18 (7). Atg2 and Atg18 are both membrane peripheral proteins, and their PAS localization depends on each other as well as Atg1, Atg9 and the PtdIns3K complex (22, 44-46). Both Atg2 and Atg18 are able to interact with Atg9 (7, 44).

1.2 Selective autophagy

Autophagy is able to work in both non-selective and selective modes. Compared to the bulk degradation of cytosol through non-selective autophagy, selective autophagy specifically recognizes and degrades a particular cargo, such as a protein complex, an organelle, or an invading pathogen (47-50). Cells employ selective autophagy for a variety of purposes under different conditions, including adaptation to the changing environment and clearance of damaged organelles.

Selective autophagy employs the same core machinery used for non-selective autophagy. Furthermore, a small group of additional proteins are

required to make the process selective. A cargo-ligand-receptor-scaffold model is generally proposed to achieve the selectivity (51). The ligand is the recognition component on the cargo that binds to the receptor. The receptor in turn interacts with the scaffold, which guarantees the selectivity and proper cargo recruitment to the PAS. In *Saccharomyces cerevisiae*, Atg11 is the general scaffold protein, mediating several types of selective autophagy, including the cytoplasm-to-vacuole targeting (Cvt) pathway, mitophagy, pexophagy, and reticulophagy (the selective degradation of mitochondria, peroxisomes or endoplasmic reticulum by autophagy, respectively); however, the mammalian homolog of Atg11 has not yet been discovered.

1.2.1 The Cvt pathway

The yeast Cvt pathway is the first characterized example of selective autophagy, and the only known biosynthetic process that utilizes the autophagy machinery (52, 53). It is a transport route through which at least three vacuolar resident enzymes are targeted from the cytosol to the vacuole, their final site of action. Enzymes that utilize the Cvt pathway include Ape1, Ape4, and Ams1 (54). Atg19 interacts with each cargo through different domains and functions as the receptor (55). Atg11 mediates the delivery of the cargo complex to the PAS though binding to Atg19 (11, 56). After completion of autophagosome formation, both the cargo and the receptor are delivered to the vacuole.

1.2.2 Mitophagy

Selective degradation of superfluous or damaged mitochondria by autophagy, termed mitophagy, has been observed both in yeast and mammals (57). In *Saccharomyces cerevisiae*, mitophagy removes excess mitochondria to achieve cellular remodeling (58). Atg32, a mitochondrial outer membrane protein, works as the receptor and sequentially interacts with Atg11 and Atg8. These interactions are critical for the formation of mitochondria-specific

autophagosomes (mitophagosomes) and ultimately degradation in the vacuole (59, 60). In mammals, both BNIP3 and BNIP3L/Nix are proposed to be the functional counterpart of Atg32 (61). BNIP3, BNIP3L and SQSTM1/p62 have been proposed to function as receptors to link mitochondria with the autophagy machinery (61, 62). During erythrocyte maturation, BNIP3L is essential for the removal of mitochondria. During depolarization-induced mitophagy, SQSTM1 may function as a receptor; in this case, PINK1 accumulates on the outer membrane of depolarized mitochondria and recruits PARK2/Parkin, an E3 ubiquitin ligase (63). PARK2 activates the ubiquitination of numerous outer mitochondrial membrane proteins, such as MFN1 and MFN2 (64).

In Chapter 2 and 3, I provide new evidence showing the upstream signaling controlling mitophagy, and the significant role of mitochondrial fission during mitophagy.

1.2.3 Pexophagy

Pexophagy, the selective autophagic degradation of peroxisomes, is important for cellular adaption to changing nutrients. When fungi are grown on oleic acid or methanol, the peroxisomes proliferate because this organelle contains the essential enzymes for the utilization of these carbon sources. When subsequently shifted to glucose or ethanol, the peroxisomes are rapidly and selectively degraded through autophagy. PpAtg30 and Atg36 function as receptors for pexophagy in *Pichia pastoris* and *Saccharoymces cerevisiae*, respectively (65, 66).

In Chapter 5, I provided new evidence suggesting an important role of peroxisomal fission during pexophagy.

1.2.4 Reticulophagy

The endoplasmic reticulum (ER) is associated with a high level of protein synthesis, and protein misfolding is a potential significant problem in this organelle. Cells have specific mechanisms for correcting misfolding errors,

including lumenal chaperones, the unfolded protein response, and ER-associated degradation; however, if the misfolding load is excessive and cannot be solved by these systems, reticulophagy is induced. Different from other types of autophagy, degradation of the impaired ER is not the immediate aim of reticulophagy; rather, sequestration of the overloaded ER within an autophagosome is sufficient to maintain cellular homeostasis (67).

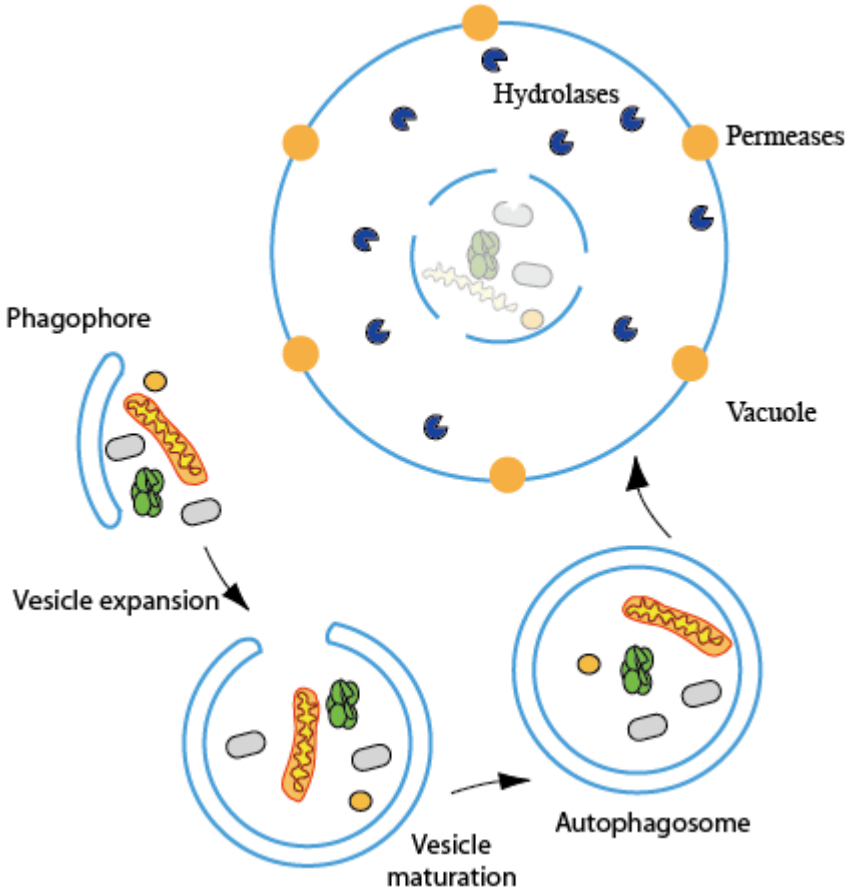

Figure 1.1 Schematic depiction of autophagy.
Cytosolic components are sequestered by an expanding membrane structure, the phagophore, resulting in the formation of a double-membrane vesicle, an autophagosome; the outer membrane of the autophagosome fuses with a vacuole, releasing the inner compartment to the lumen where it gets degraded, along with its cargo.

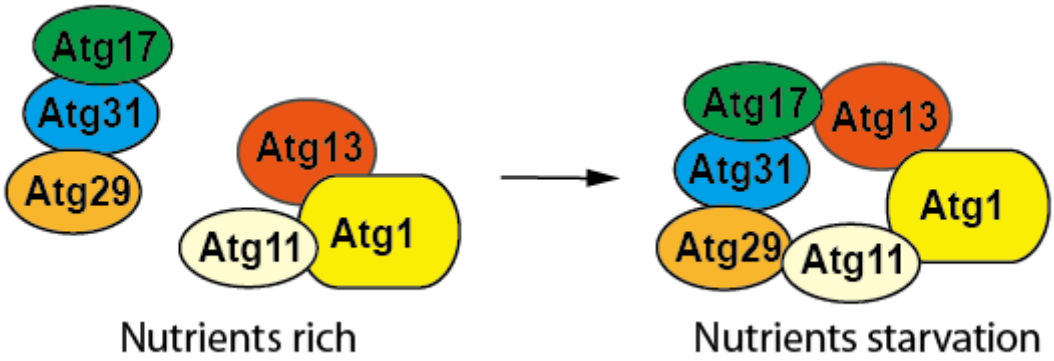

Figure 1.2 Graph of the Atg1 complex.
The Atg17-Atg31-Atg29 complex is constitutively formed, and Atg1 is associated with Atg11 and Atg13. Upon nutrient deprivation, autophagy is induced, and the intact Atg1 complex is formed. The formation of this complex is mediated by direct interaction between Atg13 and Atg17, and between Atg11 and Atg29.

Chapter 2

Two MAPK-signaling pathways are required for mitophagy in *Saccharomyces cerevisiae*[1]

2.1 Abstract

Macroautophagy (hereafter referred to simply as autophagy) is a catabolic pathway that mediates the degradation of long-lived proteins and organelles in eukaryotic cells. The regulation of mitochondrial degradation through autophagy plays an essential role in the maintenance and quality control of this organelle. Compared with our understanding of the essential function of mitochondria in many aspects of cellular metabolism such as energy production and of the role of dysfunctional mitochondria in cell death, little is known regarding their degradation and especially how upstream signaling pathways control this process. Here, we report that two mitogen-activated protein kinases (MAPKs), Slt2 and Hog1, are required for mitophagy in *Saccharomyces cerevisiae*. Slt2 is required for the degradation of both mitochondria and peroxisomes (via pexophagy), whereas Hog1 functions specifically in mitophagy. Slt2 also affects the recruitment of mitochondria to the phagophore assembly site (PAS), a critical step in the packaging of cargo for selective degradation.

2.2 Introduction

Autophagy functions as a highly conserved degradative mechanism in eukaryotic cells. During autophagy, cytosolic components and organelles are sequestered into autophagosomes, double-membrane vesicles, and then

1 Originally published in *Journal of Cell Biology* (2011; 193(4):755-67) with authors listed as Kai Mao, Ke Wang, Mantong Zhao, Tao Xu, and Daniel J. Klionsky.

delivered to the lysosome in mammalian cells or the vacuole in yeast for degradation (47). This process has attracted increasing attention in recent years because it is involved in various aspects of cell physiology, including survival during nitrogen starvation, clearance of excess or dysfunctional proteins and organelles, proper development, and aging (48). During nitrogen starvation, autophagy is generally considered to be nonselective. The unique mechanism by which the initial sequestering compartment, the phagophore, expands into an autophagosome allows for an extremely flexible capacity for cargo. In addition to this nonselective or bulk autophagy, selective types of autophagy are used for biosynthetic transport (the cytoplasm-to-vacuole targeting [Cvt] pathway), and to recognize and degrade specific cargoes or organelles. These latter include the selective degradation of mitochondria (mitophagy), peroxisomes (pexophagy), and ribosomes (ribophagy) (58, 68-71). Among different kinds of selective autophagy, mitophagy is particularly crucial because of the significance of mitochondria in cellular homeostasis. In particular, mitochondria supply energy to the cell for a variety of cellular activities. However, mitochondria are also the major source of cellular reactive oxygen species (ROS) that cause oxidative damage to cellular components including DNA, proteins, and lipids (71). Accumulation of damaged mitochondria and the concomitant increase in ROS is related to aging, cancer, and neurodegenerative diseases (72). Therefore, quality control and clearance of damaged or excess mitochondria through autophagy is an important cellular activity.

Until now, four primary signaling pathways have been characterized as playing a role in the negative regulation of nonselective autophagy. The regulatory kinases of these pathways are the target of rapamycin (TOR), Sch9, Ras/cAMP-dependent protein kinase A (PKA), and Pho85, the latter of which also plays a positive role in regulation (73-75). In the case of TOR and PKA, the corresponding signaling events negatively regulate the activity of Atg1 and Atg13 and inhibit the induction of autophagy, whereas Pho85 acts in

conjunction with various cyclins to inhibit Gcn2 and Pho4 to exert a negative effect, and inhibits Sic1 for positive regulation. In contrast to the signaling pathways upstream of bulk autophagy, which have been studied to some extent, the regulatory mechanisms of mitophagy remain largely unexplored.

In this report, we analyzed the functions of two MAPKs, Slt2 and Hog1, in the yeast *Saccharomyces cerevisiae*, and showed that both are required for mitophagy. Slt2 is a MAPK involved in the protein kinase C (Pkc1) cell wall integrity kinase signaling pathway, and responds to cell wall stress (76). Here, we show that Slt2 is required for pexophagy and mitophagy, but not the Cvt pathway or bulk autophagy. Hog1 is a MAPK homologue of mammalian p38, and responds to hyper-osmotic stress (77). Different from p38, which is a negative regulator of autophagy, Hog1 is a positive regulator only required for mitophagy, but not other types of selective autophagy or bulk autophagy. We thus propose that these two MAPK pathways play a critical role in organelle quality control.

2.3 Results

2.3.1 The MAPK Slt2 and upstream signaling components are involved in mitophagy

In a recent genome-wide yeast mutant screen for mitophagy-defective strains we found that BCK1, a gene encoding a mitogen-activated protein kinase kinase kinase (MAPKKK), is required for mitophagy (78). Bck1 is involved in the cell wall integrity signaling pathway, which includes Pkc1, Bck1, redundant Mkk1/2, and Slt2 kinases (76). Upon cell wall stress, Bck1 is activated by Pkc1 and then phosphorylates and activates Mkk1/2, which in turn transmits the signal to Slt2 (79). We asked whether all of the components of this signaling pathway are involved in mitophagy. To detect mitophagy, we first used the Om45-GFP processing assay. OM45 encodes a mitochondrial outer membrane protein, and a chromosomally tagged version with the GFP at the C terminus is correctly localized on this organelle. When mitophagy is induced,

mitochondria, along with Om45-GFP, are delivered into the vacuole for degradation. Om45 is proteolytically removed or degraded, whereas the GFP moiety is relatively stable and accumulates in the vacuole. Thus, mitophagy can be monitored based on the appearance of free GFP by immunoblot (58).

Atg32 is a mitophagy-specific receptor and is necessary for the recruitment of mitochondria to the PAS through interaction with Atg11, which is an adaptor protein for selective types of autophagy (59, 60). After 6 h of nitrogen starvation in the presence of glucose, free GFP was detected in wild-type but not *atg32Δ* cells (Figure 2.1B). Mitophagy was severely blocked in *bck1Δ* and *slt2Δ* cells. Even though the amount of free GFP derived from Om45-GFP in *mkk1Δ* or *mkk2Δ* single-mutant cells appeared essentially identical to the wild type (not depicted), an *mkk1Δ mkk2Δ* double-deletion mutant showed a strong defect in mitophagy (Figure 2.1B). Mitophagy activities of *pkc1* temperature-sensitive mutants were also measured at both permissive and restrictive temperatures. In the wild-type strain, Om45-GFP was processed at both temperatures with a greater level of free GFP detected at 35°C than at 24°C (Figure 2.1C, lanes 3 and 4, and lanes 15 and 16). In contrast, in the *pkc1-1*, *pkc1-2*, *pkc1-3*, and *pkc1-4* mutants, Om45-GFP processing was substantially reduced relative to the wild type at the nonpermissive temperature (Figure 2.1C, compare lane 4 to lanes 8 and 12, and lane 16 to lanes 20 and 24), suggesting that the Pkc1–Bck1–Mkk1/2–Slt2 signaling pathway is required for mitophagy.

To extend our analysis and precisely quantify mitophagy, we took advantage of the mitoPho8Δ60 assay to examine the extent of mitophagy defects in these mutants. PHO8encodes a vacuolar alkaline phosphatase, and its delivery into the vacuole is dependent on the ALP pathway (80). Pho8Δ60, the truncated form of Pho8 with 60 N-terminal amino acid residues including its transmembrane domain deleted, is unable to enter the endoplasmic reticulum, remains in the cytosol, and is delivered into the vacuole only through bulk autophagy (81). In this way, the magnitude of bulk autophagy is quantified by

measuring the activity of alkaline phosphatase in nitrogen starvation conditions. If PHO8Δ60 is fused with a mitochondrial targeting sequence, the encoded protein is specifically localized in mitochondria, and the ensuing alkaline phosphatase activity becomes an indicator of mitophagy (82). When mitophagy was induced, wild-type cells showed a dramatic increase in mitoPho8Δ60 activity, whereas essentially no increase was detected in *atg32Δ* cells where mitophagy was completely blocked (Fiugre. 1D). In *bck1Δ*, *mkk1/2Δ*, and *slt2Δ* cells, a severe decrease of mitoPho8Δ60 activity was seen compared with wild-type cells; these mutants displayed ~60, 53, and 62% of the mitophagy activity of the wild type, respectively. These results suggested that Bck1, Mkk1/2, and Slt2 regulate mitophagy through a linear signal transduction pathway.

2.3.2 Slt2 is required for pexophagy, but not the Cvt pathway or bulk autophagy

Considering the apparent role of Slt2 in mitophagy, we next asked whether this kinase is also involved in bulk autophagy or other types of selective autophagy. Bulk autophagy was tested by the Pho8Δ60 assay. Atg1 is a cytosolic protein kinase required for vesicle formation, and autophagic flux is absent in *atg1Δ* cells (8, 9). When bulk autophagy was induced in nitrogen starvation conditions, the Pho8Δ60-dependent alkaline phosphatase activity showed a strong increase in wild-type and *slt2Δ* cells, but remained at a basal level (i.e., the level before nitrogen starvation) in *atg1Δ* cells (Figure 2.1E).

Although the Cvt pathway is biosynthetic, it represents a selective type of autophagy and shares many of the same molecular components with bulk autophagy. The precursor form of aminopeptidase I (prApe1) is delivered to the vacuole via the Cvt pathway in rich conditions and through autophagy in nitrogen starvation conditions (53). After entering the vacuole, the N-terminal propeptide of prApe1 is cleaved to generate the mature form (mApe1) and the resulting difference in molecular mass can be differentiated by Western blot

(52). The maturation of prApe1 appeared normal in *slt2Δ* cells compared with wild-type cells in both growing and nitrogen starvation conditions, whereas *atg1Δ* cells displayed the expected block and accumulated only prApe1 (Fiugre. 1F).

As indicated above, the Cvt pathway is unusual in that it is a biosynthetic autophagy-related pathway. Therefore, we decided to examine another type of specific organelle degradation, pexophagy. PEX14 encodes a peroxisome integral membrane protein. After chromosomal tagging with GFP, the encoded protein, Pex14-GFP, is localized on the peroxisome and becomes a marker for pexophagy, similar to Om45-GFP for mitophagy; when pexophagy is induced, Pex14-GFP is delivered into the vacuole and pexophagy is detected by the release of free GFP (68). Pex14-GFP was processed after 4 h of pexophagy induction in wild-type cells, but this processing was almost completely blocked in *slt2Δ* cells similar to the *atg1Δ* negative control (Fiugre. 1G). These results indicated that Slt2 is involved in both mitophagy and pexophagy, but not the Cvt pathway or bulk autophagy.

2.3.3 The MAPK Hog1 and upstream kinase Pbs2 are mitophagy-specific regulators

Five MAPK-signaling pathways exist in *Saccharomyces cerevisiae*, and these MAPKs are involved in stress response and filamentous growth. Among these MAPKs, Hog1 responds to osmotic stress and regulates cellular metabolism. In Candida albicans, Hog1 controls respiratory metabolism and mitochondrial function (83). Because of the role of the Slt2 MAPK pathway in selective organelle degradation, we were also interested in the potential role of Hog1 in mitophagy. In the Hog1 signaling pathway, Pbs2 is the MAPKK upstream of Hog1, and the activation of Hog1 is dependent on its phosphorylation by Pbs2 (84). We again used the Om45-GFP processing assay to test mitophagy in both *hog1Δ* and *pbs2Δ* cells and found that there was minimal Om45-GFP processing relative to the wild-type positive control,

similar to the *atg32Δ* negative control, which suggested a defect in mitophagy (Figure 2.2A). Furthermore, quantification by the mitoPho8Δ60 assay showed ~50 and 52% of mitophagy activity in pbs2Δ and hog1Δ cells, respectively (Figure 2.2B). These results suggested that similar to Slt2, the Hog1 signaling pathway is also required for mitophagy.

As with Slt2, we extended our analysis by checking bulk autophagy, the Cvt pathway, and pexophagy. Our results showed that Pho8Δ60 activity (bulk autophagy), prApe1 maturation (the Cvt pathway), and Pex14-GFP processing (pexophagy) were all unaffected in *hog1Δ* cells compared with wild-type and *atg1Δ* cells (Figure 2.2C-E). These results suggested that, different from Slt2, the Pbs2 and Hog1 kinases are mitophagy-specific regulators.

2.3.4 Wsc1 and Sln1 function as upstream sensors for input into the Slt2 and Hog1 signaling pathways

To obtain more information for the extension of these two signaling pathways, we began to search for upstream and downstream components of the Slt2 and Hog1 pathways. For the Slt2 signaling pathway, six cell surface sensors, Wsc1, Wsc2, Wsc3, Wsc4, Mid2, and Mtl1, and three transcriptional factors, Rlm1, Swi4, and Swi6, function as upstream sensors and downstream effectors, respectively. Based on the Om45-GFP processing assay, mitophagy was blocked in the *wsc1Δ* strain, but not in any of the other mutants (Figure 2.3A and B). The involvement of Wsc1 in mitophagy was confirmed with the mitoPho8Δ60 assay (Figure 2.3C).

In the Hog1 signaling pathway, Sho1 and Sln1 function as sensors in the plasma membrane that function in parallel pathways (85). Mitophagy was unaffected in a *sho1Δ* strain (Figure 2.3C), but was partially blocked in a conditional *sln1* temperature-sensitive mutant at the nonpermissive temperature (Figure 2.S1A). Sln1 is a negative regulator of the Hog1 pathway (Figure 2.S1B); however, constitutively active Hog1 (e.g., due to defective Sln1) has a negative phenotype (85). Thus, a block in mitophagy in the *sln1* mutant

is in agreement with our data showing a defect in the *hog1Δ* strain (Figure 2.2). Sln1 and its effector Ypd1 inhibit the Ssk1 kinase, an activator of Hog1. To extend our analysis of the upstream components, we examined an *ssk1Δ* strain. The ssk1Δ mutant displayed a partial block in mitoPho8Δ60 activity similar to the *wsc1Δ* mutant (Figure 2.3C). There are three known transcriptional factors, Sko1, Hot1, and Smp1, that function downstream of Hog1. Mitophagy was unaffected in *sko1Δ*, *hot1Δ*, and *smp1Δ* cells (Figure 2.3B). These results indicate that the upstream sensors and effectors in the Slt2 and Hog1 signaling pathways that involve the Wsc1 and Sln1 sensors, respectively, regulate mitophagy. However, the known transcriptional factors downstream of Slt2 and Hog1 that we tested had no apparent role in mitophagy.

2.3.5 Slt2 and Hog1 are also involved in post-log phase mitophagy

Mitophagy in the yeast *Saccharomyces cerevisiae* can be induced in two different conditions: nitrogen starvation and culturing cells to the post-log phase in a nonfermentable carbon source medium (78). Atg32 is required for both types of mitophagy; however, Atg33 is specifically involved in post-log phase mitophagy, which suggests that mitophagy is induced through different mechanisms depending on the conditions. We asked whether Slt2 and Hog1 are also required for post-log phase mitophagy. Wild-type, *atg32Δ*, *slt2Δ*, *hog1Δ*, and *hog1Δ slt2Δ* cells were cultured in lactate medium to log phase, and then grown for another 12, 24, and 36 h. The mitoPho8Δ60 activities of the *slt2Δ*, *hog1Δ*, and *hog1Δ slt2Δ* mutants were significantly reduced compared with wild-type cells (Figure 2.4A). These results indicated these two MAPK signaling pathways regulate both types of mitophagy.

Finally, we examined the effect of combining the *hog1Δ* and *slt2Δ* muta tions. Mitophagy was almost completely blocked in *hog1Δ slt2Δ* double-mutant cells; the mitoPho8Δ60 activity of the *hog1Δ slt2Δ* mutant was comparable to that of *atg32Δ* cells (Figure 2.4A). This phenotype could also be detected

when mitophagy was induced by nitrogen starvation (Fiugre 2.4B). This result suggested that the strong defect of mitophagy in the *hog1Δ slt2Δ* mutant reflects an additive effect because these kinases regulate different steps of mitophagy in parallel pathways.

2.3.6 Slt2 and Hog1 are phosphorylated and remain in the cytosol during mitophagy

To investigate the response patterns of Slt2 and Hog1 during mitophagy, we examined the phosphorylation states of these proteins, which corresponds with their activation (86, 87). When cells were grown on lactate medium, both Slt2 and Hog1 were nonphosphorylated and inactive, but became phosphorylated upon nitrogen starvation (Figure 2.5A and B). Phosphorylation of Slt2 was initiated at 30 min after cells were shifted to SD-N and was subsequently reduced at 4 h (Figure 2.5A); in contrast, Hog1 was activated at 2 h and retained its phosphorylated state at 4 h (Figure 2.5B). This result indicated that Slt2 responds quickly to mitophagy-inducing signals and might function in an early stage of mitophagy, and that Hog1 responds late and might function in a correspondingly later stage of the process.

Although Slt2 and Hog1 can translocate to the nucleus and activate relevant transcription factors, depending on the stimulus, they also have cytoplasmic substrates. The observation that mitophagy was unaffected in *rlm1Δ*, *swi4Δ*, *swi6Δ*, *sko1Δ*, *hot1Δ*, and *smp1Δ* cells suggested that both Slt2 and Hog1 might control mitophagy through a mechanism other than transcriptional regulation. To monitor the distribution and localization of Slt2 and Hog1 during mitophagy, we fused both proteins with the venus variant of YFP and observed their localization during mitophagy-inducing conditions. It has been previously shown that during heat-shock stress (39°C) and hyper-osmotic stress (0.4 M NaCl), respectively, Slt2-YFP and Hog1-YFP translocate to the nucleus (86, 87). Accordingly, we used these conditions to test and verify the functionality of our constructs. As expected, Slt2-YFP and

Hog1-YFP showed clear nuclear localization under the respective stress conditions (Figure 2.5C and D). In contrast, during mitophagy Hog1-YFP and Slt2-YFP remained in the cytosol (Figure 2.5C and D). These results support the hypothesis that both Slt2 and Hog1 might activate some unknown cytoplasmic target to regulate mitophagy.

2.3.7 Atg32 recruitment to the PAS is perturbed in *slt2Δ*, but not *hog1Δ* mutants

The accumulation of the degrading portions of mitochondria at the PAS is a significant step during mitophagy (78). We first confirmed this event with the RFP-tagged mitochondria matrix protein Idh1 (Idh1-RFP) using GFP-Atg8 as the PAS marker. After 2 h of nitrogen starvation, a portion of mitochondria was located at the PAS (Figure 2.S2A).

Atg32, which functions as an organelle-specific marker, is delivered into the vacuole together with mitochondria during mitophagy (60). In *atg1Δ* cells, when the autophagic flux is completely blocked, a portion of GFP-Atg32 accumulates at the PAS, which localizes to the periphery of the vacuole in nitrogen starvation conditions (59). The PAS-localized Atg32 indicates the initiation of mitochondria-specific autophagosome (mitophagosome) formation. To further investigate how Slt2 and Hog1 regulate mitophagy, we focused on Atg32, which is the only known mitophagy receptor in yeast. We first examined the protein level of Atg32 in *slt2Δ* and *hog1Δ* mutants during mitophagy and found that the amount of the Atg32 protein was unaffected by either mutation (unpublished data). Thus, we ruled out transcriptionnal control for this mitochondria tag as being the explanation for the mitophagy defect.

As Slt2 and Hog1 are both involved in mitophagy, we asked whether Atg32 recruitment to the PAS was disturbed in the *slt2Δ* or *hog1Δ* mutant. In *atg1Δ* cells, GFP-Atg32 was present on mitochondria, but not at the PAS to an appreciable extent in vegetative conditions (SML medium). GFP-Atg32

accumulated at the PAS in ~45% (2 h) or 77% (4 h) of the *atg1Δ* cells in nitrogen starvation conditions, whereas only 17% (2 h) or 37% (4 h) of the cells displayed PAS-localized GFP-Atg32 in *atg1Δ slt2Δ* mutants (Figure 2.6). Although mitophagy was severely blocked in *hog1Δ* cells, GFP-Atg32 accumulated at the PAS in 39% (2 h) or 68% (4 h) of *atg1Δ hog1Δ* cells, which was almost similar to the extent of colocalization seen in *atg1Δ* cells (Figure 2.6). This result suggested a defect in mitochondrial recruitment to the PAS in the slt2Δ, but not hog1Δ mutant.

2.3.8 The kinase activities of Pbs2 and Hog1 are required for mitophagy

Among the autophagy core machinery proteins identified, Atg9 is the only transmembrane protein that is essential for the formation of autophagosomes. Atg9 cycles between the PAS and peripheral sites (7, 88). In mammalian cells, the MAPK p38, which is a homologue of Hog1, regulates autophagy by affecting Atg9 movement (89). Therefore, we asked whether Hog1 in yeast might also affect Atg9 cycling. Accordingly, we first investigated the retrograde transport of Atg9 in the *hog1Δ* mutant. Like the wild-type cells, Atg9 displayed multiple dots both in vegetative (SML) or nitrogen starvation (SD-N) conditions, which indicated that Hog1 had no effect on Atg9 retrograde transport (Figure 2.7A). We then examined the anterograde transport of Atg9 by the TAKA (transport of Atg9 after knocking out ATG1) assay (90). This is an epistasis analysis that relies on the accumulation of Atg9 at the PAS in the *atg1Δ* mutant background; mutants that are defective in anterograde movement of Atg9 to the PAS do not accumulate the protein at this site when combined with the *atg1Δ* mutation. However, Atg9 accumulated as a single dot in the *atg1Δ hog1Δ* mutant, similar to the result seen in the *atg1Δ* mutant (Figure 2.7B). This result indicated that, unlike p38, Hog1 is involved in mitophagy through a mechanism that does not affect Atg9 movement.

Next, we asked whether the kinase activities of Pbs2 and Hog1 are necessary for mitophagy. As expected, introduction of the wild-type HOG1 and

PBS2 genes complemented the mitophagy defect in *hog1Δ* and *pbs2Δ* cells, respectively (Figure 2.8A and B). In contrast, the kinase-dead mutants of Hog1 (K52R) and Pbs2 (K389R) were unable to recover mitophagy activity. Overall, these results suggest that upon activation by Pbs2, Hog1 phosphorylates a certain unidentified substrate(s), and that these signaling events play a significant role in mitophagy.

As a final attempt to identify targets of these signaling pathways, we examined whether the Hog1 and Slt2 kinases had any effect on the activity of the Atg1 kinase. Atg1 autophosphorylation results in a molecular mass shift that can be detected by SDS-PAGE (91). The *slt2Δ* and *hog1Δ* strains showed the same shift in mass for HA-Atg1 as seen in the wild-type strain (Figure 2.S3A). We extended this analysis by examining Atg1 kinase activity using an in vitro assay with myelin basic protein as a substrate (10). Atg1 kinase activity was reduced in the absence of Atg13 as expected, but there was no change in activity in the *slt2Δ* or *hog1Δ* mutants (Figure 2.S3B), in agreement with the normal autophosphorylation activity. We then asked whether the absence of Slt2 or Hog1 affected Atg13 phosphorylation; Atg13 is highly phosphorylated in rich conditions, and partially dephosphorylated upon shift to nitrogen starvation (92). Again, there was essentially no difference in the phosphorylation status of Atg13 in the *slt2Δ* or *hog1Δ* mutants relative to the wild type (Figure 2.S3C). Although the Slt2 and Hog1 kinases did not appear to affect the Atg1 or Atg13 proteins, we decided to examine the converse, and monitored the phosphorylation of Slt2 and Hog1 in an *atg1Δ* strain. Slt2 and Hog1 were phosphorylated after a 1- or 2-h shift to nitrogen starvation conditions, respectively, in the *atg1Δ* strain, similar to the result seen in the wild type (Figure 2.S3D).

2.4 Discussion

MAPK-signaling pathways comprise components that play major roles in cellular metabolism and resistance to stress. The Slt2-signaling pathway

participates in cell wall integrity, hypo-osmotic response, and ER stress and inheritance regulation (76, 93, 94), whereas the Hog1 signaling pathway is involved in hyper-osmotic response and the ER stress response (77, 87). In this paper, we have shown that Slt2 and Hog1 are involved in mitophagy, as both *slt2Δ* and *hog1Δ* cells showed severe defects in selective mitochondria degradation. Furthermore, the analysis of upstream components indicates that these kinases are involved in the Wsc1–Pkc1–Bck1–Mkk1/2–Slt2 and Ssk1–Pbs2–Hog1 signal transduction pathways, respectively. Both Slt2 and Hog1 are phosphorylated and remain in the cytosol during mitophagy, and none of the known downstream transcriptional factors have any apparent role in mitophagy. Bulk autophagy was unaffected in both *slt2Δ* and *hog1Δ* cells, indicating that these two signaling pathways do not act through the autophagy core machinery or by affecting overall autophagic flux.

Atg32 acts as an organelle-specific tag, and is critical for the recognition of mitochondria during mitophagy. Accordingly, the defect in Atg32 recruitment to the PAS in *slt2Δ* cells may explain why mitochondria could not be recognized, targeted, and transported to the PAS in the *slt2Δ* mutant. This defect together with the quick response of Slt2 phosphorylation suggested that a Slt2-dependent signaling event might play an early role in mitophagy induction. In contrast, no effect on Atg32 PAS localization in the *hog1Δ* mutant and a late pattern of Hog1 phosphorylation might be due to a role of Hog1 in a relatively late stage of mitophagy. Hog1-driven signaling was specific for mitophagy, whereas Slt2 also participated in pexophagy. A role for Slt2 in pexophagy was recently found by another group (95); however, in that paper, a mitophagy defect was not detected in *slt2Δ* cells, whereas pexophagy was completely blocked, the latter being consistent with our results.

Both Hog1 and Slt2 were required for mitophagy, but only the latter for pexophagy. One explanation for the apparently more stringent regulation of mitophagy may be that mitochondria play a much more important role in cellular physiology in *S. cerevisiae*. This organism has evolved such that its

metabolism favors fermentation, and unlike *Pichia pastoris* or *Hansenula polymorpha* it does not grow on methanol. Although *S. cerevisiae* can induce peroxisomes when grown in media with oleic acid as the sole carbon source, it otherwise retains relatively small numbers of this organelle. Accordingly, there may be relatively fewer mechanisms for regulating peroxisome degradation.

The Hog1, and possibly Slt2, MAPK-signaling pathway is conserved from yeast to mammals and its role in autophagy regulation also shows similarities, to some extent; in mammalian cells, the MAPKs JNK1, PKCδ, and p38 modulate autophagy (89, 96-99). Thus, the significant roles of Slt2 and Hog1 in mitophagy reveal an evolutionarily conserved function of MAPKs in autophagy control.

2.5 Materials and methods

Strains, media, and growth conditions. Yeast strains used in this study are listed in Table 2.1. Yeast cells were grown in rich (YPD; 1% yeast extract, 2% peptone, and 2% glucose) or synthetic minimal (SMD; 0.67% yeast nitrogen base, 2% glucose, and auxotrophic amino acids and vitamins as needed) media. For mitochondria proliferation, cells were grown in lactate medium (YPL; 1% yeast extract, 2% peptone, and 2% lactate) or synthetic minimal medium with lactate (SML; 0.67% yeast nitrogen base, 2% lactate, and auxotrophic amino acids and vitamins as needed). Mitophagy was induced by shifting the cells to nitrogen starvation medium with glucose (SD-N; 0.17% yeast nitrogen base without ammonium sulfate or amino acids, and 2% glucose). For peroxisome induction, cells were grown in oleate medium (1% oleate, 5% Tween 40, 0.25% yeast extract, 0.5% peptone, and 5 mM phosphate buffer). Pexophagy was also triggered by transferring the cells to SD-N.

Plasmids. pCuGFPAtg32(416) has been reported previously (59). In brief, the gene encoding GFP was inserted into the SpeI and XmaI restriction enzyme sites of pCu(416) to generate pCuGFP(416) (11). Then the *ATG32*

gene was amplified by PCR from the yeast genome and ligated into the EcoRI and SalI sites of pCuGFP(416) to construct pCuGFPAtg32(416). For other plasmids, we amplified the open reading frames along with 1 kb of upstream genomic DNA of the *SLT2*, *PBS2*, and *HOG1* genes by PCR, and introduced the PCR fragments into pDONR221 by recombination-based cloning using the Gateway system (Invitrogen). The $Hog1^{K52R}$ and $Pbs2^{K389R}$ kinase-dead alleles were generated by site-directed mutagenesis of the entry vectors. After sequencing, wild-type and kinase-dead alleles of *HOG1* and *PBS2* were separately introduced into the pAG416-ccdB-TAP destination vector (Addgene). Wild-type alleles of *SLT2* and *HOG1* were also introduced into the pDEST-vYFP destination vector (100).

Other reagents. The anti–phospho-Slt2 (phospho-p44/42 MAPK) and anti–phospho-Hog1 antibody (phospho-p38 MAPK) were from Cell Signaling Technology.

Fluorescence microscopy. For fluorescence microscopy, yeast cells were grown to OD_{600} ~0.8 in SML selective medium. Cells were shifted to SD-N for nitrogen starvation, or to 39°C for heat shock stress, or 0.4 M NaCl was added into the medium for hyper-osmotic stress. The samples were then examined by microscopy (TH4-100, Olympus; or Delta Vision Spectris, Applied Precision) using a 100x objective at 30°C and pictures were captured with a CCD camera (CoolSnap HQ; Photometrics). The imaging medium was either SML or SD-N, as indicated for each figure. For each microscopy picture, 15 Z-section images were captured with a 0.4-μm distance between two neighboring sections. FM 4-64 (Invitrogen) was applied to stain the vacuolar membrane. For quantification of GFP-Atg32 dots, the stack of Z-section images was projected into a 2D image. Images were processed in Adobe Photoshop and prepared in Adobe Illustrator.

Additional assays. The Pho8Δ60, Pex14-GFP processing, Om45-GFP processing, mitoPho8Δ60 and Atg1 in vitro kinase assays were performed as described previously (8, 68, 78, 90). For the alkaline phosphatase assay, two

A_{600} equivalents of yeast cells were harvested and resuspended in 100 µl lysis buffer (20 mM Pipes, pH 7.0, 0.5%Triton X-100, 50 mM KCl, 100 mM potassium acetate, 10 mM $MgSO_4$, 10 µM $ZnSO_4$, and 1 mM PMSF). The cells were lysed by vortexing with glass beads for 5 min, 50 µl of extract was added to 450 µl reaction buffer (250 mM Tris-HCl, pH 8.5, 0.4% Triton X-100, 10 mM $MgSO_4$, and 1.25 mM nitrophenylphosphate), and samples were incubated for 15 min at 30°C before terminating the reaction by adding 500 µl of stop buffer (2 M glycine, pH 11). Production of nitrophenol was monitored by measuring the absorbance at 400 nm using a spectrophotometer (DU-640B; Beckman Coulter), and the nitrophenol concentration was calculated using Beer's law with ε400 = 18,000 M^{-1} cm^{-1}. Protein concentration in the extracts was measured with the Pierce BCA assay (Thermo Fisher Scientific), and one activity unit was defined as nmol nitrophenol/min/mg protein.

2.6 Acknowledgments

We thank Dr. Jiefei Geng (Harvard University, Massachusetts) for providing strains, Dr. Usha Nair for providing plasmids, and Dr. Zhifen Yang for technical support. This work was supported by National Institutes of Health Public Health Service grant GM53396 to D.J. Klionsky.

Table 2.1 Yeast strain list

Name	Genotype	Reference
BY4742	*MATα his3Δ leu2Δ lys2Δ ura3Δ*	Invitrogen
JGY134	SEY6210 *RFP-APE1::LEU2 ATG9-3xGFP::URA3*	This study
JGY135	SEY6210 *RFP-APE1::LEU2 ATG9-3xGFP::URA3 atg1Δ::ble*	This study
KDM1003	SEY6210 *pho8Δ::TRP1 pho13Δ::LEU2 pRS406-ADH1-COX4-pho8Δ60 mkk1Δ::HIS5 mkk2Δ::KAN*	This study
KDM1005	SEY6210 *pho8Δ::TRP1 pho13Δ::LEU2 pRS406-ADH1-COX4-pho8Δ60 pbs2Δ::KAN*	This study
KDM1008	SEY6210 *pho8Δ::TRP1 pho13Δ::LEU2 pRS406-ADH1-COX4-pho8Δ60 slt2Δ::KAN*	This study
KDM1015	SEY6210 *pho8Δ::TRP1 pho13Δ::LEU2 pRS406-ADH1-COX4-pho8Δ60 hog1Δ::HIS5*	This study
KDM1021	SEY6210 *pho8Δ::TRP1 pho13Δ::LEU2 pRS406-ADH1-COX4-pho8Δ60 ssk1Δ::ble*	This study
KDM1022	SEY6210 *pho8Δ::TRP1 pho13Δ::LEU2 pRS406-ADH1-COX4-pho8Δ60 sho1Δ::ble*	This study
KDM1023	SEY6210 *pho8Δ::TRP1 pho13Δ::LEU2 pRS406-ADH1-COX4-pho8Δ60 wsc1Δ::ble*	This study
KDM1025	SEY6210 *pho8Δ::TRP1 pho13Δ::LEU2 pRS406-ADH1-COX4-pho8Δ60 slt2Δ::KAN hog1Δ::HIS5*	This study
KDM1101	SEY6210 *PEX14-GFP::KAN slt2Δ::URA3*	This study
KDM1102	SEY6210 *PEX14-GFP::KAN hog1Δ::URA3*	This study
KDM1203	SEY6210 *atg1Δ::HIS5 slt2Δ::ble*	This study
KDM1207	SEY6210 *RFP-APE1::LEU2 ATG9-3xGFP::URA3 hog1Δ::KAN*	This study
KDM1211	SEY6210 *atg1Δ::HIS5 hog1Δ::ble*	This study
KDM1212	SEY6210 *RFP-APE1::LEU2 ATG9-3xGFP::URA3 atg1Δ::ble hog1Δ::KAN*	This study
KDM1213	SEY6210 *slt2Δ::HIS5*	This study
KDM1214	SEY6210 *hog1Δ::HIS5*	This study
KDM1217	SEY6210 *HOG1-GFP::HIS5*	This study
KDM1218	SEY6210 *SLT2-GFP::HIS5*	This study
KDM1303	SEY6210 *OM45-GFP::TRP1 mkk2Δ::KAN mkk1Δ::HIS5*	This study
KDM1305	SEY6210 *OM45-GFP::TRP1 slt2Δ::KAN*	This study
KDM1307	SEY6210 *OM45-GFP::TRP1 hog1Δ::KAN*	This study
KDM1309	SEY6210 *OM45-GFP::TRP1 pbs2Δ::KAN*	This study
KDM1403	SEY6210 *pho13Δ pho8Δ60::HIS3 hog1Δ::KAN*	This study
KDM1401	SEY6210 *pho13Δ pho8Δ60::HIS3 slt2Δ::URA3*	This study

KDM2009	BY4742 *OM45-GFP::HIS3 pkc1-2::KAN*	This study
KDM2011	BY4742 *OM45-GFP::HIS3 pkc1-1::KAN*	This study
KDM2010	BY4742 *OM45-GFP::HIS3 pkc1-3::KAN*	This study
KDM2012	BY4742 *OM45-GFP::HIS3 pkc1-4::KAN*	This study
KDM2023	BY4742 *OM45-GFP::HIS3*	This study
KDM2024	BY4742 *OM45-GFP::HIS3 wsc1Δ::KAN*	This study
KDM2025	BY4742 *OM45-GFP::HIS3 wsc2Δ::KAN*	This study
KDM2026	BY4742 *OM45-GFP::HIS3 wsc3Δ::KAN*	This study
KDM2027	BY4742 *OM45-GFP::HIS3 wsc4Δ::KAN*	This study
KDM2028	BY4742 *OM45-GFP::HIS3 mid2Δ::KAN*	This study
KDM2029	BY4742 *OM45-GFP::HIS3 mtl1Δ::KAN*	This study
KDM2030	BY4742 *OM45-GFP::HIS3 rlm1Δ::KAN*	This study
KDM2031	BY4742 *OM45-GFP::HIS3 swi4Δ::KAN*	This study
KDM2032	BY4742 *OM45-GFP::HIS3 swi6Δ::KAN*	This study
KDM2033	BY4742 *OM45-GFP::HIS3 sko1Δ::KAN*	This study
KDM2034	BY4742 *OM45-GFP::HIS3 smp1Δ::KAN*	This study
KDM2035	BY4742 *OM45-GFP::HIS3 hot1Δ::KAN*	This study
KDM2036	BY4742 *OM45-GFP::HIS3 sln1-ts::KAN*	This study
KWY20	SEY6210 *pho8Δ::TRP1 pho13Δ::LEU2 pRS406-ADH1-COX4-pho8Δ60*	(78)
KWY22	SEY6210 *pho8Δ::TRP1 pho13Δ::LEU2 pRS406-ADH1-COX4-pho8Δ60 atg32Δ::KAN*	(78)
KWY33	SEY6210 *pho8Δ::TRP1 pho13Δ::LEU2 pRS406-ADH1-COX4-pho8Δ60 bck1Δ::KAN*	(78)
KWY51	SEY6210 *OM45-GFP::TRP1 bck1Δ::KAN*	(78)
SEY6210	*MATα ura3-52 leu2-3,112 his3-Δ200 trp1-Δ901 lys2-801 suc2-Δ9 mel GAL*	(101)
TKYM130	SEY6210 *OM45-GFP::TRP1 atg32Δ::URA3*	(78)
TKYM22	SEY6210 *OM45-GFP::TRP1*	(58)
TKYM67	SEY6210 *PEX14-GFP::KAN*	(58)
TKYM72	SEY6210 *PEX14-GFP::KAN atg1Δ::HIS5*	(58)
TKYM203	SEY6210 *atg1Δ::HIS5 IDH1-RFP::KAN*	(59)
UNY29	SEY6210 *atg13Δ::KAN atg1Δ::HIS5*	This study
WHY001	SEY6210 *atg1Δ::HIS5*	(56)
WLY176	SEY6210 *pho13Δ pho8Δ60::HIS3*	(59)
WLY192	SEY6210 *pho13Δ::KAN pho8Δ60::URA3 atg1Δ::HIS5*	(59)

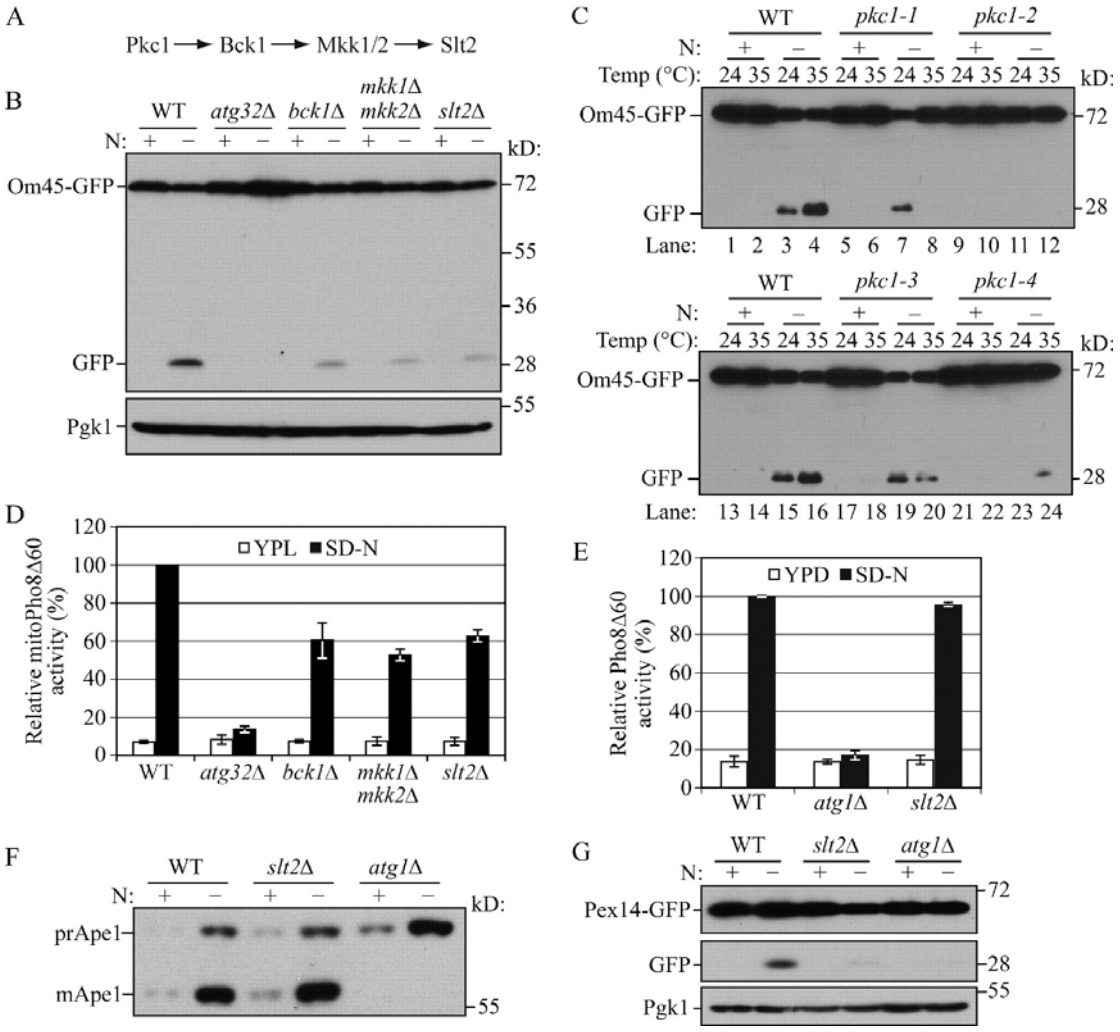

Figure 2.1 Slt2 is involved in mitophagy and pexophagy, but not bulk autophagy or the Cvt pathway.

(A) The Slt2 MAPK pathway.

(B) Om45-GFP processing is blocked in *bck1Δ*, *mkk1/2Δ*, and *slt2Δ* mutants. *OM45* was chromosomally tagged with GFP in the wild-type (TKYM22), *atg32Δ* (TKYM130), *bck1Δ* (KWY51), *mkk1Δ mkk2Δ* (KDM1303), and *slt2Δ* (KDM1305) strains. Cells were cultured in YPL to mid-log phase, then shifted to SD-N and incubated for 6 h. Samples were taken before (+) and after (−) starvation. Immunoblotting was done with anti-YFP antibody and the positions of full-length Om45-GFP and free GFP are indicated. Anti-Pgk1 was used as a loading control.

(C) Om45-GFP processing is blocked in *pkc1* mutants. Om45-GFP processing was examined in wild-type (KDM2023), *pkc1-1* (KDM2011), *pkc1-2* (KDM2009), *pkc1-3* (KDM2010), and *pkc1-4* (KDM2012) strains. Cells were cultured in YPL at 24°C to mid-log phase. For each strain, the culture was then divided into two parts. Both were shifted to SD-N and one half was incubated

for 6 h at 24°C while the other was shifted to 35°C. Protein extracts were probed with anti-YFP antibody.

(D) MitoPho8Δ60 activity is reduced in Slt2 pathway mutants. Wild-type (KWY20), *atg32Δ* (KWY22),*bck1Δ* (KWY33), *mkk1/2Δ* (KDM1003), and *slt2Δ* (KDM1008) cells were cultured as in A. The mitoPho8Δ60 assay was performed as described in Materials and methods. Error bars, standard deviation (SD) were obtained from three independent repeats.

(E) The Pho8Δ60 activity (nonspecific autophagy) is unaffected in the *slt2Δ* mutant. Wild-type (WLY176), *atg1Δ* (WLY192), and *slt2Δ* (KDM1401) cells were cultured as in A, but the time of incubation in SD-N was reduced to 2 h. The Pho8Δ60 assay was performed as described in Materials and methods. Error bars, SD were obtained from three independent repeats.

(F) The Cvt pathway is unaffected in the *slt2Δ* mutant. Wild-type (SEY6210), *atg1Δ* (WHY001), and *slt2Δ* (KDM1213) cells were cultured in YPD to mid-log phase, then shifted to SD-N and incubated for 1 h. Samples were taken before and after nitrogen starvation. Immunoblotting was done with anti-Ape1 antibody and the positions of precursor Ape1 and mature Ape1 are indicated.

(G) Pex14-GFP processing is blocked in the *slt2Δ* mutant. *PEX14* was chromosomally tagged with GFP in wild-type (TKYM67), *atg1Δ* (TKYM72), and *slt2Δ* (KDM1101) strains. Cells were grown in oleic acid–containing medium for 19 h and shifted to SD-N for 4 h. Samples were taken before and after nitrogen starvation. Immunoblotting was done with anti-YFP antibody and the positions of full-length Pex14-GFP and free GFP are indicated. Anti-Pgk1 was used as a loading control.

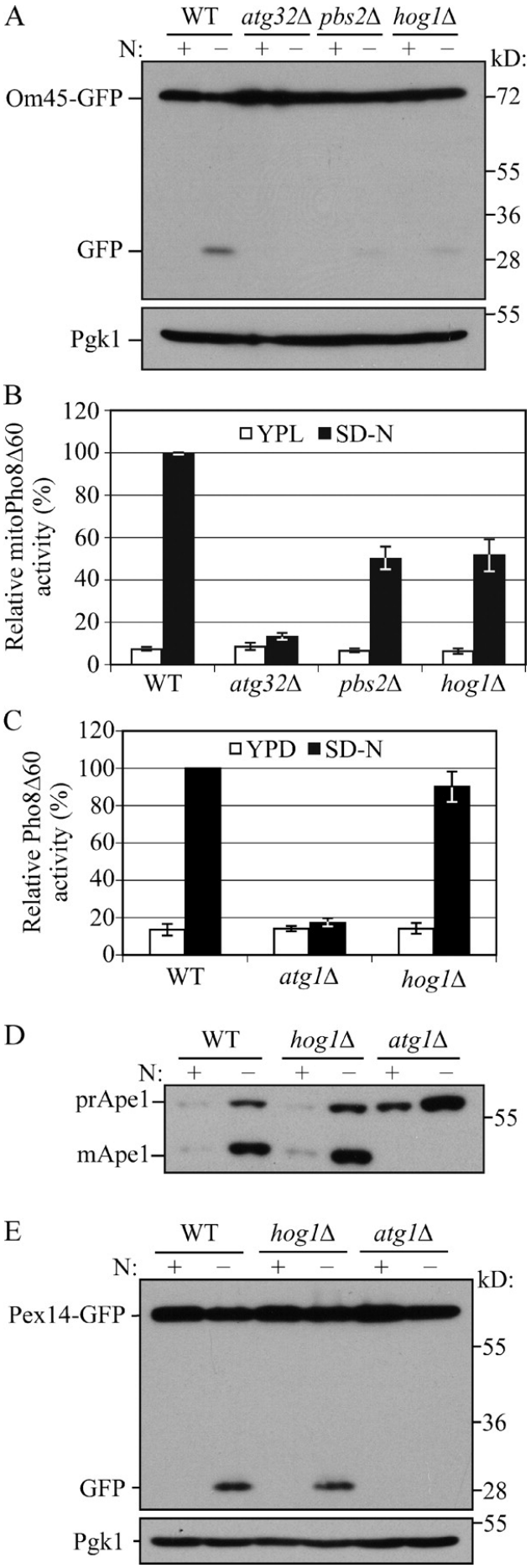
A
WT
atg32Δ
pbs2Δ
hog1Δ
N:
+ − + − + − + −
kD:
Om45-GFP
72
55
36
GFP
28
55
Pgk1
B
Relative mitoPho8Δ60 activity (%)
120
100
80
60
40
20
0
YPL
SD-N
WT
atg32Δ
pbs2Δ
hog1Δ
C
Relative Pho8Δ60 activity (%)
120
100
80
60
40
20
0
YPD
SD-N
WT
atg1Δ
hog1Δ
D
WT
hog1Δ
atg1Δ
N:
+ − + − + −
prApe1
mApe1
55
E
WT
hog1Δ
atg1Δ
N:
+ − + − + −
kD:
Pex14-GFP
55
36
GFP
28
55
Pgk1

Figure 2.2 Hog1 is involved in mitophagy, but not other types of autophagy.

(A) Om45-GFP processing is blocked in *pbs2Δ* and *hog1Δ* mutants. Om45-GFP processing was tested in wild-type (TKYM22), *atg32Δ* (TKYM130), *pbs2Δ* (KDM1309), and *hog1Δ* (KDM1307) cells with the methods described in Figure 2.1B.

(B) MitoPho8Δ60 activity is reduced in *hog1Δ* and *pbs2Δ* mutants. The mitoPho8Δ60 activity was examined in wild-type (KWY20), *atg32Δ* (KWY22), *pbs2Δ* (KDM1005), and *hog1Δ* (KDM1015) cells as in Figure 2.1D. Error bars, SD were obtained from three independent repeats.

(C) The Pho8Δ60 activity is unaffected in the *hog1Δ* mutant. The Pho8Δ60 assay was performed in wild-type (WLY176), *atg1Δ* (WLY192), and *hog1Δ* (KDM1403) cells as in Figure 2.1E. Error bars, SD were obtained from three independent repeats.

(D) The Cvt pathway is unaffected in the *hog1Δ* mutant. Maturation of prApe1 was examined in wild-type (SEY6210), *hog1Δ* (KDM1214), and *atg1Δ* (WHY001) cells as in Figure 2.1F.

(E) Pex14-GFP processing is unaffected in the *hog1Δ* mutant. Pex14-GFP processing was examined in wild-type (TKYM67), *hog1Δ* (KDM1102), and *atg1Δ* (TKYM72) cells as in Figure 2.1G.

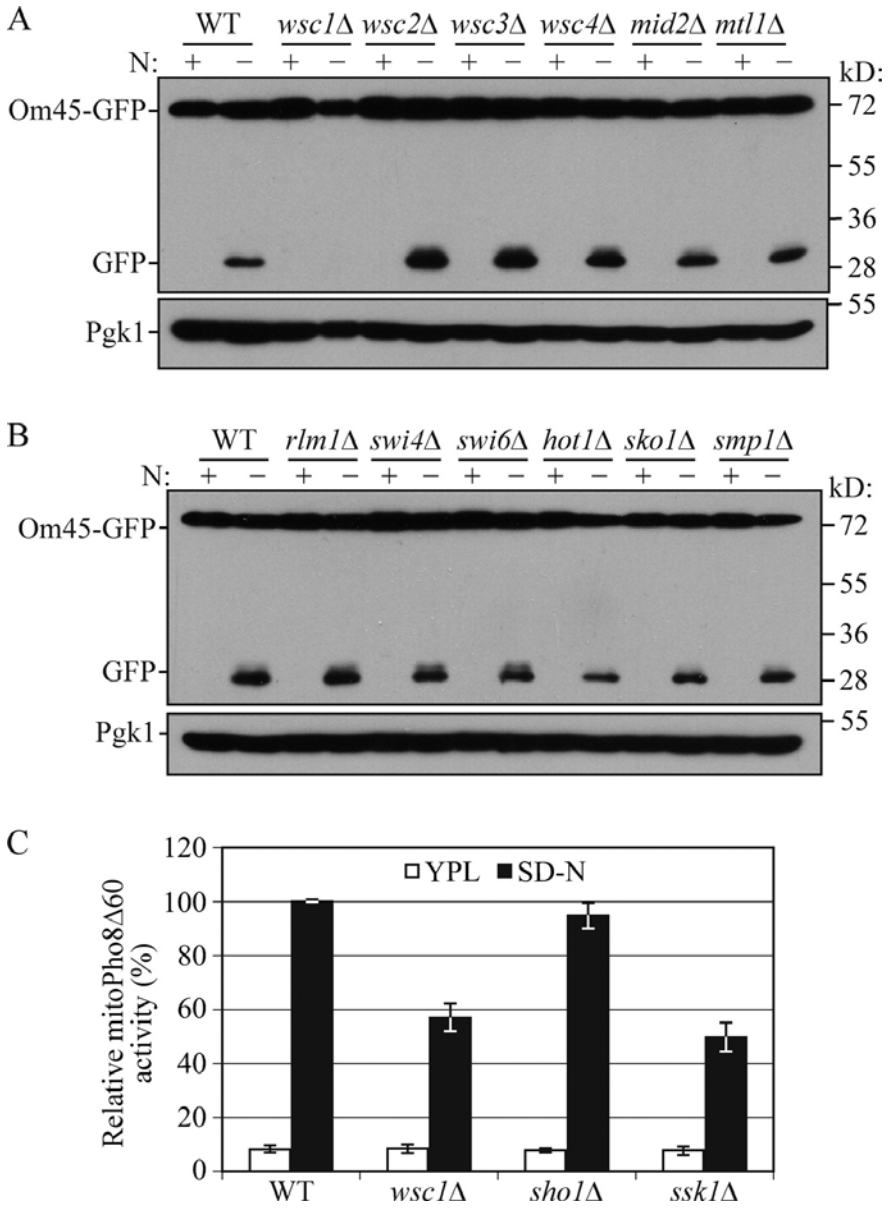

Figure 2.3 Wsc1 and Ssk1 are required for mitophagy.

(A) Om45-GFP processing is blocked in *wsc1Δ* cells but not other mutants lacking cell surface sensors. Om45-GFP processing was tested in wild-type (KDM2023), *wsc1Δ* (KDM2024), *wsc2Δ* (KDM2025), *wsc3Δ* (KDM2026), *wsc4Δ* (KDM2027), *mid2Δ* (KDM2028), and *mtl1Δ* (KDM2029) cells as in Figure 2.1B. Protein extracts were probed with anti-YFP antibodies and anti-Pgk1 as a loading control.

(B) Om45-GFP processing remains normal in *rlm1Δ* (KDM2030), *swi4Δ* (KDM2031), *swi6Δ* (KDM2032), *sko1Δ* (KDM2033), *hot1Δ* (KDM2035), and *smp1Δ* (KDM2034) mutants. Protein extracts were probed as in A.

(C) The mitoPho8Δ60 activity is reduced in *wsc1Δ* (KDM1023) and *ssk1Δ* (KDM1021) mutants but not in the *sho1Δ* (KDM1022) mutant. Error bars, SD were obtained from three independent repeats.

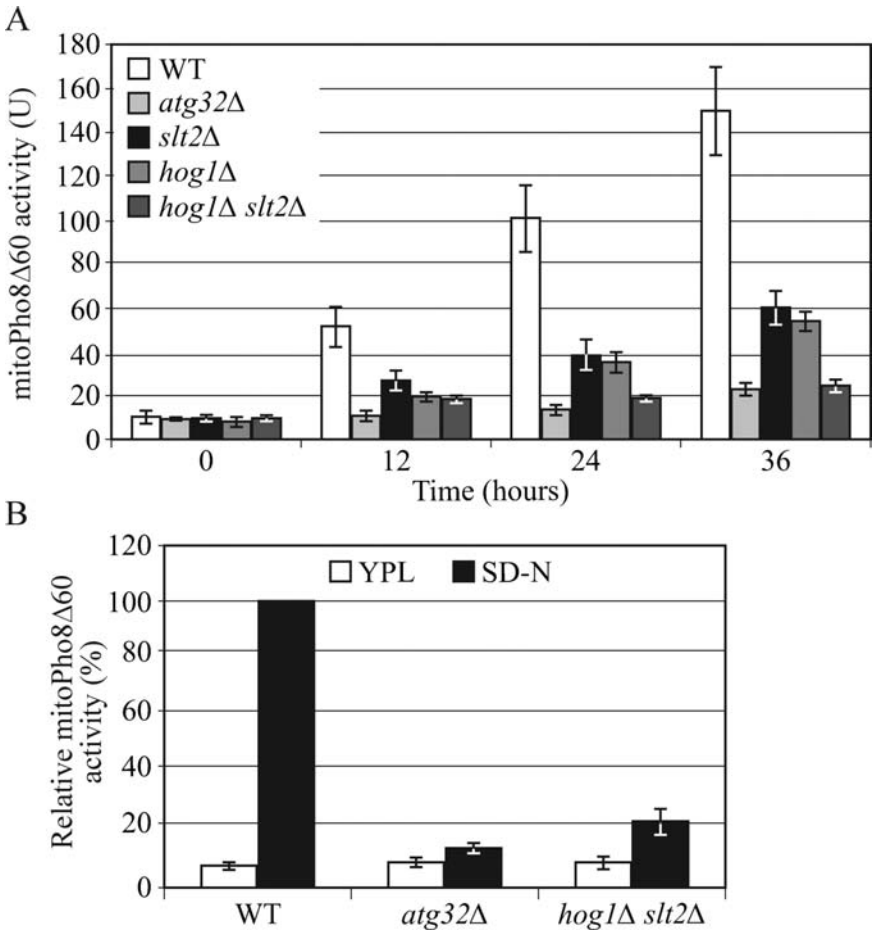

Figure 2.4 Mitophagy in post-log phase requires Slt2 and Hog1 signaling. (A) MitoPho8Δ60 activity is reduced in slt2Δ, hog1Δ, and hog1Δ slt2Δ mutants in post-log phase mitophagy. Wild-type (KWY20), *atg32Δ* (KWY22), *slt2Δ* (KDM1008), *hog1Δ* (KDM1015), and *hog1Δ slt2Δ* (KDM1025) cells were cultured in lactate medium to log phase and the cells were grown for another 12, 24, and 36 h. Samples were collected at each time point. The mitoPho8Δ60 assay was performed as described in Materials and methods. Error bars, SD were obtained from three independent repeats.
(B) MitoPho8Δ60 activity is reduced in thehog1Δ slt2Δ double mutant in nitrogen starvation–induced mitophagy conditions. The mitoPho8Δ60 assay was performed in wild-type (KWY20), atg32Δ(KWY22), and hog1Δ slt2Δ (KDM1025) cells as in Figure 2.1E.

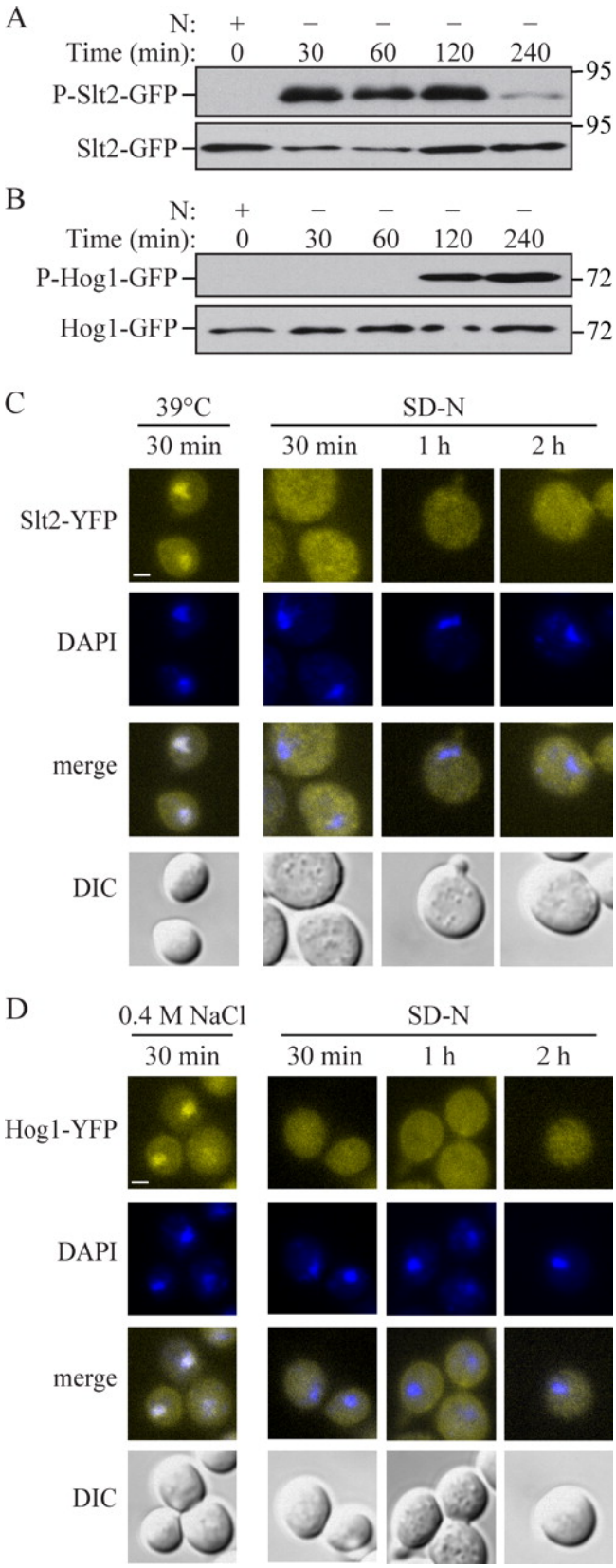

Figure 2.5 Hog1 and Slt2 are activated and remain in the cytosol during mitophagy.

(A and B) SLT2 or HOG1 were chromosomally tagged with GFP. *SLT2-GFP* (KDM1218) or *HOG1-GFP* (KDM1217) cells were cultured in YPL to mid-log

phase and shifted to SD-N for the indicated times. Samples were taken before (+) and at the indicated times after (−) nitrogen starvation. Immunoblotting was done with anti–phospho-Slt2 antibody in A, anti-phospho-Hog1 antibody in B, or anti-YFP antibody in both A and B.
(C and D) Cells (SEY6210) transformed with plasmids encoding either Hog1-YFP or Slt2-YFP were cultured in SML to mid-log phase and shifted to SD-N for the indicated times, or cultured at 39°C for Slt2-YFP in C or treated with 0.4 M NaCl for Hog1-YFP in D. Samples were taken after each specific treatment, fixed, stained with DAPI to mark the nucleus, and observed by fluorescence microscopy. Representative pictures from single Z-section images are shown. DIC, differential interference contrast. Bars, 2.5 μm.

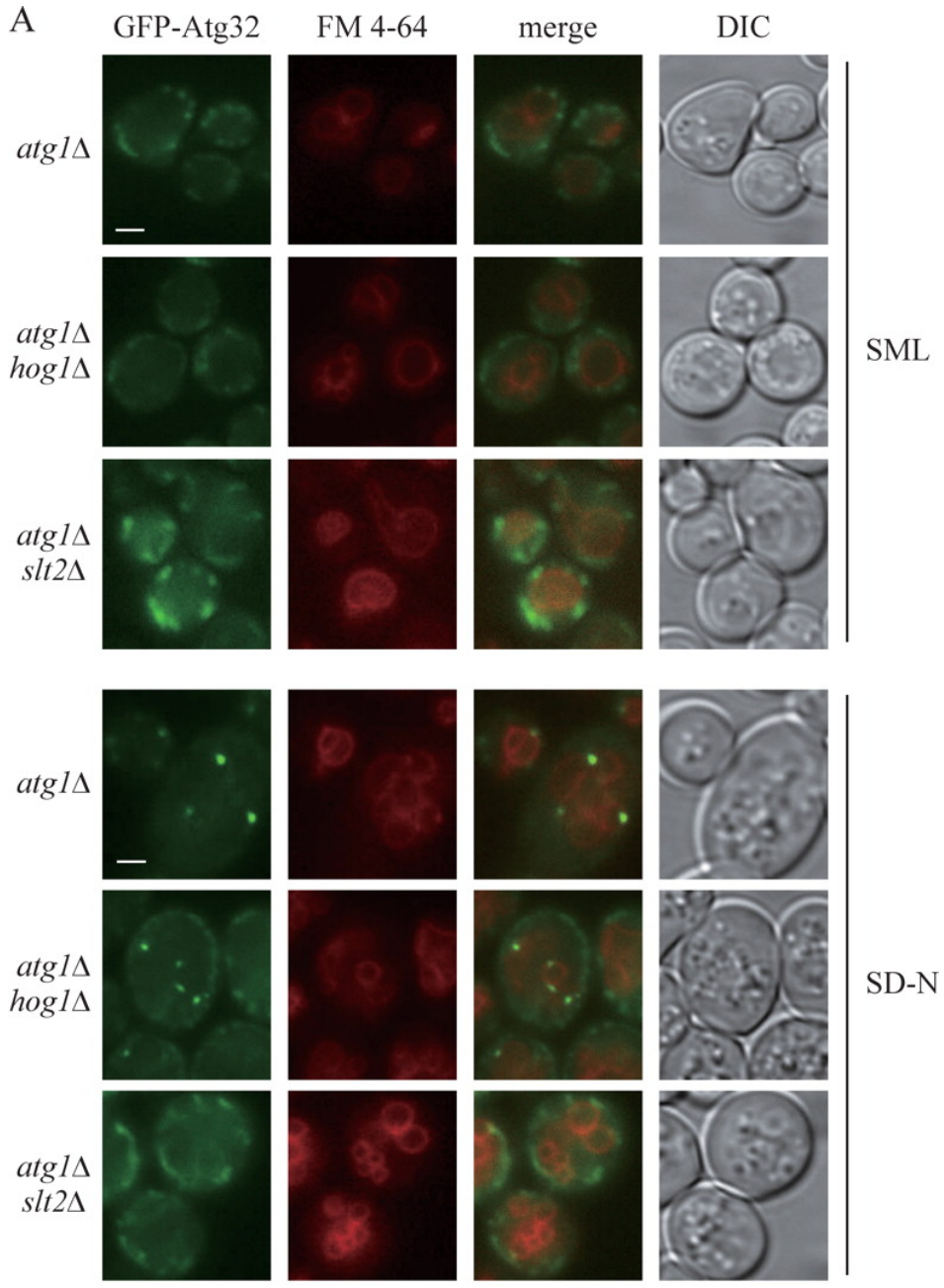

B

Strain	% Atg32 PAS localization (2 h)	% Atg32 PAS localization (4 h)
atg1Δ	44.7 ± 6.7 (n = 244)	76.7 ± 5.7 (n = 266)
atg1Δ hog1Δ	39.4 ± 4.7 (n = 218)	68.5 ± 4.0 (n = 239)
atg1Δ slt2Δ	17.4 ± 3.4 (n = 237)	36.9 ± 4.1 (n = 252)

Figure 2.6 Recruitment of Atg32 to the PAS is defective in the *slt2Δ*, but not the *hog1Δ* mutant.

(A) Plasmid-driven GFP-Atg32 was transformed into atg1Δ (WHY001), *atg1Δ slt2Δ* (KDM1203), and *atg1Δ hog1Δ* (KDM1211) strains. Cells were grown to mid-log phase in SML, shifted to SD-N for 2 or 4 h, and stained with FM 4-64 to mark the vacuole. Representative pictures from single Z-section images are

shown. DIC, differential interference contrast. Bars, 2.5 μm.
(B) Quantification of Atg32 PAS localization. 12 Z-section images were projected and the percentage of cells that contained at least one GFP-Atg32 dot on the surface of the vacuole was determined. The SD was calculated from three independent experiments.

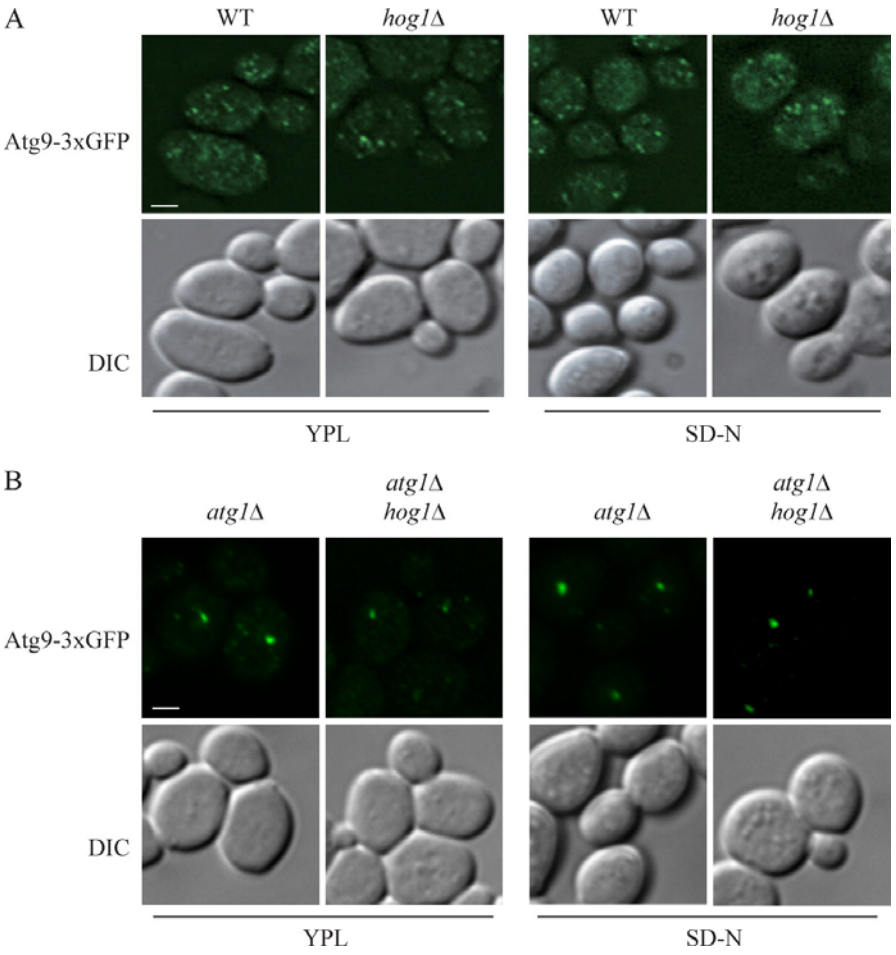

Figure 2.7 Atg9 movement is unaffected in the *hog1Δ* mutant.
(A and B) The localization of Atg9-3xGFP was tested in wild-type (JGY134) and *hog1Δ* (KDM1207) strains (A) and *atg1Δ* (JGY135) and *atg1Δ hog1Δ* (KDM1212) strains (B). Cells were cultured in growing (YPL medium) conditions and shifted to nitrogen starvation medium (SD-N) for 2 h. Cells were fixed and observed by fluorescence microscopy. Representative pictures from single Z-section images are shown. DIC, differential interference contrast. Bars, 2.5 μm.

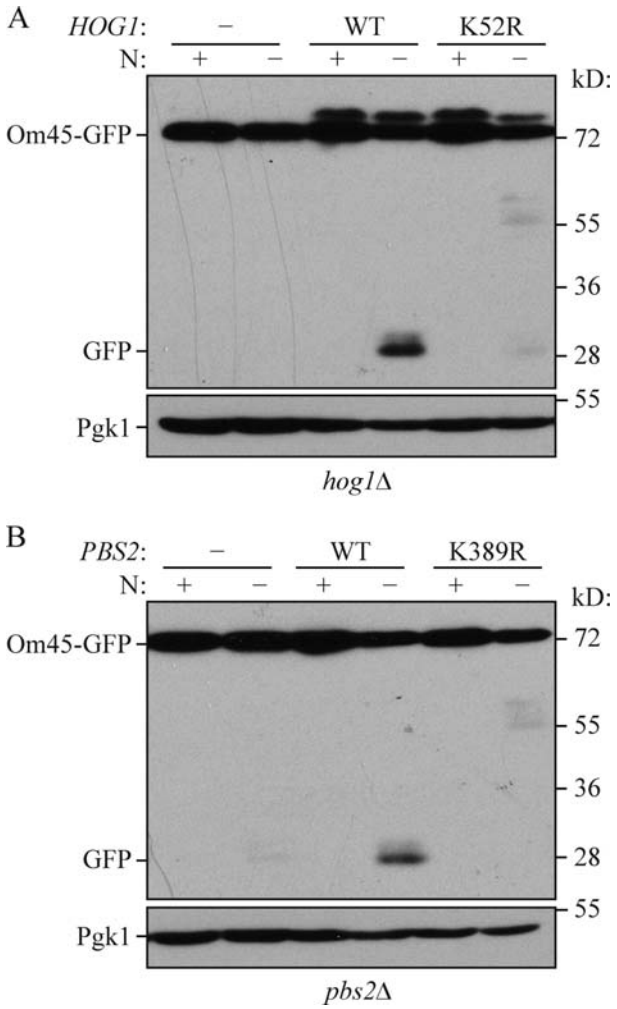

Figure 2.8 Kinase-dead mutants of Hog1 and Pbs2 have defects in mitophagy.

(A) The *hog1Δ* (KDM1307) or (B) *pbs2Δ* (KDM1309) cells were transformed with empty vector or a plasmid encoding either (A) wild-type (WT) Hog1 or a kinase-dead mutant (K52R), or (B) with empty vector or a plasmid encoding either wild-type Pbs2 or a kinase-dead mutant (K389R). (A and B) Om45-GFP processing was examined as described in Materials and methods.

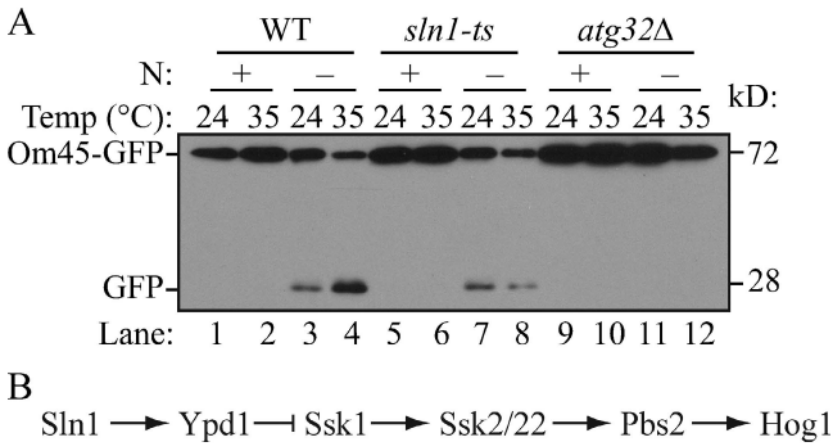

Figure 2.S1. Sln1 is required for efficient mitophagy.
(A) OM45 was chromosomally tagged with GFP in the wild-type (TKYM22), *sln1-ts* (KDM2036), and *atg32Δ* (TKYM130) strains. Cells were cultured in YPL to mid-log phase, then shifted to SD-N and incubated for 6 h. Samples were taken before (+) and after (-) starvation. Immunoblotting was done with anti-YFP antibody and the positions of full-length Om45-GFP and free GFP are indicated.
(B) The Sln1 branch of the Hog1 pathway.

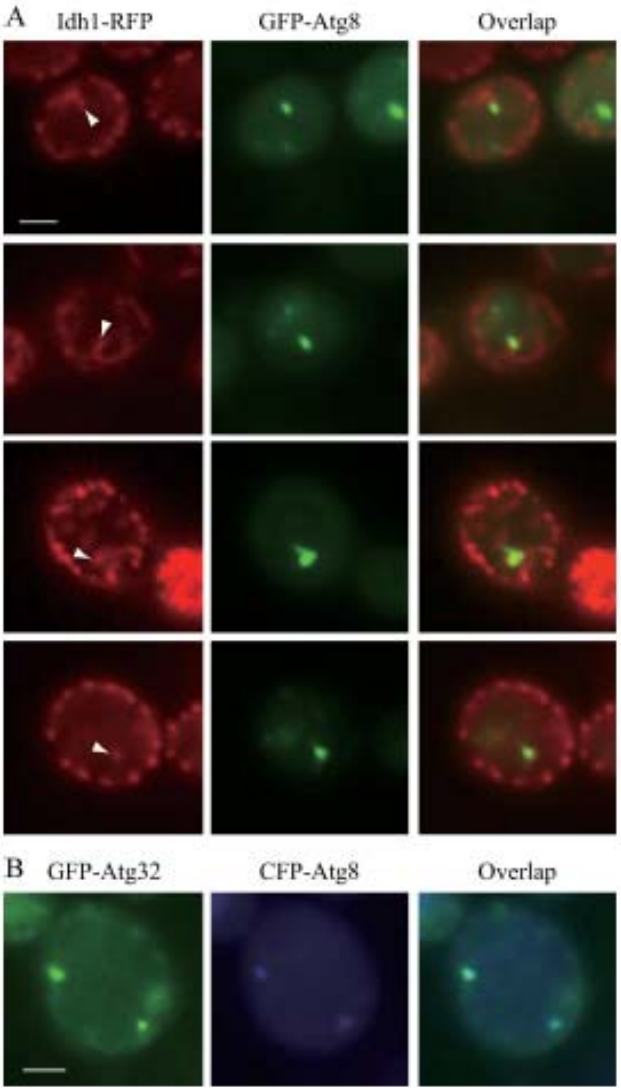

Figure 2.S2 A portion of the total mitochondria population accumulates at the PAS under mitophagy-inducing conditions.

(A) Idh1-RFP colocalized with GFP-Atg8 during mitophagy. *IDH1-RFP atg1Δ* (TKYM203) cells transformed with a plasmid expressing GFP-Atg8 were cultured in SML to mid-log phase and shifted to SD-N. Samples were taken after 2 h culturing in SD-N and observed by fluorescence microscopy. White arrowheads mark mitochondria that overlap with GFP-Atg8. Representative pictures from single Z-section images are shown.

(B) The *atg1Δ* (WHY001) cells transformed with plasmids encoding CFP-Atg8 and GFP-Atg32 were cultured in SML to mid-log phase and shifted to SD-N. Samples were taken after 2 h culturing in SD-N and observed by fluorescence microscopy. Representative pictures from single Z-section images are shown. Bars, 2.5 μm.

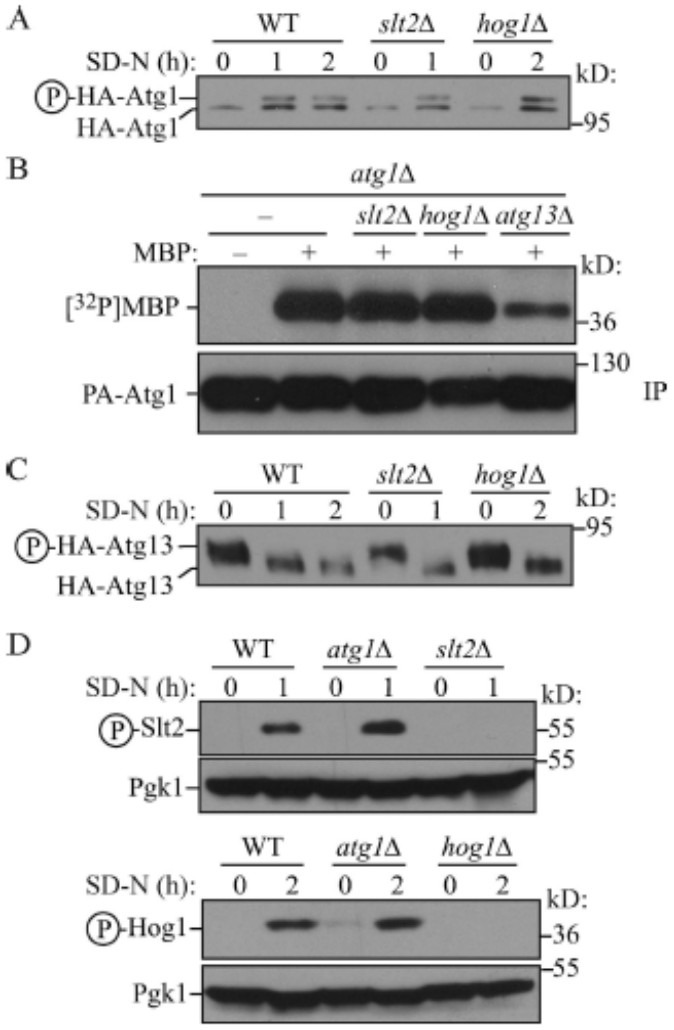

Figure 2.S3 Slt2 and Hog1 regulate mitophagy independent of the Atg1-Atg13 complex.

(A) Slt2 and Hog1 have no effect on Atg1 phosphorylation. Wildtype (SEY6210), *slt2Δ* (KDM1213), and *hog1Δ* (KDM1214) cells transformed with plasmid encoding HA-Atg1 were cultured in SML to mid-log phase and shifted to SD-N. Samples were collected before or at 1 or 2 h after nitrogen starvation. Immunoblotting was done with anti-HA antibody.

(B) Slt2 and Hog1 have no effect on Atg1 kinase activity. The *atg1Δ* (WHY001), *atg1Δ slt2Δ* (KDM1203), *atg1Δ hog1Δ* (KDM1211), and *atg1Δ atg13Δ* (UNY29) cells transformed with protein A–tagged Atg1 (PA-Atg1) were cultured in SML medium to mid-log phase and shifted to SD-N for 2 h. PA-Atg1 from the indicated strains was immunoprecipitated with IgG sepharose. MBP was used as substrate in an in vitro kinase assay with immunoprecipitated PA-Atg1 from different mutant cells. Phosphorylated MBP was detected by autoradiography and the protein input was shown by immunoblot; the molecular mass indicated is approximate.

(C) Wild-type (SEY6210), *slt2Δ* (KDM1213), and *hog1Δ* (KDM1214) cells transformed with a plasmid encoding HA-Atg13 were treated as in (A).

Immunoblotting was performed with anti-HA antibody.
(D) Atg1 has no effect on the phosphorylation of Slt2 and Hog1. Wild-type (SEY6210), *atg1Δ* (WHY001), *slt2Δ* (KDM1213), and *hog1Δ* (KDM1214) cells were treated as in A. Immunoblotting was done with anti–phospho-Slt2 or anti–phospho-Hog1 antibodies.

Chapter 3

The scaffold protein Atg11 recruits fission machinery to drive selective mitochondria degradation by autophagy[2]

3.1 Abstract

As the cellular power plant, mitochondria play a significant role in homeostasis. To maintain the proper quality and quantity of mitochondria requires both mitochondrial degradation and division. A selective type of autophagy, mitophagy, drives the degradation of excess or damaged mitochondria, whereas division is controlled by a specific fission complex; however, the relationship between these two processes, especially the role of mitochondrial fission during mitophagy, remains unclear. In this study, we report that mitochondrial fission is important for the progression of mitophagy. When mitophagy is induced, the fission complex is recruited to the degrading mitochondria through an interaction between Atg11 and Dnm1; interfering with this interaction severely blocks mitophagy. These data establish a paradigm for selective organelle degradation.

3.2 Introduction

Mitochondria are double-membrane-bound organelles that play significant roles in a variety of cellular metabolic reactions. This organelle is central to cellular physiology, supplying energy and certain metabolites, but it also generates harmful reactive oxygen species. Thus, mitochondrial homeostasis must be maintained, which can be a costly process. As a result, cells degrade superfluous, or extensively damaged, mitochondria; however, this is a considerable structural challenge considering the extended, reticular nature of

2 Originally published in *Developmental Cell* (2013; 26(1):9-18) with authors listed as Kai Mao, Ke Wang, Xu Liu, and Daniel J. Klionsky.

this organelle. Constitutive mitochondrial fusion and fission, as well as biogenesis and degradation, make the mitochondria highly dynamic. In the budding yeast *Saccharomyces cerevisiae*, a complex containing Fis1, Dnm1, Mdv1 and Caf4 controls the fission of mitochondria, whereas fusion is regulated by the action of Fzo1, Ugo1 and Mgm1 (102). The degradation of mitochondria is mediated by mitophagy, a selective type of macroautophagy (hereafter autophagy). The study of mitophagy has attracted increasing attention in recent years; this process plays significant roles in various aspects of normal physiology such as the removal of mitochondria during the maturation of erythroid cells, whereas its dysfunction is associated with certain pathophysiologies such as Wolfram Syndrome 2 and Parkinson disease (59-61, 63, 103-106).

Autophagy functions as a lysosome/vacuole-dependent mechanism for the degradation of damaged or obsolete proteins and organelles, and can occur in either nonselective or selective modes. Nonselective autophagy functions to sequester bulk cytoplasm into double-membrane vesicles, termed autophagosomes, which are then transported to the lysosome/vacuole where the cargo is degraded (47). In contrast, selective autophagy targets specific proteins or organelles as cargos, such as peroxisomes (pexophagy) and mitochondria. In the case of selective autophagy, a general model has been established in which a ligand on the target interacts with a specific receptor; the receptor in turn binds a scaffold protein, which links the cargo-receptor complex with the autophagy machinery (107). For example, in yeast mitophagy, Atg32 is a mitochondrial protein that serves as a selective receptor (a ligand, if one exists, has not been identified), which binds the Atg11 scaffold. Atg11 is needed for subsequent engagement of the mitochondria with Atg8–PE, which lines the initial sequestering compartment, the phagophore. Due to its potentially large size, one key question with regard to mitophagy concerns the role of mitochondrial fission. Work in mammalian cells suggests that mitochondrial fission facilitates the process of mitophagy (64, 108); however, it

is not clear whether these two processes occur independently, or whether they function in a coordinated manner.

Here, we show that the Atg32-Atg11 interaction marks degrading mitochondria. Furthermore, Dnm1 is recruited to these mitochondria through an interaction with Atg11. When Dnm1 loses its interaction with Atg11, the degradation of mitochondria is severely blocked. These results support the hypothesis that mitochondrial fission machinery participates in, and facilitates, mitochondrial division in an early step of mitophagy, and indicate that Atg11 plays a unique role as a scaffold that recruits the fission components in addition to its role in connecting the target with the autophagic machinery.

3.3 Results

3.3.1 The mitochondrial fission complex is required for mitophagy

In our recent genome-wide yeast mutant screen for mitophagy-defective strains, we found that *DNM1*, a gene encoding a dynamin-related GTPase required for mitochondrial fission, is required for efficient mitophagy (78). In *Saccharomyces cerevisiae*, the mitochondrial fission complex consists of four components, Fis1, Dnm1, Mdv1 and Caf4. Fis1 is a conserved integral membrane protein and is required for the proper localization of Dnm1 and Mdv1 on mitochondria (109-111). Dnm1 assembles specifically at the sites where mitochondrial fission occurs (112). Mdv1 and Caf4 redundantly bridge the interaction between Fis1 and Dnm1 (109, 113). Although Fis1 is distributed evenly on mitochondria, Dnm1 and Mdv1 show colocalized puncta on mitochondrial tubules, and it is thought that those puncta are the sites where mitochondrial division takes place. We first sought to determine whether all four of the corresponding gene products are involved in mitophagy.

In *Saccharomyces cerevisiae*, mitochondria proliferate when cells are cultured in a non-fermentable carbon source, such as lactic acid or glycerol. When these cells are subjected to conditions of nitrogen starvation in the presence of a fermentable carbon source, such as glucose, mitophagy is

induced to degrade the excess mitochondria (58). We examined the activity of mitophagy in the absence of *DNM1*, *FIS1*, *MDV1* or *CAF4*, using an enzymatic assay in which a mitochondrially-targeted zymogen, mitoPho8Δ60, is activated following mitophagic delivery to the vacuole (78). *PHO8* encodes an alkaline phosphatase that is transported to the vacuole via the ALP pathway (80). Pho8Δ60, a mutant form of Pho8 in which the N-terminal 60 amino acids including the transmembrane domain have been removed, localizes to the cytoplasm and is unable to be transported to the vacuole through the ALP pathway. We fused cytochrome c oxidase subunit IV (Cox4) with Pho8Δ60 and named the fusion protein mitoPho8Δ60. This fusion protein is localized on mitochondria and its transport to the vacuole, which results in enzyme activation, is dependent on mitophagy (78). Therefore, calculating the phosphatase activity of mitoPho8Δ60 can be used to monitor mitophagy activity. We found that mitophagy was severely blocked in *dnm1*Δ and *fis1*Δ cells, partially blocked in *mdv1*Δ cells, and essentially normal in *caf4*Δ cells (Figure 3.1). Previous work implied a redundant function for Mdv1 and Caf4, with Mdv1 being more important than Caf4 in mitochondrial fission (114). Accordingly, we examined the *mdv1*Δ *caf4*Δ double-deletion mutant, which showed a strong defect in mitophagy, similar to *dnm1*Δ and *fis1*Δ (Figure 3.1). These results suggest that the intact mitochondrial fission machinery is required for mitophagy.

Previously, it was reported that mitochondrial fission is not required for rapamycin-induced mitophagy (115). In this study, the diminished mitophagy activity in *fis1*Δ cells is reported to be due to a secondary mutation in the *WHI2* gene. Therefore, we tested mitophagy activity in *whi2*Δ cells using the mitoPho8Δ60 assay. Mitophagy activity in *whi2*Δ cells was essentially identical to that of the isogenic wild-type cells (Figure 3.1). The discrepancy between our results and those of Mendl et al. may be due to the different methods used to induce mitophagy. In the previous study, yeast cells were cultured in medium containing glycerol, and mitophagy was induced by the addition of

rapamycin; however, these conditions require 24 h of drug treatment to induce a high level of mitophagy. In our study, mitochondrial proliferation was achieved by growth in lactic acid, and mitophagy was induced by nitrogen starvation in the presence of glucose; a similar level of mitoPho8Δ60 activity was detected in the wild-type and *whi2*Δ strains within 6 h. In general, nitrogen starvation induces a substantially stronger response than treatment with rapamycin.

3.3.2 The Atg32-Atg11 interaction marks degrading mitochondria during mitophagy

Mitochondrial fission is proposed to occur on mitochondrial termini (113), which may therefore represent a very early stage of mitophagy. Thus, the first requirement was to identify a marker that would enable us to specifically identify mitochondria destined for degradation. Previously, others and we showed that Atg32 and Atg11 directly participate in an early event of mitophagy (59, 60, 116, 117). When mitophagy is induced, Atg32 recruits Atg11 to the mitochondria, and their interaction is required for the delivery of mitochondria to the phagophore assembly site (PAS), the location of autophagosome formation, and eventually into the vacuole for degradation. In mammalian cells, PARK2/Parkin is recruited to, and thereby selectively marks, depolarized mitochondria (103); in yeast, however, Atg32 is evenly distributed on the mitochondrial tubules, even though only a relatively small portion of the total mitochondrial population will ultimately be degraded (118). Therefore, Atg32 alone cannot serve as the sole marker of the degrading mitochondria.

We took advantage of the bimolecular fluorescence complementation (BiFC) assay (119), in which the Venus yellow fluorescent protein (vYFP) is split into two fragments, VN (N terminus of vYFP) and VC (C terminus of vYFP); we fused VN to Atg32, and VC to Atg11 by integrating the corresponding constructs at the chromosomal *ATG32* and *ATG11* loci. Fluorescence from these chimeras can only be observed when the two proteins interact and bring

the two fluorophore fragments into close proximity. We tested the VN-Atg32-VC-Atg11 interaction in both growing (YPL) and mitophagy-inducing (SD-N) conditions. When expressing both VN-Atg32 and VC-Atg11, ~9% of the cells showed vYFP dots in growing conditions; however, when mitophagy was induced, ~42% of the cells displayed vYFP dots, indicating the colocalization of these two proteins (Figure 3.2A and B). In contrast, neither VN-Atg32 in combination with another autophagy-related protein fusion construct, Atg9-VC, nor a different chimera containing the OM45 mitochondrial outer membrane protein fused to VN (OM45-VN) in combination with VC-Atg11, generated fluorescent puncta in either growing or mitophagy-inducing conditions (Figure 3.2A). These results were consistent with our previous report that the interaction of Atg32 and Atg11 is enhanced when mitophagy is induced (59). The chimeric constructs were stable under mitophagy-inducing conditions and did not show an appreciable change in protein level, indicating that the appearance of the fluorescent dots reflected colocalization, and was not due to a change in protein concentration (Figure 3.S1B).

We next asked whether the VN-Atg32-VC-Atg11 BiFC fluorescent puncta (hereafter, 32-11 dots) represented degrading mitochondria. We first examined the activity of mitophagy in the presence of the fusion proteins VN-Atg32 and VC-Atg11. Wild-type and VN-Atg32-VC-Atg11 cells were grown in a non-fermentable carbon source, then shifted to SD-N to induce mitophagy. The mitoPho8Δ60 activity of VN-Atg32-VC-Atg11 cells was similar to that of wild-type cells, which indicated that mitophagy occurred normally when Atg32 and Atg11 were fused with VN and VC, respectively (Figure 3.S1C). The *atg32*Δ strain served as a negative control, and displayed only a background level of activity. Second, we stained the mitochondria with MitoTracker Red dye and examined the localization of the 32-11 dots relative to the organelle. When mitophagy was induced following a 30 min shift to SD-N, most of the 32-11 dots were localized on the mitochondrial reticulum (Figure 3.S1D). Subsequently, we used the FM 4-64 dye to mark the vacuole. Immediately

after the shift to SD-N, no 32-11 dots were detected in proximity to the vacuole (data not shown). Within 1 h after mitophagy induction, however, we detected 32-11 dots localized close to the vacuole limiting membrane (Figure 3.S1E); this perivacuolar location likely corresponds to the PAS. Finally, by 6 h after shifting to SD-N, very few 32-11 dots could be detected in wild-type cells; however, *atg1*Δ mutant cells that are defective in mitophagy continued to accumulate 32-11 dots, which indicated that the degradation of mitochondria marked by the VN-Atg32-VC-Atg11 BiFC interaction was dependent on an intact autophagy pathway (Figure 3.S1F and G). Therefore, based on the observations that 1) VN-Atg32 and VC-Atg11 are functional fusion proteins; 2) 32-11 dots localized on mitochondria shortly after inducing mitophagy; 3) at a later time point, the 32-11 dots subsequently showed a vacuole-peripheral PAS localization; and 4) the loss of the 32-11 signal was dependent on autophagy, we concluded that the 32-11 dots were an appropriate marker to monitor degrading mitochondria.

In order to clarify the sequential steps of mitophagy, we used a plasmid containing Mito-RFP and CellTracker Blue CMAC dye to mark the mitochondria and vacuole lumen, respectively, which enabled us to observe both organelles and determine the localization of the 32-11 signal. In growing conditions, when mitophagy was not induced, very few 32-11 dots were detected, which was defined as Stage 0 (Figure 3.2C, row 1). After a short time of starvation (10 to 30 min), when mitophagy was initiated, 32-11 puncta were formed on the mitochondrial reticulum, which was defined as Stage 1 (Figure 3.2C, rows 2 and 3). After longer times of starvation (approximately 40 to 60 min), even though most of the 32-11 puncta were still localized on the mitochondrial reticulum, some of the puncta were detected in proximity to the vacuole, which corresponded to the presence of mitophagosomes. We defined this step as Stage 2 (Figure 3.2C, row 4). The earliest we were able to detect the vYFP signal in the vacuole was after approximately 50 min starvation, and the RFP signal was also seen in the vacuole at this time, which suggested the

degradation of mitochondria in the vacuole lumen. We defined this step as Stage 3 (Figure 3.2C, rows 5 and 6).

3.3.3 Dnm1 is recruited to the degrading mitochondria through its interaction with Atg11

Dnm1 assembles specifically at the sites where mitochondrial fission occurs. Therefore, we next asked whether Dnm1 accumulated on the degrading mitochondria, which were marked by 32-11 dots. Accordingly, we chromosomally tagged Dnm1 with mCherry and examined its localization together with the 32-11 dots. Several Dnm1-mCherry puncta that colocalized with 32-11 dots were seen when mitophagy was induced by nitrogen starvation, and this colocalization occurred on the mitochondrial reticulum, which was marked by Mito-BFP (Figure 3.3A). We also chromosomally tagged Mdv1 and Caf4 with mCherry. Similar to Dnm1-mCherry, both Mdv1-mCherry and Caf4-mCherry were colocalized with 32-11 dots (Figure 3.S2A and B).

Based on these observations, we hypothesized that there were two groups of Dnm1, one of them assembling on the mitochondria destined for degradation in order to promote mitophagy-specific fission, with the other functioning in the normal process of constitutive mitochondrial division. A key question with regard to this first population would be the mechanism through which Dnm1 can be specifically recruited to sites that correspond to mitochondria that are destined for degradation. We hypothesized that Atg32 or Atg11 might be able to interact with Dnm1, Fis1, Mdv1 and/or Caf4. To determine whether Atg32 or Atg11—which we just showed mark this population of mitochondria—played a role in Dnm1 localization, we constructed eight strains expressing different combinations of Atg11, Atg32 and the fission machinery components as BiFC chimeras: VC-Atg11 co-expressed with Dnm1-VN, VN-Atg11 with VC-Fis1, VC-Atg11 with Mdv1-VN, VC-Atg11 with Caf4-VN, VN-Atg32 with Dnm1-VC, VN-Atg32 with VC-Fis1, VN-Atg32 with Mdv1-VC, and VN-Atg32 with Caf4-VC; we used the BiFC

assay to test the interactions of these chimeric pairs. All eight strains were tested in both growing (YPL) and mitophagy-inducing (SD-N) conditions. The fluorescent signal could only be observed in cells expressing VC-Atg11 and Dnm1-VN or VN-Atg11 and VC-Fis1 (Figure 3.S2C). The chimeric constructs were stable and did not change in expression level during the course of the analysis, indicating that the fluorescent signals reflected protein localization rather than changes in protein concentration (Figure 3.S2D).

To extend our analysis, we then examined where the interactions occurred. Therefore, we stained the mitochondria with MitoTracker Red dye and examined the localization of the Atg11-Dnm1 and Atg11-Fis1 dots relative to the organelle. Atg11-Fis1 dots were localized on the mitochondrial reticulum in both growing and starvation conditions (Figure 3.3B). However, in VC-Atg11 Dnm1-VN cells, although Atg11-Dnm1 dots were observed on the mitochondrial reticulum, the mitochondrial morphology was abnormal, which resembled that in *dnm1*Δ cells. It was reported that the BiFC assay allows the detection of weak and transient interactions, but that these interactions are stabilized by the formation of an intact YFP. Thus, we considered that the stabilized binding of VC-Atg11 and Dnm1-VN prevented the free Dnm1, which functions as an oligomer, from participating in the normal process of constitutive mitochondrial fission. Therefore, in order to provide additional free Dnm1 in the cells, we either transformed a plasmid harboring Dnm1-3HA into the VC-Atg11 VN-Dnm1 cells or a plasmid harboring Dnm1-VN into the chromosomally integrated VC-Atg11 cells. In both cases, the mitochondrial morphology was normal and the Atg11-Dnm1 dots were localized on the mitochondrial reticulum (Figure 3.3B).

To further demonstrate the existence of two different populations of Dnm1, one of which interacted with Atg11, we asked whether the localization of Dnm1 was affected when Atg11 or Atg32 was absent. Accordingly, we chromosomally tagged Dnm1 with GFP in wild-type, *atg11*Δ and *atg32*Δ cells, and tracked the mitochondria with a plasmid-driven Mito-RFP. In both growing and nitrogen

starvation conditions, the cellular pattern of Dnm1-GFP and mitochondrial morphology was normal in either *atg11*Δ or *atg32*Δ cells, which suggested that neither Atg11 nor Atg32 would affect the function of the normal mitochondrial fission machinery (Figure 3.S2E). We also noticed that even though many Dnm1-GFP puncta were detected in each cell (Figure 3.S2E), only a few Dnm1-Atg11 interacting dots were formed (Figure 3.3B), which also supported our hypothesis that there were two different population of Dnm1. To directly observe these two groups of Dnm1, we generated a yeast strain with VC-Atg11 and Dnm1-mCherry on the genome and transformed these cells with a plasmid harboring Dnm1-VN. The Dnm1 puncta corresponded to an oligomeric mixture of both Dnm1-mCherry and Dnm1-VN, and as a result all of the Dnm1 puncta showed a mCherry signal; however, only the small population associated with VC-Atg11 also showed a vYFP signal (Figure 3.3C).

A previous report demonstrated that mitochondrial fission happens at the ER-mitochondria contact sites (120). We wondered whether mitophagy-specific fission also occurred at these sites. Accordingly, we co-transformed plasmids containing Mito-BFP and HDEL-DsRed to track the mitochondria and ER, respectively. We found that some of the 32-11 dots were indeed localized at the ER-mitochondria contact sites (Figure 3.4A). Previous work also reported an ERMES (ER-mitochondria encounter structure) complex localized at the ER-mitochondria contact sites (121). This complex includes four proteins: Mmm1 and Mdm12, which are on the ER side, and Mdm10 and Mdm34, which are on the mitochondria side of the complex. We fused mCherry at the C terminus of Mdm12 or Mdm34 in the yeast genome, and observed the localization of these proteins together with the 32-11 dots. We observed the colocalization of 32-11 dots with some of the Mdm12-mCherry and Mdm34-mCherry puncta (Figure 3.4B and C). These observations suggested that the ER, in particular at the ER-mitochondria contact sites, might also participate in mitophagy-specific fission.

3.3.4 The Dnm1-Atg11 interaction is required for mitophagy

Dnm1 contains four domains: GTPase, middle, insert B, and GED (GTPase effector domain) (122). In order to find a Dnm1 mutant that lost its binding to Atg11, we examined the interaction of Dnm1 mutants with Atg11 by the BiFC assay. Almost no interacting dots were observed when the GED (~87 amino acids at the C terminus) was deleted (Figure 3.6A and B), which implied that the GED is required for binding to Atg11. We then made truncations of Dnm1 from the C terminus. The interacting dots were detected when we deleted the last 24 amino acids (Dnm1-VN 24Δ); however, very few fluorescent dots were seen when the last 30 amino acids were absent (Dnm1-VN 30Δ) (Figure 3.6A and B). To verify the observation from the BiFC assay, we carried out protein A affinity isolation with IgG-Sepharose. Protein A-tagged wild-type Dnm1 or the mutant without the last 24 amino acids co-precipitated HA-Atg11; however, the Dnm1 mutant lacking the last 30 amino acids was not able to precipitate this protein (Figure 3.6C).

We hypothesized that the six amino acids (EDQTLA) that exist in Dnm1 24Δ, but not Dnm1 30Δ, might be important for Dnm1 binding to Atg11. Therefore, we made two Dnm1 mutants: Dnm1 4R in which the first four amino acids, EDQT, were substituted with arginine, and Dnm1 5A in which the first five amino acids, EDQTL, were substituted with alanine. We then examined the interaction of these two Dnm1 mutants with Atg11 by the BiFC assay. Interacting dots were detected with wild-type Dnm1, but almost none were seen with the Dnm1 4R or 5A mutants (Figure 3.6D and E). Consistent with this result, protein A-tagged Dnm1 4R or 5A were not able to co-precipitate HA-Atg11 by affinity isolation using IgG-Sepharose (Figure 3.6F). Furthermore, these mutants resulted in a block in mitophagy activity similar to that seen with the complete absence of Dnm1 (Figure 3.S3A).

Even though Dnm1 4R or 5A lost the ability to interact with Atg11, we asked whether these two mutants still retained the normal function of Dnm1. Therefore, we used the plasmid-driven Mito-RFP to determine the

mitochondrial morphology in the presence of the Dnm1 4R or 5A mutant. Mitochondrial morphology was normal in wild-type cells, whereas enlarged mitochondria were seen in *dnm1*Δ cells (Figure 3.S3B). The expression of proteinA-tagged wild-type Dnm1 from the plasmid was able to rescue the defect of mitochondrial fission in *dnm1*Δ cells, whereas neither Dnm1 4R nor 5A could rescue the defect (Figure 3.S3B). We suspected the loss of function of Dnm1 4R or 5A was due to the loss of interaction with Mdv1, Caf4 and/or Fis1. Therefore, we carried out affinity isolation with IgG-Sepharose and found that proteinA-tagged Dnm1 4R or 5A were unable to co-precipitate HA-Mdv1, HA-Caf4, GFP-Fis1 or GFP-Atg32 (Figure 3.S4). Accordingly, we generated additional Dnm1 mutants with single amino acid changes in the interaction domain that we had identified. We found that Dnm1 E728R and D729R, but not Q730R or T731R, had a reduced interaction with Atg11 (Figure 3.7A), but maintained the normal function of Dnm1 with regard to mitochondrial fission, and interaction with Mdv1, Caf4, and Fis1 (Figure 3.S4A, B, and C). In contrast, Dnm1 E728R and D729R were not able to co-precipitate GFP-Atg32, in contrast to Dnm1 Q730R or T731R, in agreement with a role for Atg11 as a scaffold that bridges the interaction between Dnm1 and Atg32 (Figure 3.S4D).

Finally, we asked whether the Dnm1 mutants that lost binding to Atg11 were competent for mitophagy. Therefore, we determined the mitophagy activity of the *dnm1*Δ strain containing empty vector, or vector harboring either wild-type Dnm1, or the single amino acid mutants using the mitoPho8Δ60 assay. The presence of wild-type Dnm1 largely suppressed the mitophagy defect in the *dnm1*Δ mutant strain, and similar results were obtained with the Dnm1 Q730R or T731R mutants. In contrast, the Dnm1 E728R or D729R mutants displayed decreased mitoPho8Δ60 activity (Figure 3.7B). Based on these results, we suggest that the interaction of Dnm1 and Atg11 is required for efficient mitophagy, although we do not yet know if this interaction is direct or is mediated by another protein(s).

3.4 Discussion

Autophagy regulates the degradation of cytoplasmic components and organelles. In nonselective autophagy, the amount of Atg8 controls the size of the autophagosomes (123). In contrast, during selective types of autophagy the phagophore membrane is in close apposition to the cargo, excluding bulk cytoplasm. Thus, partly different mechanisms may be involved in determining curvature of the phagophore, and the ultimate size of the autophagosome. In the cytoplasm-to-vacuole targeting (Cvt) pathway, a biosynthetic route that delivers resident hydrolases to the vacuole, the size of the cargo is relatively small; however, when the primary cargo of the Cvt pathway is overexpressed, it forms a larger complex that is no longer efficiently sequestered (124), indicating that there is a size limit for Cvt vesicle formation. Similarly, size may be an issue for organelles that are destined for degradation, especially for organelles such as mitochondria, which exist largely as an extended, reticular structure. Therefore, it is possible that large organelles need to be divided into smaller pieces in order to be effectively engulfed by phagophores.

Here, we showed that mitochondrial division is important for mitophagy, which leads to the question of how mitochondrial fission participates in this process. If fission and mitophagy occur independently, we could imagine that mitochondrial fission happens constitutively and only the resulting small mitochondrial fragments would be chosen for degradation. In this case, there would be no requirement for a direct connection between the fission complex and the mitophagy machinery. In contrast, if fission and mitophagy occur in a coordinated manner, the mitochondria destined for degradation should be selected first, and then the fission complex would be recruited to drive the separation of these mitochondria from the mitochondrial reticulum. The direct interaction between Atg11 and Dnm1 supports the second model. Therefore, we propose that when mitophagy is induced, Atg32 recruits Atg11 to the degrading mitochondria. Atg11 in turn brings Dnm1 and other mitochondrial fission proteins to these “marked” mitochondria, and promotes their division.

These small fragments of mitochondria are subsequently transported to the PAS where other Atg proteins accumulate, initiating the formation of mitochondria-specific autophagosomes (mitophagosomes).

As a scaffold protein and selective autophagy adaptor, Atg11 binds to a variety of cargo receptors to mediate different types of selective autophagy. For example, Atg11 binds to the Cvt pathway receptor, Atg19, to Atg32 and to Atg36 for cargo selection during the Cvt pathway, mitophagy and pexophagy, respectively (11, 56, 59, 66, 125). Atg11 also interacts with Atg1 and Atg17, which connects the step of cargo selection to the initiation of autophagosome formation (125). Here, we unveil a new role forAtg11: recruiting mitochondrial fission machinery to facilitate mitophagy.

Previous results indicated that Atg32 is evenly distributed on the mitochondria, even in mitophagy-inducing conditions (118). In contrast, the BiFC Atg32-Atg11 interacting pair displayed a punctate pattern on the mitochondrial tubules. We suggest that these dots represent the degrading mitochondria. However, it remains unknown as to how Atg11 recognizes and binds only the Atg32 that marks the organelles, or segments of the organelles, that are to be degraded. Thus, some other factor(s) might determine this very early event in mitophagy.

The degradation of peroxisomes and chloroplasts through autophagy pathways in *Pichia pastoris*, *S. cerevisiae*, *Arabidopsis thaliana* and other organisms have been reported (65, 66, 126, 127). It was also reported that the mitochondrial fission complex (Dnm1, Fis1, Mdv1 and Caf4) controls the fission of peroxisomes in yeast, and peroxisomes and chloroplasts in plants (128-130). Thus, we propose that the mechanism we show in this study (receptor-adaptor-fission complex) may also be relevant in selective pexophagy and chloroplast autophagy.

3.5 Materials and methods

Strains, Media, and Growth Conditions. Yeast strains used in this study

are listed in Table 3.1. Yeast cells were grown in rich (YPD; 1% yeast extract, 2% peptone, and 2% glucose) or synthetic minimal (SMD; 0.67% yeast nitrogen base, 2% glucose, and auxotrophic amino acids and vitamins as needed) media. For mitochondria proliferation, cells were grown in lactate medium (YPL; 1% yeast extract, 2% peptone, and 2% lactic acid) or synthetic minimal medium with lactic acid (SML; 0.67% yeast nitrogen base, 2% lactic acid, and auxotrophic amino acids and vitamins as needed). Mitophagy was induced by shifting the cells to nitrogen starvation medium with glucose (SD-N; 0.17% yeast nitrogen base without ammonium sulfate or amino acids, and 2% glucose).

Plasmids.pMito-RFP(URA) was a gift from Dr. Lois Weisman (University of Michigan). pCuHA-Atg11(416) has been reported previously (59). For pCuHA-Mdv1(416) and pCuHA-Caf4(416), the ORF of *MDV1* and *CAF4* was amplified by PCR from the yeast genome. The HA tag is included in the 5' primer. The resulting PCR products, HAMDV1 and HACAF4, were digested by XmaI and XhoI and ligated into pCu416 (131) to generate pCuHA-Mdv1(416) and pCuHA-Caf4(416). For pCuGFP-Fis1(416), the ORF of *FIS1* was amplified from the yeast genome. The DNA fragment of GFP was ligated into pCu416 cut with SpeI and XmaI and that of *FIS1* after digestion with XmaI and XhoI to generate pCuGFP-Fis1(416). For other plasmids, the DNA fragments of *DNM1-3HA*, *DNM1-VN*, *DNM1-VC* and *DNM1-PA* containing the endogenous promoter of the *DNM1* gene and the *ADH1* terminator were amplified by PCR from the genome of the yeast strains KDM1215, KDM1523, KDM1521 and KDM1247 respectively, and digested with SpeI and KpnI. *DNM1-3HA*, *DNM1-VN* and *DNM1-VC* were ligated into pRS416 to generate pDnm1-3HA(416), pDnm1-VN(416), and pDnm1-VC(416). *DNM1-PA* was ligated into pRS314 to generate pDnm1-PA(314). pDnm1(4R)-VC(416), and pDnm1(5A)-VC(416) were generated by site-directed mutagenesis from pDnm1-VC(416), and pDnm1(4R)-PA(314), pDnm1(5A)-PA(314), pDnm1(E728R)-PA(314), pDnm1(D729R)-PA(314), pDnm1(Q730R)-PA(314),

and pDnm1(T731R)-PA(314) were from pDnm1-PA(314).

Fluorescence Microscopy. For fluorescence microscopy, yeast cells were grown to OD_{600} ~0.6 in YPL or SML media and shifted to SD-N for nitrogen starvation. Samples were then examined by microscopy (Delta Vision, Applied Precision) using a 100x objective and pictures were captured with a CCD camera (CoolSnap HQ; Photometrics). For each microscopy picture, 12 Z-section images were captured with a 0.3-μm distance between two neighboring sections. MitoTracker Red (Invitrogen/Molecular Probes) was used to stain the mitochondria, CellTracker Blue CMAC (Invitrogen/Molecular Probes) to stain the vacuolar lumen, and FM 4-64 (Invitrogen) to stain the vacuolar membrane.

Additional Assays. The mitoPho8Δ60 assay and immunoprecipitation were performed as described previously (59, 78)

3.6 Acknowledgements

This work was supported by grant GM053396 to DJK.

Table 3.1 Yeast strain list

Name	Genotype	Reference
KDM1001	SEY6210 *pho8Δ::TRP1 pho13Δ::LEU2 pRS406-ADH1-COX4-pho8Δ60 RPL7Bp-VN-ATG32::KAN RPL7Bp-VC-ATG11::HIS3*	This study
KDM1002	SEY6210 *pho8Δ::TRP1 pho13Δ::LEU2 pRS406-ADH1-COX4-pho8Δ60 fis1Δ::HIS5*	This study
KDM1006	SEY6210 *pho8Δ::TRP1 pho13Δ::LEU2 pRS406-ADH1-COX4-pho8Δ60 mdv1Δ::HIS5*	This study
KDM1009	SEY6210 *pho8Δ pho13Δ pRS406-ADH1-COX4-pho8Δ60*	This study
KDM1010	SEY6210 *pho8Δ::TRP1 pho13Δ::LEU2 pRS406-ADH1-COX4-pho8Δ60 whi2Δ::HIS5*	This study
KDM1011	SEY6210 *pho8Δ::TRP1 pho13Δ::LEU2 pRS406-ADH1-COX4-pho8Δ60 caf4Δ::KAN*	This study
KDM1012	SEY6210 *pho8Δ::TRP1 pho13Δ::LEU2 pRS406-ADH1-COX4-pho8Δ60 caf4Δ::KAN mdv1Δ::HIS5*	This study
KDM1013	SEY6210 *pho8Δ::TRP1 pho13Δ::LEU2 pRS406-ADH1-COX4-pho8Δ60 dnm1Δ::HIS5*	This study
KDM1014	SEY6210 *pho8Δ pho13Δ pRS406-ADH1-COX4-pho8Δ60 dnm1Δ::HIS5*	This study
KDM1209	SEY6210 *DNM1-GFP::HIS3*	This study
KDM1210	SEY6210 *DNM1-GFP::HIS3 atg11Δ::LEU2*	This study
KDM1236	SEY6210 *DNM1-GFP::HIS3 atg32Δ::LEU2*	This study
KDM1252	SEY6210 *dnm1Δ::LEU2*	This study
KDM1215	SEY6210 *DNM1-3HA::HIS5*	This study
KDM1247	SEY6210 *atg11Δ::LEU2 DNM1-PA::HIS3*	This study
KDM1248	SEY6210 *atg11Δ::LEU2 DNM1(C24Δ)-PA::HIS3*	This study
KDM1249	SEY6210 *atg11Δ::LEU2 DNM1(C30Δ)-PA::HIS3*	This study
KDM1251	SEY6210 *atg11Δ::LEU2 dnm1Δ::HIS5*	This study
KDM1501	SEY6210 *pRPL7b-VN-ATG32::TRP1 RPL7Bp-VC-ATG11::HIS5*	This study
KDM1505	SEY6210 *RPL7Bp-VN-ATG32::TRP1 RPL7Bp-VC-ATG11::HIS5 atg1Δ::LEU2*	This study
KDM1517	SEY6210 *RPL7Bp-VC-ATG11::HIS3*	This study
KDM1519	SEY6210 *RPL7Bp-VN-ATG32::TRP1 ATG9-VC::HIS3*	This study
KDM1520	SEY6210 *RPL7Bp-VC-ATG11::HIS5 OM45-VN::TRP1*	This study
KDM1521	SEY6210 *RPL7Bp-VN-ATG32::TRP1 DNM1-VC::HIS3*	This study
KDM1523	SEY6210 *RPL7Bp-VC-ATG11::HIS5*	This study

	DNM1-VN::TRP1	
KDM1528	SEY6210 *RPL7Bp-VC-ATG11::HIS5 DNM1 (c-100Δ)-VN::TRP1*	This study
KDM1532	SEY6210 *RPL7Bp-VC-ATG11::HIS3 DNM1(C-24Δ)-VN::TRP1*	This study
KDM1533	SEY6210 *RPL7Bp-VC-ATG11::HIS3 DNM1(C-30Δ)-VN::TRP1*	This study
KDM1535	SEY6210 *RPL7Bp-VN-ATG11::TRP1*	This study
KDM1540	SEY6210 *RPL7Bp-VN-ATG32::TRP1 MDV1-VC::HIS3*	This study
KDM1541	SEY6210 *RPL7Bp-VN-ATG32::TRP1 CAF4-VC::HIS3*	This study
KDM1542	SEY6210 *RPL7Bp-VC-ATG11::HIS3 MDV1-VN::TRP1*	This study
KDM1543	SEY6210 *RPL7Bp-VC-ATG11::HIS3 CAF4-VN::TRP1*	This study
KDM1544	SEY6210 *RPL7Bp-VN-ATG32::TRP1 RPL7Bp-VC-FIS1::HIS3*	This study
KDM1545	SEY6210 *RPL7Bp-VN-ATG11::TRP1 RPL7Bp-VC-FIS1::HIS3*	This study
KDM1550	SEY6210 *RPL7Bp-VN-ATG32::KAN RPL7Bp-VC-ATG11::HIS3 DNM1-mCherry::TRP1*	This study
KDM1558	SEY6210 *RPL7Bp-VC-ATG11::HIS3 DNM1-mCherry::TRP1*	This study
KDM1559	SEY6210 *HIS3::RPL7Bp-VN-ATG11-PA::TRP1*	This study
KDM1560	SEY6210 *HIS3::RPL7Bp-VN-ATG11-PA::TRP1 RPL7Bp-VC-ATG32::KAN*	This study
KDM1561	SEY6210 *RPL7Bp-VN-ATG32::KAN RPL7Bp-VC-ATG11::HIS3 MDV1-mCherry::TRP1*	This study
KDM1562	SEY6210 *RPL7Bp-VN-ATG32::KAN RPL7Bp-VC-ATG11::HIS3 CAF4-mCherry::TRP1*	This study
KDM1563	SEY6210 *RPL7Bp-VN-ATG32::KAN RPL7Bp-VC-ATG11::HIS3 MDM12-mCherry::TRP1*	This study
KDM1564	SEY6210 *RPL7Bp-VN-ATG32::KAN RPL7Bp-VC-ATG11::HIS3 MDM34-mCherry::TRP1*	This study
KWY20	SEY6210 *pho8Δ::TRP1 pho13Δ::LEU2 pRS406-ADH1-COX4-pho8Δ60*	(78)
KWY22	SEY6210 *pho8Δ::TRP1 pho13Δ::LEU2 pRS406-ADH1-COX4-pho8Δ60 atg32Δ::KAN*	(78)
SEY6210	MATα *leu2-3,112 ura3-52 his3-Δ200 trp1-Δ901 suc2-Δ9 lys2-801; GAL*	(101)
TKYM22	SEY6210 *OM45-GFP::TRP1*	This study
XLY050	SEY6210 *dnm1Δ::LEU2 atg32Δ::HIS3*	This study

XLY051	SEY6210 *dnm1Δ::LEU2 mdv1Δ::HIS3*	This study
XLY052	SEY6210 *dnm1Δ::LEU2 fis1Δ::HIS3*	This study
XLY053	SEY6210 *dnm1Δ::LEU2 caf4Δ::HIS3*	This study
YTS147	SEY6210 *atg11Δ::LEU2*	(58)

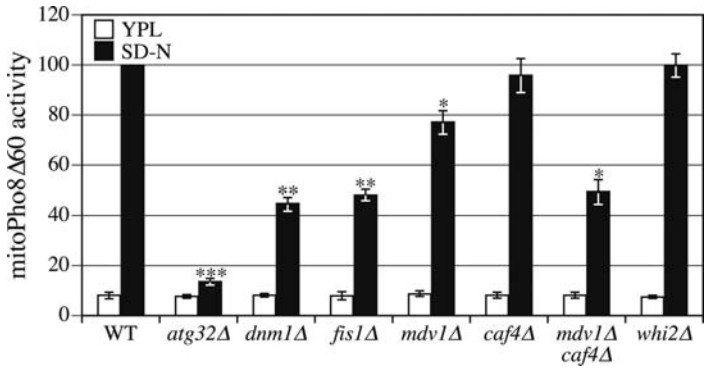

Figure 3.1 Mitochondrial fission is required for mitophagy.
MitoPho8Δ60 activity is reduced in strains with deletions of genes encoding mitochondrial fission proteins. Wild-type (KWY20), *atg32*Δ (KWY22), *dnm1*Δ (KDM1013), *fis1*Δ (KDM1002), *mdv1*Δ (KDM1006), *caf4*Δ (KDM1011), *mdv1*Δ *caf4*Δ (KDM1012) and *whi2*Δ (KDM1010) cells in the mitoPho8Δ60 background were cultured in YPL to mid-log phase, then shifted to SD-N for 6 h. The mitoPho8Δ60 assay was performed as described in Experimental Procedures. Error bars correspond to the standard error, and were obtained from three independent repeats. * $p<0.01$; ** $p<0.001$; *** $p<0.0001$.

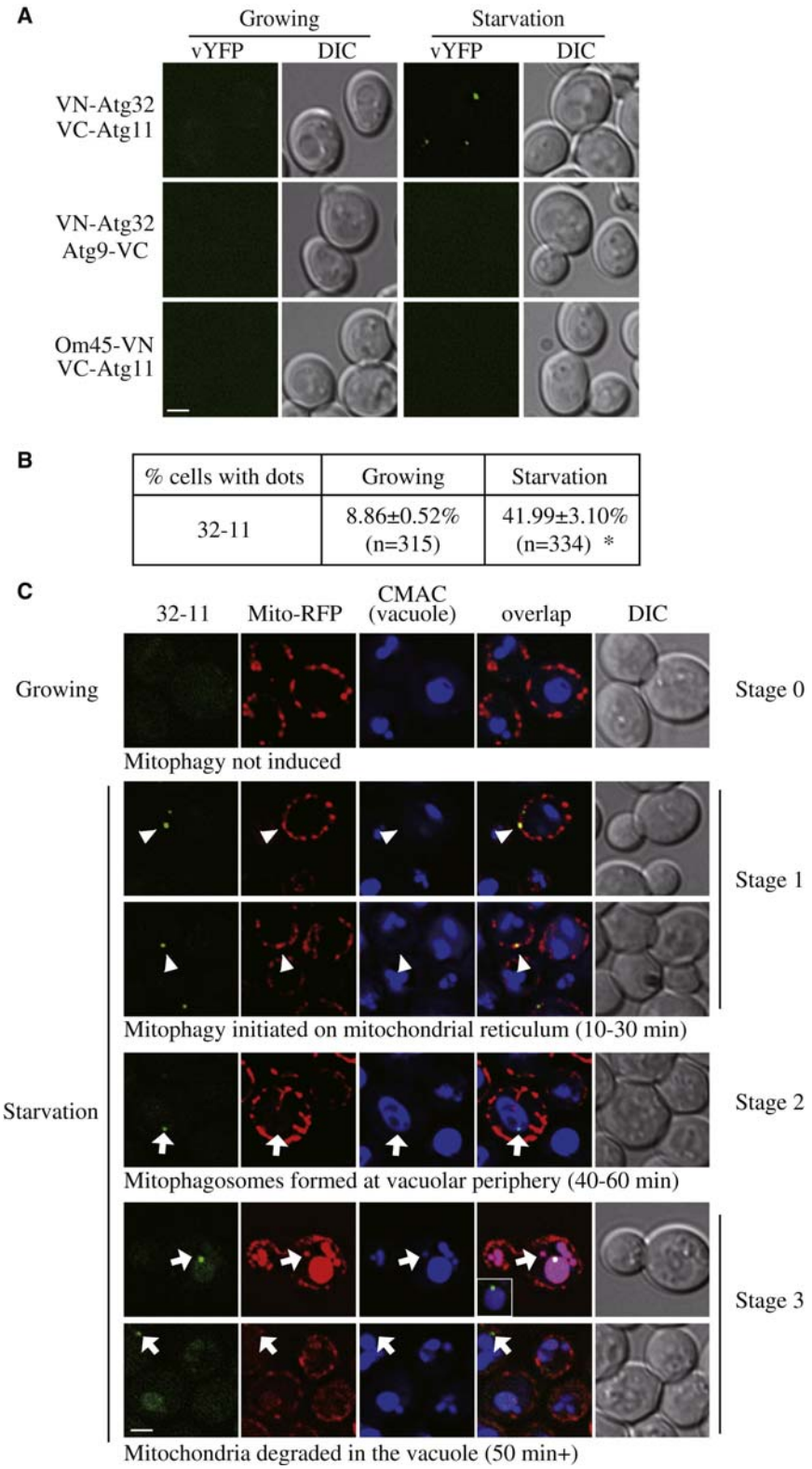

Figure 3.2 BiFC 32-11 dots mark degrading mitochondria during mitophagy.

(A) A BiFC assay was performed for Atg32, Atg11, Om45 and Atg9. Cells containing BiFC pairs (Atg32-Atg11 in KDM1501, Atg32-Atg9 in KDM1519 and Atg11-Om45 in KDM1520) were cultured in YPL and shifted to SD-N for 1 h, followed by analysis by fluorescence microscopy; images are representative

pictures from single Z-sections. DIC, differential interference contrast. Scale bar, 2 μm.
(B) Quantification of (A). 12 Z-section images were projected and the percentage of cells that contained 32-11 dots was determined. Standard error was calculated from three independent experiment. * $p<0.01$.
(C) *VN-ATG32 VC-ATG11* (KDM1501) cells, transformed with pMito-RFP, were cultured in SML and shifted to SD-N from 10 min to 1 h, and the cell samples were observed by fluorescence microscopy. CellTracker Blue CMAC was used to stain the vacuolar lumen. Arrowheads indicate the 32-11 dots that localized on the mitochondrial reticulum; and arrows indicate the 32-11 dots that localized on the vacuolar periphery. All of the images are representative pictures from single Z-sections. DIC, differential interference contrast. Scale bar, 2 μm. The inset in row 5, panel 4 corresponds to the large vacuole, reducing the red intensity to demonstrate that the intravacuolar punctum corresponds to a green 32-11 dot that has not yet been degraded.

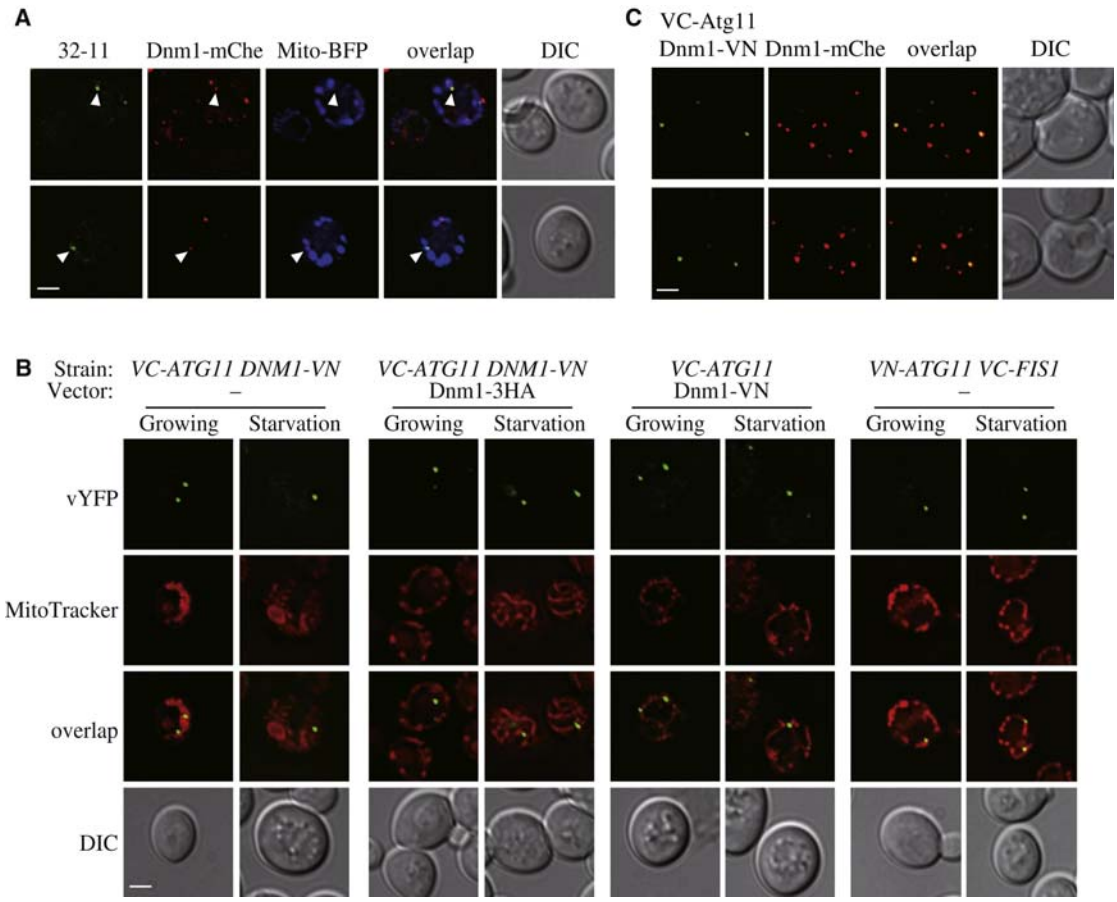

Figure 3.3 Atg11 recruits Dnm1 to the degrading mitochondria.
(A) *VN-ATG32 VC-ATG11 DNM1-mCherry* cells, transformed with pMito-BFP, were cultured in SML and shifted to SD-N for 1 h, and samples were observed by fluorescence microscopy. Arrowheads indicate the colocalized 32-11 dots with Dnm1-mCherry on the mitochondrial reticulum. All of the images are representative pictures from single Z-sections. DIC, differential interference contrast. Scale bar, 2 μm.
(B) *VC-ATG11 DNM1-VN* cells transformed with empty vector or pDnm1-3HA, *VC-ATG11* cells transformed with pDnm1-VN, and *VN-ATG11 VC-FIS1* cells transformed with empty vector were cultured in SML and shifted to SD-N for 1 h. Samples were observed by fluorescence microscopy as in (A). Scale bar, 2 μm.
(C) *VC-ATG11 DNM1-mCherry* cells, transformed with pDnm1-VN, were cultured in SML and shifted to SD-N for 30 min. Samples were observed by fluorescence microscopy as in (A). Scale bar, 2 μm.

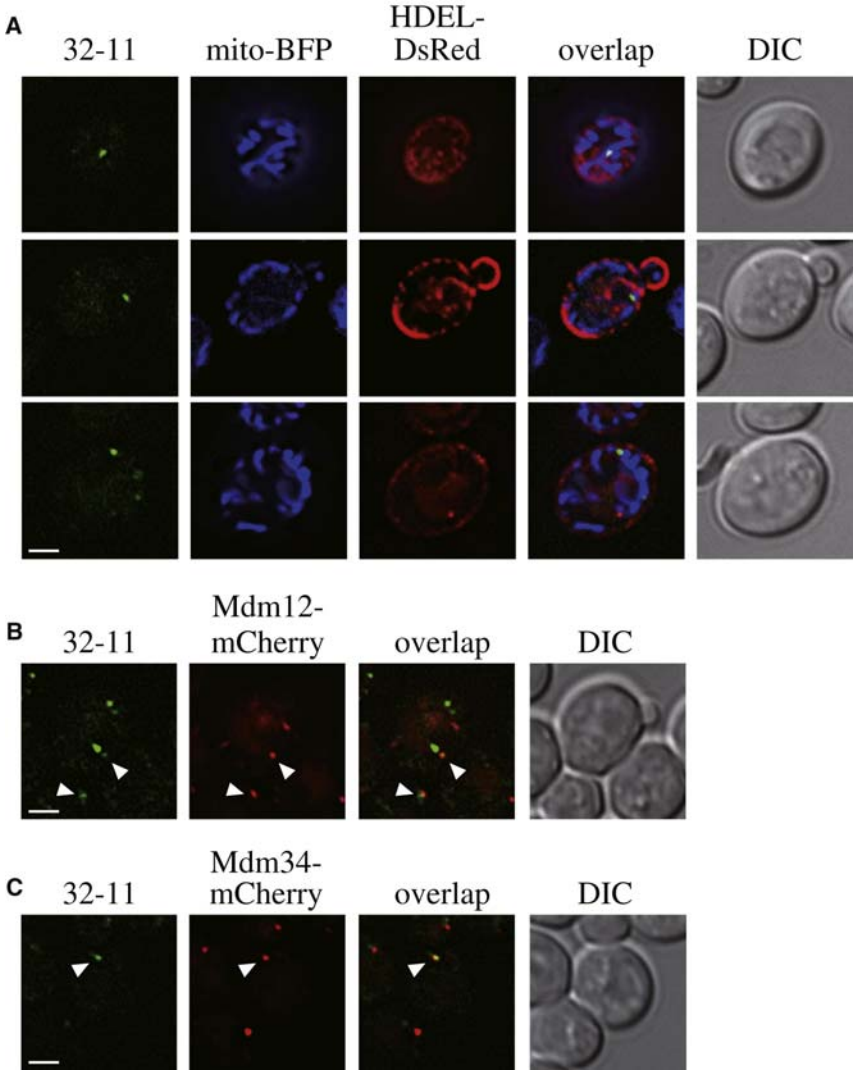

Figure 3.4 The ER participates in mitophagy-specific fission.
(A) *VN-ATG32 VC-ATG11* (KDM1501) cells, transformed with pMito-BFP and pHDEL-DsRed, were cultured in SML and shifted to SD-N for 30 min.
(B, C) *VN-ATG32 VC-ATG11 MDM12-mCherry* (KDM1561) and *VN-ATG32 VC-ATG11 MDM34-mCherry* (KDM1562) cells were cultured in YPL and shifted to SD-N for 30 min. The cells in (A, B, and C) were analyzed by fluorescence microscopy. The images are representative pictures from single Z-sections. DIC, differential interference contrast. Scale bars, 2 μm.

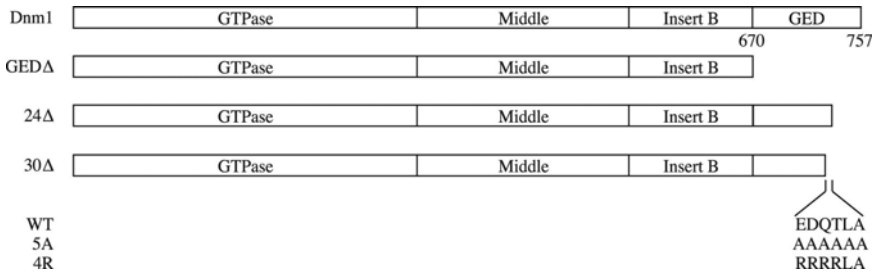

Figure 3.5 Domain structure of Dnm1 and GED mutations.
The domains of Dnm1 are depicted in the top diagram, and the position of the GED domain (amino acids 670-757) are indicated. The C-terminal truncations, GEDΔ, 24Δ and 30Δ are depicted in the middle diagrams. The sequence of the six amino acid residues comprising E728 through A733 in the GED that are required for the interaction with Atg11 and the mutations 5A and 4R are shown at the bottom.

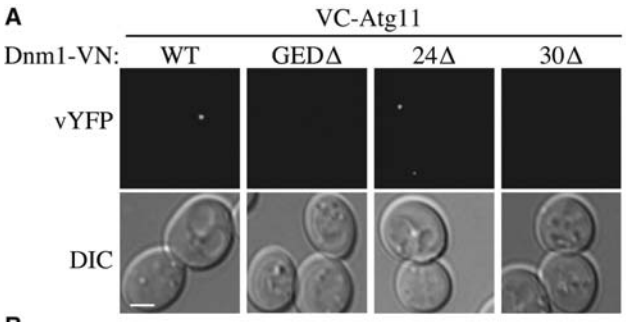

B

% cells with dots	WT	GEDΔ
32-11	37.02±3.38% (n=282)	1.98±0.46% (n=258) *
% cells with dots	24Δ	30Δ
32-11	34.84±3.25% (n=291)	3.80±1.03% (n=299) *

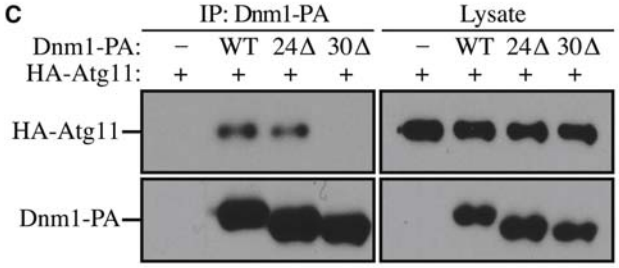

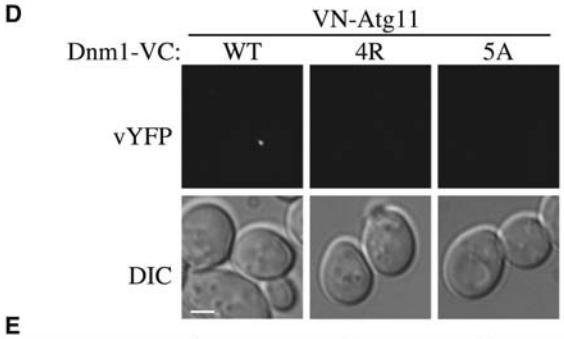

E

% cells with dots	WT	4R	5A
32-11	33.40±3.57% (n=317)	3.32±0.81% (n=279) *	5.89±0.77% (n=272) *

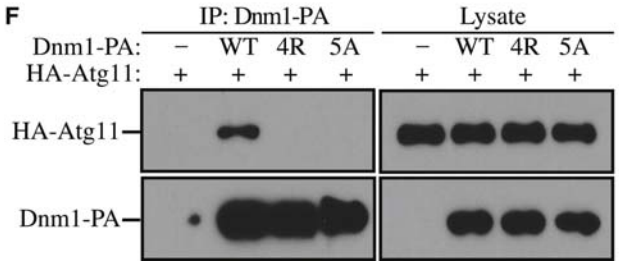

Figure 3.6 Mutation of the Dnm1 C terminus blocks mitophagy.
(A) Cells containing BiFC pairs (Atg11-Dnm1 in KDM1523, Atg11-Dnm1 (GEDΔ) in KDM1528, Atg11-Dnm1 (24Δ) in KDM1532, and Atg11-Dnm1 (30Δ) in KDM1533) were cultured in YPL and shifted to SD-N for 1 h. Samples were

observed by fluorescence microscopy, and all the images are representative pictures from single Z-sections. DIC, differential interference contrast.
(B) Quantification of (A). 12 Z-section images were projected and the percentage of cells that contained BiFC Dnm1-Atg11 dots was determined. Standard error was calculated from three independent experiment. * $p<0.01$.
(C) The plasmid pCuHA-Atg11 was transformed into *atg11*Δ (YTS147), *atg11*Δ *DNM1-PA* (KDM1247), *atg11*Δ *DNM1(24Δ)-PA* (KDM1248), and *atg11*Δ *DNM1(30Δ)* (KDM1249) cells. Cells were cultured in SML and shifted to SD-N for 1.5 h. Cell lysates were prepared and incubated with IgG-Sepharose for affinity isolation as described in Experimental Procedures. The eluted proteins were separated by SDS-PAGE and detected with monoclonal anti-HA antibody and an antibody that binds to PA.
(D) VN-ATG11 (KDM1535) cells, transformed with pDnm1-VC, pDnm1(4R)-VC, or pDnm1(5A)-VC, were cultured in SML and shifted to SD-N for 1 h. Samples were observed by fluorescence microscopy as in (A).
(E) Quantification of (D). 12 Z-section images were projected and the percentage of cells that contained BiFC Dnm1-Atg11 dots was determined. Standard error was calculated from three independent experiment. * $p<0.01$.
(F) The plasmid pCuHA-Atg11 together with pDnm1-VC, pDnm1(4R)-VC, or pDnm1(5A)-VC were transformed into *atg11*Δ *dnm1*Δ (KDM1251) cells. The cells were cultured in SML and shifted to SD-N for 1.5 h. Cell lysates were prepared and analyzed as in (C).

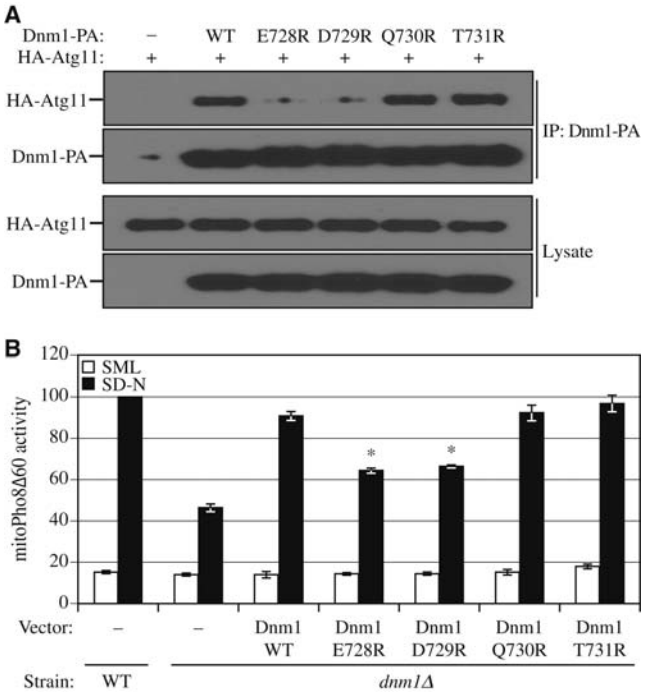

Figure 3.7 Dnm1 mutants that lose binding to Atg11 are mitophagy defective.

(A) The plasmid pCuHA-Atg11 together with pDnm1-PA, pDnm1(E728R)-PA, pDnm1(D729R)-PA, pDnm1(Q730R)-PA, or pDnm1(T731R)-PA was co-transformed into *atg11*Δ *dnm1*Δ (KDM1251) cells. Cells were cultured in SML and shifted to SD-N for 1.5 h. Cell lysates were prepared and incubated with IgG-Sepharose for affinity isolation as described in Experimental Procedures. The eluted proteins were separated by SDS-PAGE and detected with monoclonal anti-HA antibody and an antibody that binds to PA.

(B) MitoPho8Δ60 wild-type (KDM1009) cells were transformed with empty vector; mitoPho8Δ60 *dnm1*Δ (KDM1014) cells were transformed with empty vector, pDnm1-PA, pDnm1(E728R)-PA, pDnm1(D729R)-PA, pDnm1(Q730R)-PA, or pDnm1(T731R)-PA. Cells were cultured in SML to mid-log phase, then shifted to SD-N for 6 h. The mitoPho8Δ60 assay was performed as described in Experimental Procedures. Error bars correspond to the standard error, and were obtained from three independent repeats. * $p<0.01$.

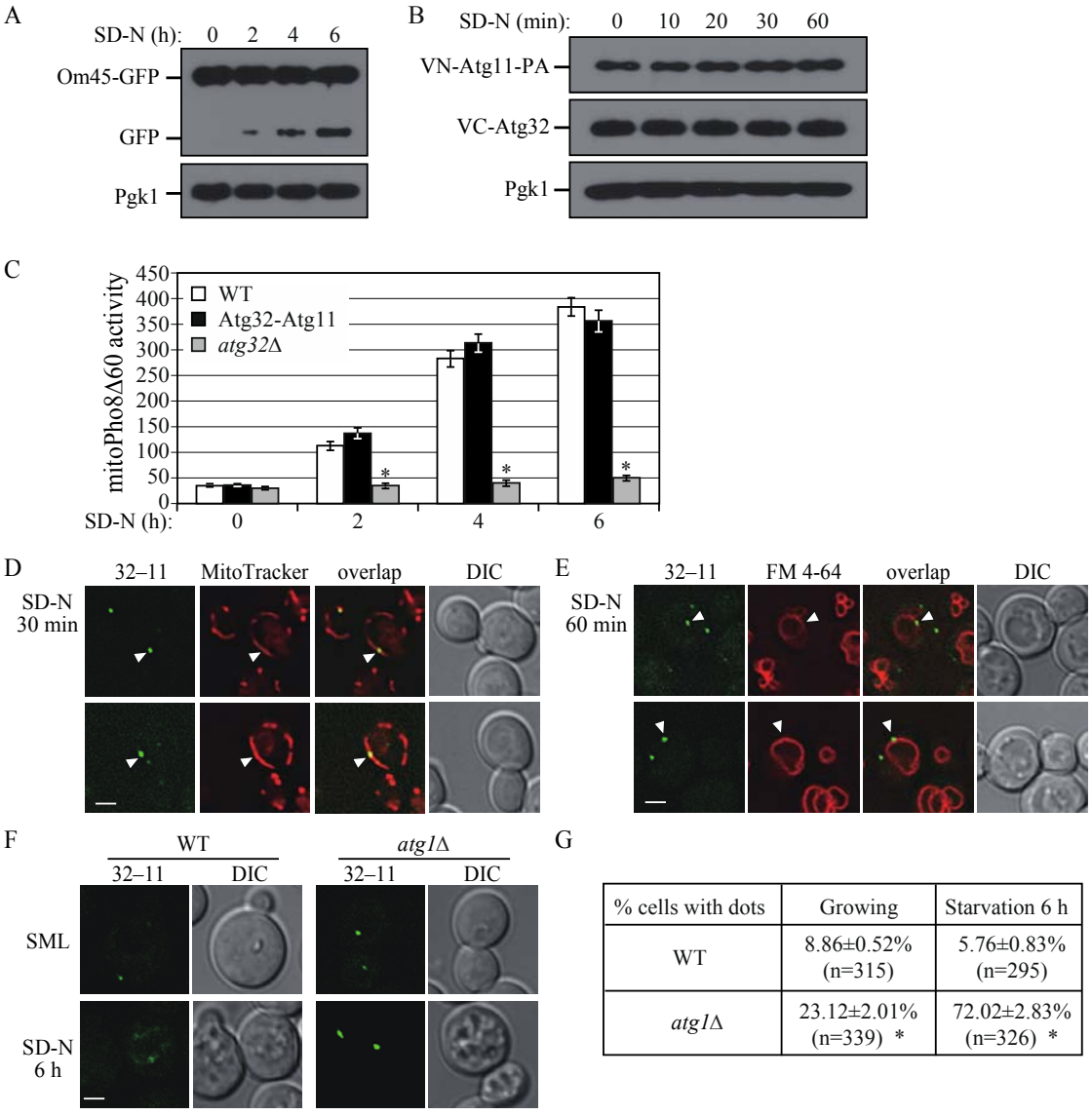

% cells with dots	Growing	Starvation 6 h
WT	8.86±0.52% (n=315)	5.76±0.83% (n=295)
*atg1*Δ	23.12±2.01% (n=339) *	72.02±2.83% (n=326) *

Figure 3.S1 BiFC Atg32-Atg11 puncta mark degrading mitochondria.
(A) Cells with *OM45-GFP* integrated into the genome were cultured in YPL to mid-log phase and shifted to SD-N for 2, 4 and 6 h. Immunoblotting was done with anti-YFP antibody. Only a small part of the total mitochondrial pool, marked b Om45-GFP, is degraded during mitophagy, as measured by the release of free GFP in the vacuole.
(B) *VN-ATG11-PA VC-ATG32* (KDM1560) cells were cultured in YPL and shifted to SD-N from 10 min to 1 h. Immunoblotting was carried out with anti-YFP antibody for VC-Atg32 detection and an antibody that binds to PA for VN-Atg11-PA.
(C) The mitoPho8Δ60 assay was performed in wild-type (KWY20), *atg32*Δ (KWY22) and *VN-ATG32 VC-ATG11* (KDM1001) cells with the indicated times of nitrogen starvation. Error bars correspond to the standard error, and were obtained from three independent repeats. * $p<0.01$.
(D, E) *VN-ATG32 VC-ATG11* (KDM1501) cells were cultured in YPL and

shifted to SD-N for 30 min (D), or 1 h (E). All samples were analyzed by fluorescence microscopy. MitoTracker Red was used to stain the mitochondria in (D) and FM 4-64 to stain the vacuole in (E). Arrowheads indicate the 32-11 dots, which localized on the mitochondrial reticulum (D) or the vacuole membrane (E). All of the images are representative pictures from single Z-sections. DIC, differential interference contrast. Scale bars, 2 μm.
(F) *VN-ATG32 VC-ATG11* (KDM1501) and *VN-ATG32 VC-ATG11 atg1*Δ (KDM1505) cells were cultured in YPL and shifted to SD-N for 6 h. Cell samples were analyzed by fluorescence microscopy. The images are representative pictures from single Z-sections. DIC, differential interference contrast. Scale bar, 2 μm.
(G) Quantification of (F). 12 Z-section images were projected and the percentage of cells that contained 32-11 dots was determined. Standard error was calculated from three independent experiment. * $p<0.01$.

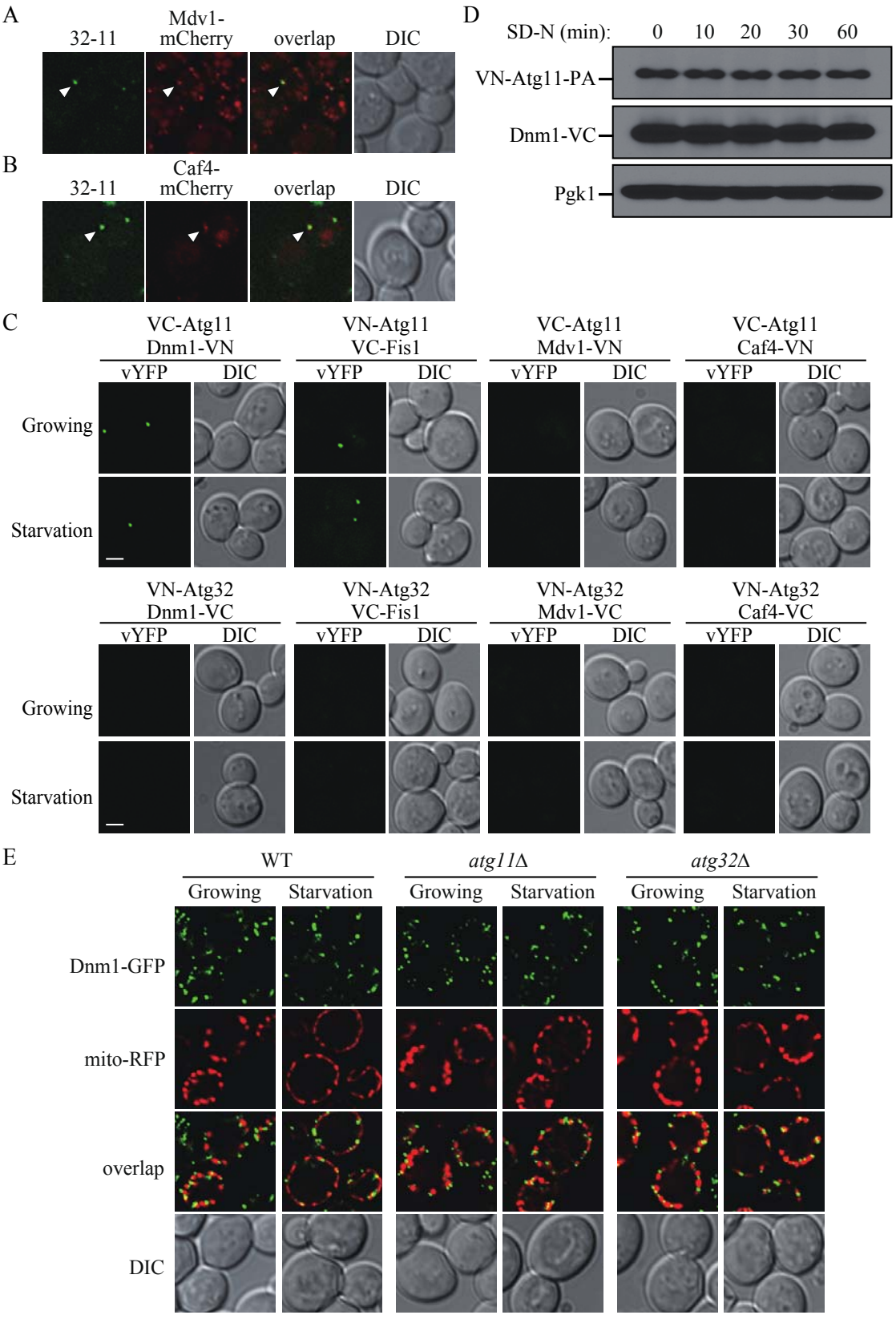

Figure 3.S2 Atg11 interacts with Dnm1.

(A,B) *VN-ATG32 VC-ATG11 MDV1-mCherry* (KDM1561) and *VN-ATG32*

VC-ATG11 CAF4-mCherry (KDM1562) cells were cultured in YPL and shifted to SD-N for 30 min.
(C) A BiFC assay was performed for Atg32, Atg11, Dnm1, Fis1, Mdv1 and Caf4. Cells containing BiFC pairs (Atg11-Dnm1 in KDM1523, Atg11-Fis1 in KDM1545, Atg11-Mdv1 in KDM1542, Atg11-Caf4 in KDM1543, Atg32-Dnm1 in KDM1521, Atg32-Fis1 in KDM1544, Atg32-Mdv1 in KDM1540, and Atg32-Caf4 in KDM1541) were cultured in YPL and shifted to SD-N for 1 h.
The cells in (A, B, and C) were analyzed by fluorescence microscopy. The images are representative pictures from single Z-sections. DIC, differential interference contrast. Scale bar, 2 μm.
(D) *VN-ATG11-PA* (KDM1559) cells, transformed with pDnm1-VC, were cultured in SML and shifted to SD-N from 10 min to 1 h. Immunoblotting was carried out with anti-YFP antibody for Dnm1-VC detection and an antibody that binds to PA for VN-Atg11-PA.
(E) *DNM1-GFP* wild-type (KDM1209), *atg11*Δ (KDM1210), and *atg32*Δ (KDM1236) cells, transformed with pMito-RFP, were cultured in SML and shifted to SD-N for 30 min. The cells were analyzed by fluorescence microscopy as in (A).

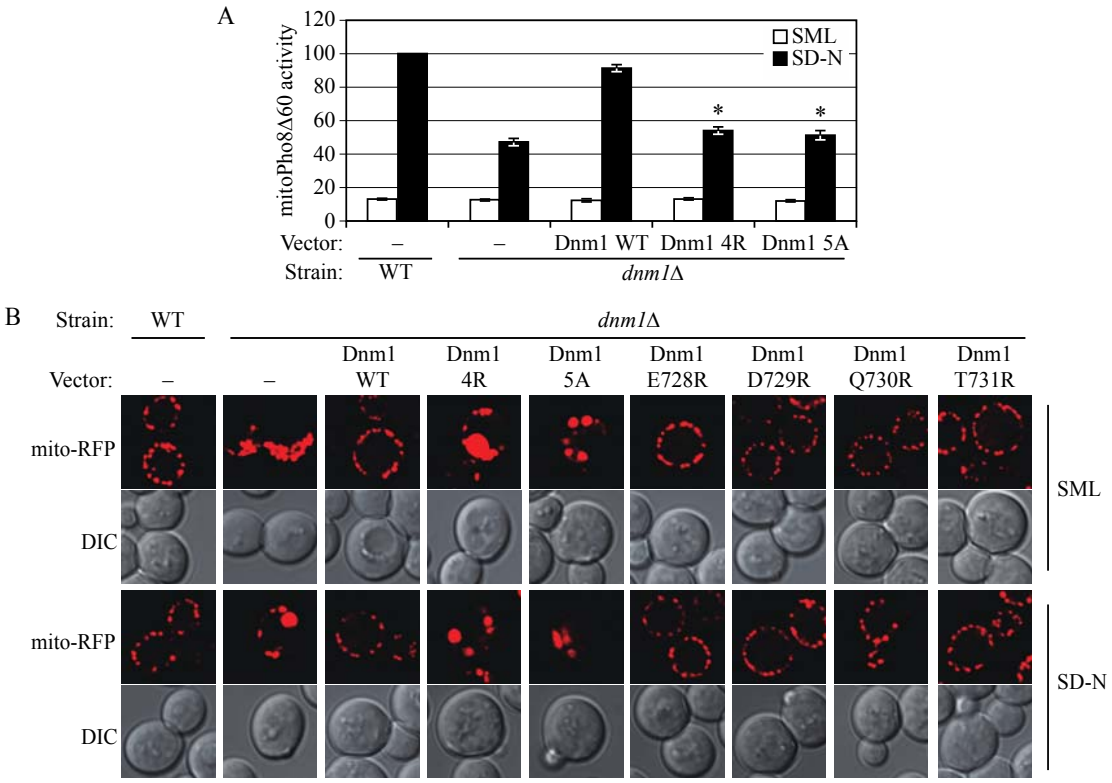

Figure 3.S3 Dnm1 4R and Dnm1 5A result in defective mitophagy and mitochondrial morphology.

(A) MitoPho8Δ60 wild-type (KDM1009) cells were transformed with empty vector; mitoPho8Δ60 *dnm1*Δ (KDM1014) cells were transformed with empty vector, pDnm1-PA, pDnm1(4R)-PA, or pDnm1(5A)-PA. The mitoPho8Δ60 assay was performed as described in Experimental Procedures. Error bars correspond to the standard error, and were obtained from three independent repeats. * $p<0.01$.

(B) Wild-type (SEY6210) cells were co-transformed with pMito-RFP and empty vector, and *dnm1Δ* (KDM1252) cells with pMito-RFP and empty vector, pDnm1-PA, pDnm1(4R)-PA, pDnm1(5A)-PA, pDnm1(E728R)-PA, pDnm1(D729R)-PA, pDnm1(Q730R)-PA, or pDnm1(T731R)-PA. Cells were cultured in SML and shifted to SD-N for 1 h. Samples were observed by fluorescence microscopy, and all the images are representative pictures from single Z-sections. DIC, differential interference contrast.

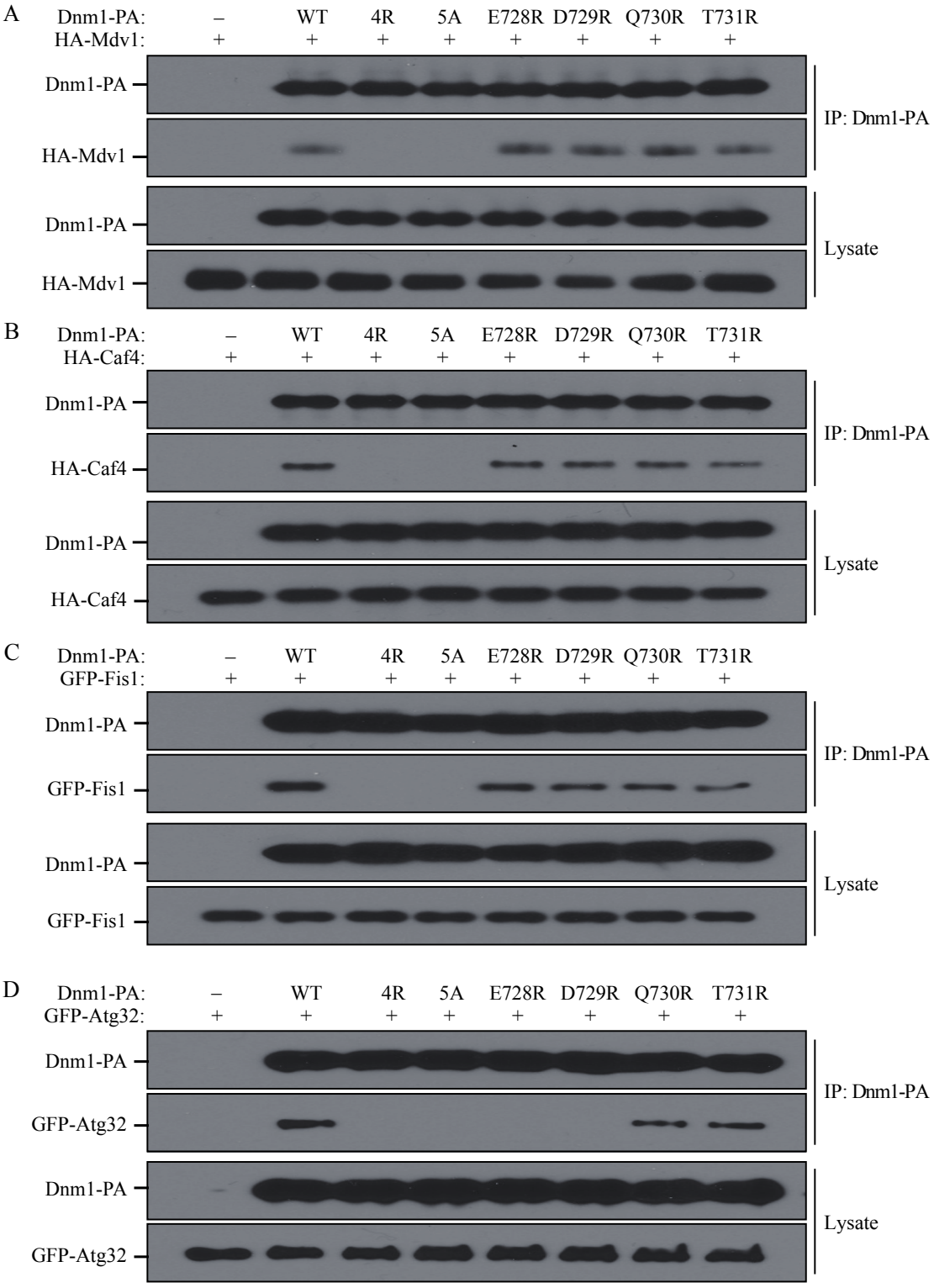

Figure 3.S4 Co-immunoprecipitation analysis of Dnm1 mutants.
Cells were cultured in SML and shifted to SD-N for 1.5 h. Cell lysates were prepared and incubated with IgG-Sepharose for affinity isolation as described in Experimental Procedures. The eluted proteins were separated by SDS-PAGE and detected with monoclonal anti-HA antibody, monoclonal

anti-YFP antibody and an antibody that binds to PA.
(A) The plasmid pCuHA-Mdv1 together with empty vector, pDnm1-PA, pDnm1(4R)-PA, pDnm1(5A)-PA, pDnm1(E728R)-PA, pDnm1(D729R)-PA, pDnm1(Q730R)-PA, or pDnm1(T731R)-PA was co-transformed into *mdv1*Δ *dnm1*Δ (XLY051) cells.
(B) The plasmid pCuHA-Caf4 together with empty vector, pDnm1-PA, pDnm1(4R)-PA, pDnm1(5A)-PA, pDnm1(E728R)-PA, pDnm1(D729R)-PA, pDnm1(Q730R)-PA, or pDnm1(T731R)-PA was co-transformed into *caf4*Δ *dnm1*Δ (XLY053) cells.
(C) The plasmid pCuGFP-Fis1 together with empty vector, pDnm1-PA, pDnm1(4R)-PA, pDnm1(5A)-PA, pDnm1(E728R)-PA, pDnm1(D729R)-PA, pDnm1(Q730R)-PA, or pDnm1(T731R)-PA was co-transformed into *fis1*Δ *dnm1*Δ (XLY052) cells.
(D) The plasmid pCuGFP-Atg32 together with empty vector, pDnm1-PA, pDnm1(4R)-PA, pDnm1(5A)-PA, pDnm1(E728R)-PA, pDnm1(D729R)-PA, pDnm1(Q730R)-PA, or pDnm1(T731R)-PA was co-transformed into *atg32*Δ *dnm1*Δ (XLY050) cells.

Chapter 4

Atg29 phosphorylation regulates coordination of the Atg17-Atg31-Atg29 complex with the Atg11 scaffold during autophagy initiation[3]

4.1 Abstract

Macroautophagy (hereafter autophagy) functions in the nonselective clearance of cytoplasm. This process participates in many aspects of cell physiology, and is conserved in all eukaryotes. Autophagy begins with the organization of the phagophore assembly site (PAS), where most of the AuTophaGy-related (Atg) proteins are at least transiently localized. Autophagy occurs at a basal level, and can be induced by various types of stress; the process must be tightly regulated because insufficient or excessive autophagy can be deleterious. A complex composed of Atg17-Atg31-Atg29 is vital for PAS organization and autophagy induction, implying a significant role in autophagy regulation. In this study, we demonstrate that Atg29 is a phosphorylated protein and that this modification is critical to its function; alanine substitution at the phosphorylation sites blocks its interaction with the scaffold protein Atg11, and its ability to facilitate assembly of the PAS. Atg29 has the characteristics of an intrinsically disordered protein, suggesting that it undergoes dynamic conformational changes upon interaction with a binding partner(s). Finally, single-particle electron microscopy analysis of the Atg17-Atg31-Atg29 complex reveals an elongated structure with Atg29 located at the opposing ends.

4.2 Introduction

Autophagy is the major lysosome/vacuole-dependent cellular degradative

---

3 Originally published in *PNAS* (2013; 110(31):E2875-84) with authors listed as Kai Mao, Leon H. Chew, Yuko Inoue, Heesun Cheong, Usha Nair, Hana Popelka, Calvin K. Yip and Daniel J. Klionsky.

pathway. During autophagy, cytoplasmic constituents including proteins, lipids and even entire organelles, are surrounded by the phagophore, the initial sequestering compartment. The phagophore then expands to form double-membrane vesicles, termed autophagosomes. The completed autophagosomes fuse with lysosomes/vacuoles allowing access of the cargo to the degradative enzymes within this organelle; the resulting breakdown products are released back into the cytosol as building blocks or catabolic substrates (47, 132, 133). Autophagy is not only critical for survival upon nutrient deprivation, but is also involved in various human pathophysiologies, including cancer and neurodegeneration (48).

Upon autophagy induction, Atg proteins accumulate at the PAS and initiate autophagosome formation. Among the 36 known Atg proteins, Atg1 is the only kinase, and it plays a particularly important role in autophagy induction by controlling the movement of other Atg proteins including Atg9 and Atg23 (7), and in the proper organization of the PAS (8, 9). Atg1 interacts with several proteins, including direct binding to Atg13 (which interacts with Atg17) and Atg11; the kinase activity of Atg1 is regulated in part by its binding to, and/or interaction with, some of these components (10, 11).

Atg17 constitutively forms a stable protein complex with Atg29 and Atg31 in both growing and nitrogen starvation conditions (12), and Atg31 directly interacts with Atg17 and Atg29 to bridge these two proteins (13). When autophagy is initiated, the Atg17-Atg31-Atg29 complex is first targeted to the PAS and recruits other Atg proteins, including Atg1 and Atg13, highlighting the significance of the ternary complex (15, 16). Along these lines, a single deletion of the *ATG17*, *ATG29*, or *ATG31* genes results in a dramatic decrease in autophagy activity (134-136).

In this study, we examined the role of posttranslational modification of Atg29. We found that Atg29 is a phosphoprotein, and that phosphorylation on the C-terminal domain is critical for autophagy activity; the N terminus of Atg29 contains the functional domain, whereas the C terminus plays a regulatory role.

We continued and extended our study to include a structural and functional analysis of the Atg17-Atg31-Atg29 complex. Single-particle electron microscopy reveals that the recombinant Atg17-Atg31-Atg29 complex is present as an elongated “S”-shaped dimerized structure, with Atg17 forming the backbone. We further demonstrate that Atg29 has the characteristics of an intrinsically disordered protein (IDP), suggesting that the C-terminal half is flexible and capable of altering its conformation upon binding to one or more interacting proteins. Finally, we determined that Atg11 is necessary and sufficient to recruit this complex to the PAS, and that phosphorylation of Atg29 is required for its interaction with Atg11 and proper PAS localization.

4.3 Results

4.3.1 Atg29 is a phosphoprotein

The activity of Atg1 kinase is regulated in part by various binding partners (10, 137). For example, Atg13 is critical for Atg1 kinase activity, and Atg13 function is regulated through phosphorylation (92, 138, 139). Similarly, a stable ternary complex composed of Atg17, Atg29 and Atg31 also interacts with the Atg1 kinase complex (16, 134); while the function of the Atg17-Atg31-Atg29 complex is not known, the absence of any of these proteins results in a substantial decrease in autophagy activity, suggesting that, similar to Atg13, they affect Atg1 kinase activity. Atg31 is a phosphoprotein (12), but the functional significance of its phosphorylation has not been demonstrated. To gain further insight into the mechanism of regulation of the Atg1 kinase complex, we decided to examine the phosphorylation status of Atg29. Following a shift from nutrient-rich to nitrogen starvation conditions, we noted that protein A (PA)-tagged Atg29 migrated as multiple bands (Figure 4.1A). The highest molecular mass corresponded to an apparent increase of ~9 to 10 kDa. To determine whether the reduced migration corresponded to phosphorylation, we performed a phosphatase treatment. Cells expressing Atg29-PA were shifted to starvation conditions,

and lysates were generated. Treatment of cell lysates with λ protein phosphatase resulted in a collapse of the multiple bands to a single, lower mass band, whereas phosphatase treatment combined with phosphatase inhibitor resulted in a migration pattern that appeared similar to lysates without treatment (Figure 4.1A). These data suggest that Atg29 is a phosphorylated protein, and that phosphorylation, as assessed by SDS-PAGE, occurs when autophagy is induced.

To identify phosphorylation sites in Atg29 that affect autophagy activity, we generated several truncated forms of Atg29 and examined their migration pattern. All of the Atg29 constructs displayed multiple bands except for one construct that contained the N-terminal half of the protein, Atg29[1-100] (Figure 4.1B). This finding suggested that most of the phosphorylated sites of Atg29, or at least those that contribute to the molecular mass shift detected by SDS-PAGE, are in the C terminus (amino acids 101-213), but not the N terminus (amino acids 1-100).

4.3.2 The N-terminal domain of Atg29 is functional

Considering that the two halves of Atg29 displayed different migration/phosphorylation characteristics, we decided to separately examine the two parts of the protein for their ability to complement the autophagy defect of the *atg29*Δ strain. The C terminus of Atg29 expressed by itself was unstable, whereas the N-terminal half of the protein displayed essentially normal stability (Figure 4.1B). Therefore, we transformed the *atg29*Δ strain with a plasmid encoding either wild-type Atg29 or Atg29[1-100], or with the empty vector, and monitored autophagy activity using the Pho8Δ60 assay (81). In brief, Pho8Δ60 is a truncated version of vacuolar alkaline phosphatase that lacks the N-terminal transmembrane domain. As a result of this deletion, Pho8Δ60 cannot enter the endoplasmic reticulum and remains in the cytosol, where is serves as a non-selective cargo for autophagy. Pho8Δ60-dependent alkaline phosphatase activity thus provides a quantitative readout for autophagy

activity. The *atg29*Δ strain (*atg29*Δ with empty vector) displayed a significant block in autophagy activity under starvation conditions (Figure 4.2A), in agreement with previous data (135), whereas transformation with the plasmid expressing wild-type Atg29 or the N-terminal half of the protein, Atg29[1-100], restored the autophagy activity to approximately 80% of that seen in wild-type cells transformed with empty vector.

Thus, Atg29[1-100] largely suppressed the autophagy defect of the *atg29*Δ mutant. Atg29 is associated with Atg17 and Atg31 though direct interaction with the latter (13). To further investigate the functionality of the N-terminal half of Atg29 we asked whether Atg29[1-100] retained the ability to associate with Atg31. Accordingly, we transformed the *atg29*Δ strain with plasmids encoding Atg29-PA and Atg31-GFP, and carried out protein A affinity isolation with IgG-Sepharose. Both protein A-tagged wild-type Atg29 and Atg29[1-100] co-precipitated Atg31-GFP (Figure 4.2B). Therefore, we conclude that the N terminus of Atg29 constitutes a functional domain (Figure 4.2C).

4.3.3 The C terminus of Atg29 plays a regulatory role

Since the N-terminal domain of Atg29 is able to complement the *atg29*Δ strain with regard to autophagy activity, we hypothesized that the C-terminal domain containing multiple phosphorylation sites plays a regulatory role. The C terminus of Atg29 contains 23 serine or threonine residues. Individual mutations of serine or threonine to alanine had no significant effect on Atg29 function, and deletions of individual genes encoding kinases did not completely eliminate phosphorylation. Because the number of possible permutations of kinase deletions is quite large, and the number of potential mutation combinations in Atg29 phosphorylation sites makes systematic mutagenesis analysis impractical, we mutated all of these sites to alanine to generate Atg29[23STA]. This mutant migrated as a single lower mass band during SDS-PAGE when extracts were prepared from cells in either growing or

nitrogen-starvation conditions (Figure 4.2D). We then carried out a Pho8Δ60 assay to assess the functionality of this construct. Atg29[23STA] was completely unable to complement the autophagy defect of the *atg29*Δ strain (Figure 4.2A). The *atg29*Δ strain displays approximately 40% of the autophagy activity of the wild-type strain. Therefore, for ease of comparison to the mutant constructs, we set the Pho8Δ60 activity of the *atg29*Δ strain expressing wild-type Atg29 to 100% and that of the *atg29*Δ strain expressing empty vector to 0, and normalized the results with the other forms of Atg29 as shown in Figure 4.2E. The result with the Atg29[23STA] mutant indicated that the phosphorylation of Atg29 at its C terminus is crucial for activity. Furthermore, considering that the N-terminal half of Atg29 is able to complement the null strain for autophagy activity, these data suggest that the C terminus, or some portion of it, constitutes a negative regulatory domain (Figure 4.2C).

During the course of mapping the phosphorylation sites in Atg29, we generated a series of C-terminal truncations (Figure 4.1B). We began to systematically combine these truncations with the Atg29[23STA] construct to define a domain that no longer inhibited the function of the N terminus. The C-terminal 11 amino acids of Atg29 (residues 203-213) lack any potential phosphorylation sites, and Atg29[1-202] retained ~90% of the Pho8Δ60 activity of the wild-type protein (Figure 4.2A and E). When the truncation of the extreme C-terminal 11 amino acids was combined with the non-phosphorylable mutant, which by itself lacked autophagy activity, the double mutant construct Atg29[1-202/23STA] displayed ~80% of the Pho8Δ60 activity of the wild type (Figure 4.2A and E). Therefore, we conclude that the last 11 amino acids play a negative role in Atg29 function, indicating that the extreme C terminus of Atg29 acts as an inhibitory peptide (Figure 4.2C). The observation that the truncation of the extreme C terminus restores function to Atg29[23STA] suggests that at least one function of phosphorylation is to alter the conformation of Atg29 such that the inhibitory peptide is displaced, presumably altering its interaction with another component of the Atg1 kinase

complex.

4.3.4 Residues adjacent to the inhibitory peptide are important in Atg29 function

Of the 23 serine and threonine residues in the C-terminal half of Atg29, the last three serines (S197, S199, and S201) are very close to the inhibitory peptide. Therefore, we proposed that these residues would have a particularly important role in Atg29 function. Accordingly, we mutated S197, S199 and S201 to alanine to generate Atg29[3SA]. We also generated the complementary construct by mutating the first 20 serines and threonines to alanine to generate Atg29[20STA] in which the last three potential phosphorylation sites were left unchanged. In contrast to Atg29[23STA], which displayed essentially no Pho8Δ60 activity, Atg29[20STA] retained ~65% of the activity of wild-type Atg29, which was presumably due to phosphorylation of one or more of the last three serines (Figure 4.3A and B). Along these lines, mutation of only the last three serine residues had an even stronger effect, as Atg29[3SA] only exhibited ~45% of the Pho8Δ60 activity of the wild type (Figure 4.3A and B). These results suggest that the phosphorylation of the last three serines plays a particularly important role for Atg29 function.

To extend our analysis of the serines at positions 197, 199 and 201 of Atg29, we made phosphomimetic mutants, Atg29[3SD] or Atg29[3SE] by substituting them with either aspartic acid or glutamic acid, and examined the effect with regard to autophagy activity. Both Atg29[3SD] and Atg29[3SE] retained ~80% of the wild-type activity (Figure 4.3A and C), indicating that the phosphomimetic mutants functioned similar to wild-type Atg29. Even in the context of the Atg29 mutant where the remainder of the C-terminal sites could not be phosphorylated (i.e., Atg29[20STA]), the phosphomimetic mutants (Atg29[20STA/3SD] or Atg29[(20STA/3SE]) retained ~80% of the wild-type Atg29 activity (Figure 4.3A and C). Together, these data suggest that phosphorylation of multiple residues of the Atg29 C terminus results in a

mass-action effect that alters the conformation of the inhibitory peptide with respect to Atg29 (i.e., auto-inhibition) or another component of the Atg1 kinase complex.

4.3.5 Atg29 is an intrinsically disordered protein

The results of the above analysis indicate that Atg29 undergoes significant conformational changes upon phosphorylation. This behavior is not unusual for a large group of functional proteins that are either entirely disordered or contain long disordered domains under physiological conditions. These polypeptides are referred to as intrinsically disordered proteins (140-143). Since IDPs can clearly be discriminated from the group of globular proteins that gain a fixed rigid 3D structure in solution, we examined whether or not Atg29 is an IDP.

The presence of long disordered regions makes IDPs very sensitive to proteolytic cleavage, and disordered regions correspond to missing electron density in protein structures (141). The ribbon model of Atg29 that was obtained as part of the crystal structure of the Atg17-Atg31-Atg29 complex (144), lacks the C-terminal half of the protein, due to sensitivity to proteolytic cleavage. Furthermore, from the 79 residues that were used in the attempted crystallization, residues 41-50 are missing and 51-79 could not be assigned to specific amino acids. These results indicate that Atg29 is a solvent-accessible polypeptide with a high degree of mobility that leads to noncoherent X-ray scattering, making flexible atoms unobservable or hard to distinguish.

Unfoldedness of IDPs is encoded in their amino acid sequence (140-142). We carried out a disorder prediction for Atg29 (Figure 4.4B) using IUPred, an algorithm that evaluates the tendency for intrinsic disorder based on the observation that globular proteins have an ordered structure that is stabilized by a large number of inter-residue interactions, whereas intrinsically disordered proteins possess an amino acid composition that does not allow these interactions (145). IDPs contain random coil domains of at least 40

consecutive amino acid residues (141). The IUPred analysis predicts that only the first half of Atg29, up to Ser96, is structured, while the remaining part of Atg29 (>100 amino acids including the entire C terminus) is disordered when the protein is present alone in solution. However, in the presence of a structured binding partner, this domain may undergo a disorder-to-order transition. The ANCHOR predictor (146) identifies small hydrophobic domains present within disordered regions; these domains are too small to favor intramolecular interactions (i.e., aggregation), but facilitate intermolecular binding, whereas the disordered regions themselves are generally low in binding capacity. The residues Ile, Leu, Phe and Val tend to predominate in these short ordered regions in small -helical linear motifs. Analysis using this algorithm revealed a high probability for disordered binding regions in the regulatory domain Figure 4.4B). In this regard it is noteworthy that the inhibitory peptide at the very C terminus of Atg29 was identified as the longest disordered binding region and exhibited the highest binding tendency, in agreement with its proposed regulatory role involving interaction with another component of the Atg1 kinase complex.

A very typical characteristic of IDPs is their special position in the CH plot given by a combination of their low mean hydrophobicity <H> and high mean net charge <R> (140, 141). Atg29 occupies the same area in the CH plot as known IDPs such as Sic1 (147); Figure 4.S1B].

Since disorder propensity is embedded directly in the amino acid sequence, it follows that IDPs in the DisProt database (148) are depleted in rigid, order-promoting residues and enriched in flexible, disorder-promoting residues (142). Compositional profiler (149) in Figure 4.4D shows that Atg29 has an amino acid composition similar to IDPs in the DisProt database (Figure 4B).

Another feature that Atg29 shares with IDPs is its anomalous migration during SDS-PAGE (Figure 4C). The molecular mass of Atg29 calculated from its amino acid sequence is 24.7 kDa. With the 17-kDa MOCR purification tag

(see Materials and Methods), the expressed and purified Atg29 migrated as an ~48-kDa protein, and with the 10-kDa PA tag, the molecular mass of the Atg29-PA fusion protein in yeast was ~45 kDa. Untagged Atg29 purified from *E. coli* appeared to be 31- to 35-kDa (Figure 4.5A). Thus, Atg29 migrates at a molecular mass approximately 8.3 kDa larger than predicted. This type of aberrant migration typically results from poor interaction of the protein with SDS due to a higher content of charged amino acid residues compared to globular proteins (150). Taken together, these data suggest that Atg29 is an IDP.

4.3.6 Single-particle electron microscopy analysis of the Atg17-Atg31-Atg29 Complex

Atg29 exists in a stable protein complex that also contains Atg17 and Atg31. To better understand the structure and function of Atg29, we carried out negative stain single-particle electron microscopy (EM) analysis. Coomassie Blue-stained SDS-PAGE analysis confirmed that the ternary complex purified using the previously published procedure contained stoichiometric quantities of Atg17, Atg31, and Atg29 (Figure 4.5A) (12). Next, negative stained specimens were prepared by adsorbing purified Atg17-Atg31-Atg29 to glow discharged carbon-coated EM grids and staining with uranyl formate. Initial images obtained for these specimens revealed that the purified complex was relatively homogeneous and had an elongated shape (Figure 4.5A).

To gain further insights into the structural features of the Atg17-Atg31-Atg29 complex, we selected a total of 6,788 particles from the raw images, and subjected these particle images to reference-free alignment and classification. The gallery of average images revealed that Atg17-Atg31-Atg29 contained a backbone that had an overall shape resembling a stretched out letter “S”, with two circular domains attached to opposite “ends” (Figure 4.5B). These averages also showed that

Atg17-Atg31-Atg29 is dimeric, with the two-fold symmetry axis located at the center of the complex. The observed stoichiometry is in agreement with yeast two-hybrid studies, which showed that Atg17 self-associates (134), and with recent analytical ultracentrifugation experiments, which showed that Atg17 forms a 2:2:2 complex with Atg29 and Atg31 (12). The overall architecture of this complex resembles the recently determined crystal structure of the *Lachancea thermotolerans* Atg17-Atg31-Atg29 core complex (144), suggesting that the *S. cerevisiae* complex has a similar subunit organization as the *L. thermotolerans* complex. In other words, *S. cerevisiae* Atg17 forms the backbone while Atg31 and Atg29 constitute the terminal globular domains.

The crystallized complex, however, lacks more than 100 C-terminal residues of Atg29, the domain that we determined was subject to regulatory phosphorylation and that contains the C-terminal inhibitory peptide, whereas the *S. cerevisiae* complex we analyzed contains full-length components. To localize the Atg29 C-terminal domain, a difference mapping approach was implemented. This approach involves generating a series of 2D projections corresponding to different views of the high-resolution model and then experimentally determining the projection that correlates best with a representative 2D average obtained for the *S. cerevisiae* complex. Next, a difference image was calculated by subtracting the identified 2D projection from the experimental 2D average. Strong difference densities adjacent to each of the two globular domains were observed, suggesting that the C-terminal domains of Atg29 may be projecting away from these domains (Figure 4.5C). The two weaker densities were also located on opposite ends of the complex, but these could be attributed to flattening of the particle by the negative staining procedure, leading to a slight extension to its overall length (Figure 4.5C).

The recombinant Atg17-Atg31-Atg29 complex that we structurally characterized is non-phosphorylated and presumably in the non-autophagy-inducing state. To examine the autophagy-inducing state of

Atg17-Atg31-Atg29, we reconstituted complexes containing the phosphomimetic mutants Atg29[3SD] or Atg29[20STA/3SD], and subjected the purified complexes to negative stain 2D EM analysis. Two galleries of class averages were obtained from the classification of 4,671 Atg29[3SD]-containing and 6,558 Atg29[20STA/3SD]-containing particles, respectively (Figure 4.5D and E). These averages indicated that the phosphomimetic mutations did not significantly alter the overall structure of the ternary complex. This finding is in agreement with the earlier assignment of the C-terminal regulatory domain of Atg29 to the periphery of the Atg17-Atg31-Atg29 complex (Figure 4.5C). Although the Atg29 regulatory domain is not directly engaged in assembling and/or stabilizing this complex, it localizes to a highly accessible region suitable for engaging in interactions with other Atg proteins and/or components of the Atg1 signaling machinery.

4.3.7 *In vivo* reconstitution and analysis of the Atg17-Atg31-Atg29 complex

The Atg17-Atg31-Atg29 complex is considered to be one of the first sets of proteins that assemble at the PAS, and it plays a role in the recruitment of other Atg proteins. However, the complexity of the interaction network of Atg proteins has made it difficult to completely dissect the process of PAS organization. Therefore, we tried to reconstitute assembly of the ternary complex in vivo in our multiple-knockout (MKO) strain (151), and used Atg17-GFP as the reporter to observe the PAS localization of the complex. In the MKO strain, the *ATG* genes whose products are involved in autophagosome formation have been deleted; this allows us to eliminate contributions from other Atg proteins and determine the minimum components needed for the assembly and correct localization of the complex. When we expressed both Atg29 and Atg31 together with Atg17-GFP, we were unable to observe puncta corresponding to Atg17-GFP (Figure 4.6A). In contrast, if Atg11 was co-expressed with all three proteins, the Atg17-GFP puncta were

now detected (Figure 4.6A). Thus, in the absence of all other known Atg proteins, Atg11 is necessary and sufficient to recruit the Atg17-Atg31-Atg29 complex to the PAS.

Previous studies from our lab suggested that Atg17 interacts with Atg11 (125); however, neither *ATG29* nor *ATG31* had been identified at that time. Therefore, we decided to reexamine which component of the Atg17-Atg31-Atg29 complex was the direct binding partner of Atg11. In order to carry out this analysis, we took advantage of the bimolecular fluorescence complementation assay (119). In this system, the Venus yellow fluorescent protein is split into two fragments, corresponding to the N terminus (VN) and C terminus (VC). We fused VC to Atg11, and VN to Atg17, Atg29, or Atg31, by integrating the corresponding constructs at the *ATG11*, *ATG17*, *ATG29* or *ATG31* loci on the yeast genome. Fluorescence from these chimeras can only be observed when the two proteins interact and bring the two fluorophore fragments into close proximity. Bright dots were observed in cells expressing VC-Atg11 and Atg29-VN, but no fluorescent signal was observed in cells expressing either VC-Atg11 and Atg17-VN, or VC-Atg11 and Atg31-VN (Figure 4.6B). To confirm the interaction between Atg29 and Atg11, we carried out protein A affinity isolation with IgG-Sepharose. PA-tagged Atg17 and Atg29 were both able to co-precipitate HA-Atg11. When Atg17 was absent, Atg29 could still pull down Atg11; however, when Atg29 was absent, Atg17 no longer interacted with Atg11 (Figure 4.6C). These results indicate that Atg29, but not Atg17, directly interacts with Atg11 to facilitate the association of Atg11 with the complex and to achieve its PAS localization.

Atg11 is a scaffold protein required for selective autophagy that appears to be dispensable for non-selective autophagy, as deletion of the *ATG11* gene has no obvious effect on autophagy activity (11). However, some lines of evidence also suggest that Atg11 might have a role in non-selective autophagy. For example, a small number of autophagic bodies (the single-membrane vesicles that result from the fusion of autophagosomes with

the vacuole) are detected in the vacuole in *atg17*Δ cells (9), consistent with the fact that autophagy is not completely blocked when Atg17 is absent. However, no autophagic bodies are detected in *atg11*Δ *atg17*Δ cells, suggesting that Atg11 contributes to autophagic body (and hence autophagosome) formation in the absence of Atg17. Atg11 is proposed to function as the initial component localizing to the PAS in vegetative conditions, facilitating the formation of the starvation-specific PAS upon the induction of autophagy (9). In the present study, we found that Atg11 interacted with Atg29 and was required for the PAS targeting of the Atg17-Atg31-Atg29 complex in MKO cells. Therefore, we extended our analysis of the role of Atg11 in non-selective autophagy with the Pho8Δ60 assay. In *atg11*Δ cells, autophagy activity was normal in agreement with previous studies, whereas in *atg29*Δ cells, autophagy activity was ~40-45% the level of the wild type. In contrast, when both *ATG11* and *ATG29* were deleted, autophagy was almost completely blocked (Figure 4.6D). Therefore, Atg11 appears to contribute to non-selective autophagy when Atg29 is absent.

4.3.8 The phosphorylation of Atg29 is required for its binding to Atg11 and the PAS targeting of the Atg17-Atg31-Atg29 complex

Because we found that the phosphorylation of Atg29 is important for autophagy activity, we decided to examine the role of Atg29 phosphorylation in the PAS targeting of the Atg17-Atg31-Atg29 complex. We co-expressed Atg11, Atg31 and either wild-type or mutant Atg29 in the MKO strain, and again used Atg17-GFP as the reporter. With wild-type Atg29, ~22% or ~33% of the cells contained Atg17-GFP puncta in growing or nitrogen starvation conditions, respectively (Figure 4.7A and B). The phosphomimetic mutants Atg29[3SD] and Atg29[3SE] were also able to support Atg17-GFP puncta formation at essentially wild-type levels (Figure 4.7A and B). In contrast, no Atg17-GFP puncta were observed with the non-phosphorylable Atg29[23STA] mutant in either growing or nitrogen starvation conditions (Figure 4.7A and B). These

results suggest that the phosphorylation of Atg29 is required for the PAS recruitment of the Atg17-Atg31-Atg29 complex.

Since Atg29[23STA] could not promote the PAS targeting of the Atg17-Atg31-Atg29 complex, we suspected that the phosphorylation of Atg29 was required for its association with the complex, or for interaction with Atg11. Therefore, we used wild-type Atg29-PA or Atg29[23STA]-PA to pull down Atg17-GFP and HA-Atg11 in MKO cells. Atg17-GFP was co-precipitated by both wild-type Atg29-PA and Atg29[23STA]-PA, in agreement with the observation that the Atg17-Atg31-Atg29 complex is present in vegetative conditions (i.e., when we do not detect phosphorylation of the C terminus) (12); however, only wild-type Atg29-PA was able to co-precipitate HA-Atg11 (Figure 4.7C). Therefore, the phosphorylation of Atg29 is dispensable for its association with Atg31 and Atg17, but is required for interaction with Atg11, and the PAS targeting of the Atg17-Atg31-Atg29 complex.

4.3.9 The Atg17-Atg31-Atg29 complex and Atg11 cooperate to recruit the intact Atg1 kinase complex

Previous work showed that Atg11 directly interacts with Atg1, although the physiological role of this interaction is unknown (9, 11). In the absence of Atg17 or Atg29, Atg11 permits the cells to retain residual autophagy activity (9). Therefore, we hypothesized that the intact Atg1 complex consists of (at least) six subunits, which form an interacting structure that controls autophagy induction. To test our hypothesis and gain further insight into the physiological role of the Atg1-Atg11 interaction, we combined random mutagenesis and yeast two-hybrid assays and identified an Atg1 mutant, $Atg1^{L825H,W826S}$ (hereafter Atg1(LHWS)). Atg1(LHWS) showed a significant decrease in its interaction with Atg11, as detected by protein A affinity isolation (Figure 4.8A). Importantly, Atg1(LHWS) has normal Atg1 function other than decreased interaction with Atg11, as the plasmid-driven Atg1(LHWS) was able to rescue the defect of autophagy activity as well as wild-type Atg1 (Figure 4.8B).

Atg1 protein kinase is the key subunit of Atg1 complex, and we showed that Atg11 is necessary and sufficient to recruit the Atg17-Atg31-Atg29 complex to the PAS (Figure 4.6A). We hypothesized that the Atg17-Atg31-Atg29 complex and Atg11 together form a scaffold for the recruitment of Atg1 to the PAS. To test this possibility and to preclude interference from the endogenous wild-type Atg1, we transformed plasmids expressing chimeras of GFP fused to either wild-type Atg1 or Atg1(LHWS) into *atg1*Δ cells. Wild-type GFP-Atg1 and GFP-Atg1(LHWS) displayed similar levels of puncta formation in both growing and starvation conditions (Figure 4.8C and D). Loss of the Atg1-Atg11 interaction may not have had an obvious effect on autophagy activity (Figure 4.8B) or puncta formation (Figure 4.8C and D) because of compensation from the Atg11-Atg29 interaction, which was able to retain Atg11 within the Atg1 complex. To test this hypothesis, we next deleted the *ATG29* gene. In *atg1*Δ *atg29*Δ cells, wild-type GFP-Atg1 showed reduced puncta formation compared to that in *atg1*Δ cells in both growing and starvation conditions (Figure 4.8C and D), which suggested that Atg29 is important for the PAS recruitment of Atg1. GFP-Atg1(LHWS) showed a further decrease in puncta formation in the double deletion background (Figure 4.8C and D), which implied that the Atg1-Atg11 interaction is essential for Atg1 recruitment when Atg29 is absent.

Finally, we asked whether the change in puncta formation corresponded to a change in autophagy activity. Even though both wild-type Atg1 and Atg1(LHWS) expressed from plasmids were able to rescue the defect of autophagy activity in cells with only an *ATG1* deletion (Figure 4.8B), when we also deleted the *ATG29* gene, only plasmid-driven wild-type Atg1, but not Atg1(LHWS), rescued the autophagy defect (Figure 4.8B). Therefore, the Atg1-Atg11 interaction is also essential for autophagy activity when Atg29 is absent.

4.4 Discussion

Autophagy is crucial for cellular metabolism, but either excessive or insufficient autophagy can be deleterious. Therefore, the activity of this process has to be tightly controlled. The Atg1 kinase complex, which includes Atg1, Atg13, Atg17, Atg29, and Atg31, is a key regulator of autophagy induction and inhibition, and the activity of these proteins is modulated in part by posttranslational modifications. For example, Atg1, Atg13 and Atg31 are all phosphoproteins, and the functions of at least Atg1 and Atg13 are regulated by phosphorylation (12, 91, 92, 139). Here, we show that Atg29 is also a phosphoprotein and we determine the physiological role of its phosphorylation.

Based on our results, we suggest that in nutrient-rich conditions, when autophagy is at a basal level, the activity contributed by Atg29 is blocked by an inhibitory peptide located at its extreme C terminus. Upon autophagy induction, Atg29 is phosphorylated, and the modification of the last three serine residues in particular promotes a conformational change and release of the inhibition, thus allowing the full activity of the N-terminal functional domain.

The phosphorylation of Atg29 affected its ability to interact with Atg11. All these results are consistent with our protein analysis that Atg29 belongs to a new class of very flexible polypetides called intrinsically disordered proteins. IDPs have a number of functional advantages over the function of structured proteins. For example, they have larger interacting surfaces compared to their ordered partners, exhibit increased speed of interactions and high specificity coupled with low affinity, carry recognition segments that can fold after binding to a native partner or cofactor, have accessible posttranslational modification sites, and possess conformational flexibility that allows for structural adaptation in interaction with several partners, or they can be involved in very distinct functional modes, for example, acting as both inhibitors and activators of their partner enzyme(s) (140, 150, 152, 153). The very same regions of these proteins are involved in very distinct functional modes (e.g., activation as well as inhibition) (140, 150, 152).

The lines of evidence that Atg29 is an IDP come mainly from the characteristics that originate in the protein's amino acid sequence and that have been shown by numerous studies (140-143, 147) to be distinct for IDPs relative to ordered (globular) proteins. We were not able to apply a full set of experimental techniques that would provide comprehensive characterization of this protein, because the purified Atg29 could not be obtained in the monomeric form; the protein a very significant propensity for aggregation under different experimental conditions. This tendency to aggregate further supported our finding that Atg29 is disordered, because this type of proteins exists as an ensemble of conformations without a single minimum in the energy landscape model, and as a result is always more prone to inter-molecular interactions or aggregation in the absence of a natural binding partner in solution (143). Given the enormous versatility of IDPs, we conclude that the presence of at least Atg29 as one component representing this class of proteins in the constitutively formed regulatory Atg1 kinase complex is consistent with the requirement for prompt regulation of autophagy induction in response to changing intracellular conditions.

Our single-particle electron microscopy analysis of the Atg17-Atg31-Atg29 complex revealed an "S"-shaped architecture that is consistent with the crystal structure of the recently published *L. thermotolerans* complex (144), although we note that the crystal structure does not include substantial portions of Atg29 or Atg31, including the entire C-terminal half of Atg29 that we show in the present study is subject to phosphorylation. Atg29 is located at the ends of the dimeric scaffold that is formed primarily by the rigid structure of Atg17. Considering this location, it is not surprising that the introduction of phosphomimetic mutations to substitute for the last three serine residues in Atg29 does not change the overall structure of the complex at this level of resolution. We have not yet succeeded in purifying the complex from yeast under autophagy-inducing conditions, so we cannot rule out the possibility that the phosphorylated protein will display a more obvious conformational change.

At any rate, we found that the phosphorylation state of Atg29 affected its ability to interact with Atg11.

Atg11 is a selective autophagy scaffold protein, binding to a variety of cargo receptors to mediate different types of selective autophagy (56, 59) (51). Atg11 directly interacts with Atg1 and is involved in the activation of Atg1 kinase activity (10, 11). In the absence of Atg17 or Atg29, Atg11 permits the cells to retain residual autophagy activity, even though the deletion of the *ATG11* gene by itself does not have an obvious effect on autophagy activity (9, 11). The hierarchical study of the Atg proteins along with other work suggests that the Atg17-Atg31-Atg29 complex comprises the first set of proteins localized to the PAS (15, 16). However, in the absence of other Atg proteins (as in our MKO strain), this complex is diffuse in the cytosol rather than accumulating at the PAS; under these conditions, Atg11 is necessary and sufficient for PAS recruitment (Figure 4.5A).

Atg11 directly interacts with Atg1, although the physiological role of this interaction is unknown (11). With regard to Atg1 kinase activity, the Atg17-Atg31-Atg29 complex can interact with Atg1 via the binding of Atg13 to Atg17, or through the binding of Atg11 to Atg29. This finding may explain the residual autophagy activity seen in *atg17*Δ or *atg29*Δ cells, and the complete loss of autophagy activity in *atg11*Δ *atg17*Δ or *atg11*Δ *atg29*Δ cells. Atg1 and Atg13 are the core subunits within the complex; therefore, both non-selective and selective autophagy are blocked when *ATG1* or *ATG13* are deleted. Atg11 and the Atg17-Atg31-Atg29 complex have partly redundant roles as scaffolds for PAS organization (9); under starvation conditions, the Atg17-Atg31-Atg29 complex plays a major role, whereas Atg11 is critical for selective autophagy, and for facilitating the transition to non-selective autophagy.

In summary, the function and organization of the PAS is a critical issue in the autophagy field. A continued structure-function analysis of the Atg17-Atg31-Atg29 complex will help us better understand the molecular mechanism of phagophore initiation. In particular, further structural studies that

include additional components of the Atg1 kinase complex combined with molecular genetic data should provide tremendous insight into autophagy regulation.

4.5 Materials and methods

Strains, Media, and Growth Conditions. Yeast strains used in this study are listed in Table 4.1. Yeast cells were grown in rich (YPD; 1% yeast extract, 2% peptone, and 2% glucose) or synthetic minimal (SMD; 0.67% yeast nitrogen base, 2% glucose, and auxotrophic amino acids and vitamins as needed) media. Autophagy was induced by shifting the cells to nitrogen starvation medium (SD-N; 0.17% yeast nitrogen base without ammonium sulfate or amino acids, and 2% glucose).

Plasmids. pCuHAAtg11(416), pCuHAAtg11(414) and pCuPA-Atg1(416) has been reported previously (9, 59). For constructing wild-type or truncation forms of the ATG29-PA plasmid, the full-length or corresponding truncation forms of the *ATG29* gene with its endogenous promoter were amplified by PCR and ligated into pNopPA(314) after removing the *NOP1* promoter, which was described elsewhere (154). The DNA fragments of ATG29-PA[23STA] and ATG29-PA[20STA] were synthesized by GenScript, and ligated into pNopPA(314). The plasmids pAtg29[3SA]-PA, pAtg29[3SD]-PA, and pAtg29[3SE]-PA were generated by site-directed mutagenesis from pAtg29-PA. pAtg29[20STA/3SD]-PA and pAtg29[20STA/3SE]-PA were generated from pAtg29[23STA]. For pAtg29[1-202/23STA], the DNA fragment lacking the last 33 nucleotides was amplified by PCR and ligated into pNopPA(314). To construct pAtg1(414), the open reading frame along with 1763 bp of upstream and 566 bp of downstream of *ATG1* gene was amplified from yeast genome and inserted in the BamHI site of pRS414. pGFP-Atg1(316) was a kind gift from Dr. Yoshinori Ohsumi (National Institute for Basic Biology, Okazaki, Japan). pAtg1(LHWS)(414) was generated by site-directed mutagenesis from pAtg1(414), pGFP-Atg1(LHWS)(316) was from pGFP-Atg1(316), and

pCuPA-Atg1(LHWS)(416) was from pCuPA-Atg1(416).

Fluorescence Microscopy. For fluorescence microscopy, yeast cells were grown to OD_{600} ~0.6 in YPD or SMD and shifted to SD-N for autophagy induction. Samples were then examined by microscopy (Olympus; or Delta Vision, Applied Precision) using a 100x objective and pictures were captured with a CCD camera (CoolSnap HQ; Photometrics). For each microscopy picture, 12 Z-section images were captured with a 0.3-µm distance between two neighboring sections.

Expression and purification of MOCR-Atg29. The *ATG29* gene was cloned using LIC technology (155) into the multiple cloning site of the pMOCR expression vector (156). The recombinant fusion protein MOCR-Atg29 was expressed for 3 h at 28°C in BL21-AI *E. coli* cells after induction with 0.2 mM IPTG and 0.2% arabinose. The protein was purified in the first step using the His tag. The soluble fraction of the bacterial lysate was batch bound to Ni-NTA agarose (Qiagen) for 3 h. Resin was washed with 20 mM imidazole in a buffer containing 50 mM sodium phosphate, pH 8, 300 mM NaCl and 10% betaine. The protein was eluted with 250 mM imidazole in the same buffer and dialyzed overnight in 50 mM sodium phosphate, pH 8, 10 mM NaCl, 1 mM DTT, and 5% betaine. The second purification step was performed by gel filtration in dialysis buffer using a Superdex 200 column and ÄKTApurifierTM FPLC system (GE Healthcare). The protein eluted in the void peak as a soluble aggregate.

Purification of Recombinant Atg17-Atg31-Atg29 Complexes and Variants. N-terminal GST (glutathione-S-transferase)-tagged or N-terminal hexahistidine-MBP (maltose binding protein)-tagged Atg17, was co-expressed with N-terminal hexahistidine-tagged Atg31, and untagged Atg29 in the same *E. coli* expression host. The recombinant complex was purified using glutathione-agarose (for GST-tagged Atg17) or nickel sepharose (for His-MBP tagged Atg17) followed by PreScission or TEV protease cleavage to remove the affinity tag. The cleaved complex was further purified by gel filtration chromatography using a Superose 6 column.

Single-Particle Electron Microscopy. Negatively stained specimens were prepared as previously described (157). Raw images were recorded at a nominal magnification of 49,000x on a 4K x 4K Eagle camera (FEI) with a Tecnai Spirit transmission electron microscope operated at an accelerating voltage of 120 kV. Images for two-dimensional (2D) analysis were collected using the same instrument with operating parameters and at a defocus value of −1.2 μm. For 2D analysis, particles were interactively selected using Boxer (158) . The selected particles were windowed into 112 x 112-pixel images, rotationally and translationally aligned, and subjected to ten cycles of multi-reference alignment using SPIDER. Each round of alignment was followed by K-means classification specifying 50 classes.

Additional Assays. The Pho8Δ60 assay and immunoprecipitation were performed as described previously (59).

4.6 Acknowledgements

This work was supported by NIH grant GM053396 to DJK, by a University of Michigan Rackham Predoctoral Fellowship to MK, by a Natural Sciences and Engineering Research Council of Canada Discovery Grant, a Michael Smith Foundation for Health Research Career Investigator Award, and a Canadian Institutes of Health Research New Investigator award to CKY, and by a Natural Sciences and Engineering Research Council of Canada Postgraduate Scholarship award to LHC.

Table 4.1 Yeast strain list

Name	Genotype	Reference
HCY107	YCY123 *ATG17-GFP::HIS3*	This study
HCY108	YCY131 *ATG17-GFP::HIS3*	This study
HCY109	SEY6210 *atg29Δ::KAN*	This study
HCY125	SEY6210 *atg17Δ::KAN Atg29-PA::TRP1*	This study
HCY129	SEY6210 *Atg29-PA::TRP1*	This study
KDM1233	SEY6210 *atg29Δ::KAN ATG31-GFP::HIS3*	This study
KDM1234	SEY6210 *ATG17-PA::HIS3*	This study
KDM1235	SEY6210 *atg29Δ::KAN ATG17-PA::HIS3*	This study
KDM1270	SEY6210 *atg1Δ::HIS5 atg11Δ::LEU2*	This study
KDM1406	TN124 *atg11Δ::URA3*	This study
KDM1407	TN124 *atg29Δ::KAN atg11Δ::URA3*	This study
KDM1408	SEY6210 *pho13Δ pho8Δ60 atg1Δ::LEU2*	This study
KDM1409	SEY6210 *pho13Δ pho8Δ60 atg29Δ::HIS5*	This study
KDM1410	SEY6210 *pho13Δ pho8Δ60 atg1Δ::LEU2 atg29Δ::HIS5*	This study
KDM1551	SEY6210 *pRPL7b-VC-ATG11::HIS3 ATG17-VN::TRP1*	This study
KDM1552	SEY6210 *pRPL7b-VC-ATG11::HIS3 ATG29-VN::TRP1*	This study
KDM1553	SEY6210 *pRPL7b-VC-ATG11::HIS3 ATG31-VN::TRP1*	This study
SEY6210	MATα *leu2-3,112 ura3-52 his3-Δ200 trp1-Δ901 suc2-Δ9 lys2-801 GAL*	(101)
TKY12	SEY6210 *atg29Δ::KAN atg1Δ::LEU2*	This study
TN124	*MATa leu2-3,112 trp1 ura3-52 pho8::pho8Δ60 pho13*::*LEU2*	(81)
WHY1	SEY6210 *atg1Δ::HIS5*	This study
WLY176	SEY6210 *pho13Δ pho8Δ60*	This study
YCY123	SEY6210 *atg1Δ, 2Δ, 3Δ, 4Δ, 5Δ, 6Δ, 7Δ, 8Δ, 9Δ, 10Δ, 11Δ, 12Δ, 13Δ, 14Δ, 16Δ, 17Δ, 18Δ, 19Δ, 20Δ, 21Δ, 23Δ, 24Δ, 27Δ, 29Δ*	(151)
YCY131	SEY6210 *atg1Δ, 2Δ, 3Δ, 4Δ, 5Δ, 6Δ, 7Δ, 8Δ, 9Δ, 10Δ, 11Δ, 12Δ, 13Δ, 14Δ, 16Δ, 17Δ, 18Δ, 19Δ, 20Δ, 21Δ, 23Δ, 24Δ, 27Δ, 29Δ, 31Δ::ble*	This study
YIY36	TN124 *atg29Δ::KAN*	This study

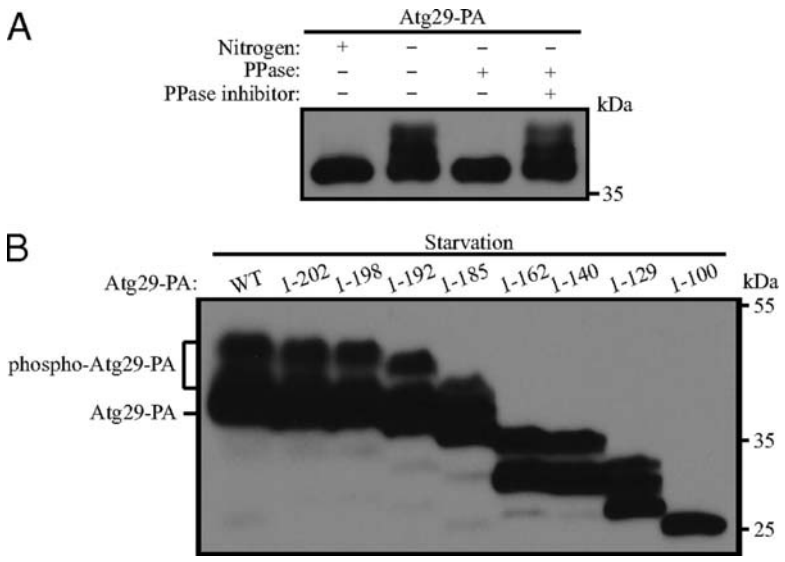

Figure 4.1 Atg29 is a phosphoprotein.
(A) Cells containing a chromosomal protein A-tagged Atg29 (HCY129) were grown in YPD and shifted to SD-N for 2 h. λ phosphatase and phosphatase inhibitor were added to the cell lysate as indicated.
(B) Different forms of plasmid-encoded Atg29-PA with the indicated truncations were transformed into *atg29*Δ cells (HCY109). Cells were grown in SMD and shifted to SD-N for 2 h. Cell lysates were separated by SDS-PAGE and analyzed by western blot.

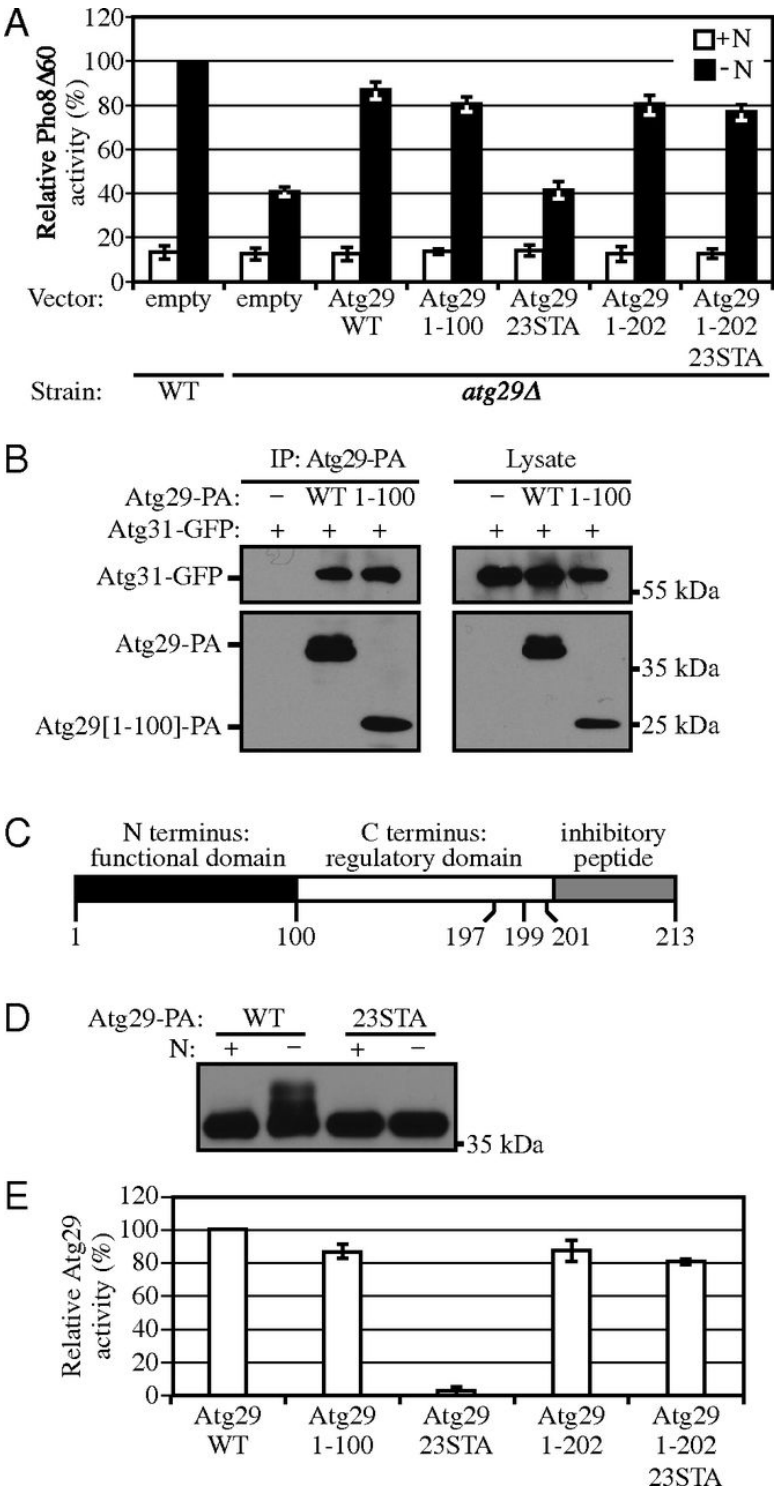

Figure 4.2 Atg29 contains distinct functional, regulatory and inhibitory domains.

(A) Pho8Δ60 wild-type (TN124) cells were transformed with empty vector; Pho8Δ60 *atg29*Δ (YIY36) cells were transformed with empty vector, or a plasmid containing wild-type or different mutant forms of Atg29-PA as indicated. Cells were cultured in SMD to mid-log phase (+N), and shifted to SD-N for 4 h. The Pho8Δ60 assay was performed as described in Materials and Methods. Error bars correspond to the standard deviation (SD), and were obtained from

three independent repeats.
(B) Empty vector, or plasmids encoding Atg29-PA, or Atg29[1-100]-PA were transformed into *atg29*Δ cells expressing Atg31-GFP (KDM1233). Cells were cultured in SMD to mid-log phase, and cell lysates were prepared and incubated with IgG-Sepharose for affinity isolation as described in Materials and Methods.
(C) A schematic diagram of the Atg29 protein.
(D) The plasmid pAtg29-PA or pAtg29[23STA] was transformed into *atg29*Δ cells (HCY109). Cells were cultured in SMD, shifted to SD-N for 2 h, and analyzed by immunoblot.
(E) Relative activities of different Atg29 mutants based on the results in (A). The conversion from percent Pho8Δ60 to relative Atg29 activity was carried out as described in the text.

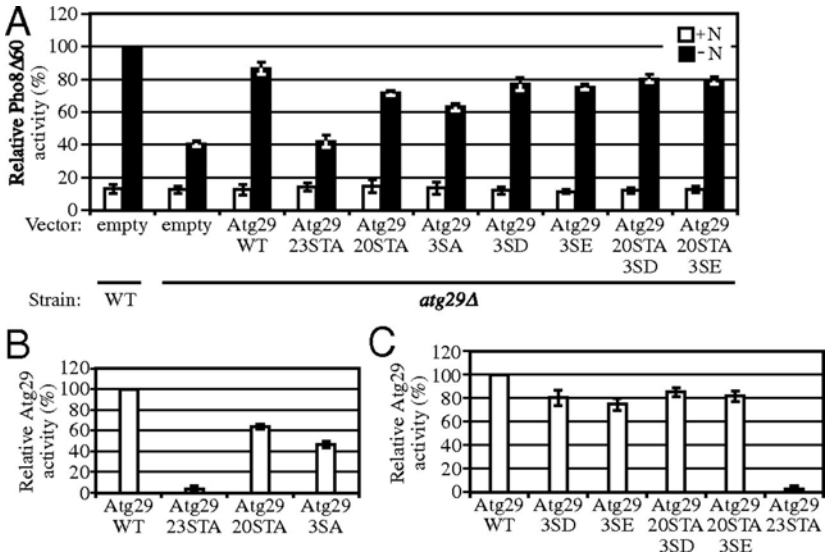

Figure 4.3 Phosphorylation of serine residues adjacent to the inhibitory peptide is important for Atg29 function.

(A) Pho8Δ60 wild-type (TN124) cells were transformed with empty vector; Pho8Δ60 *atg29*Δ (YIY36) cells were transformed with empty vector, or a plasmid containing wild-type or different mutant forms of Atg29-PA as indicated. Cells were cultured in SMD (+N) to mid-log phase, and shifted to SD-N for 4 h. Protein extracts were analyzed using the Pho8Δ60 assay. Error bars correspond to the standard deviation (SD), and were obtained from three independent repeats.

(B,C) Relative activities of different Atg29 mutants based on the results in (A).

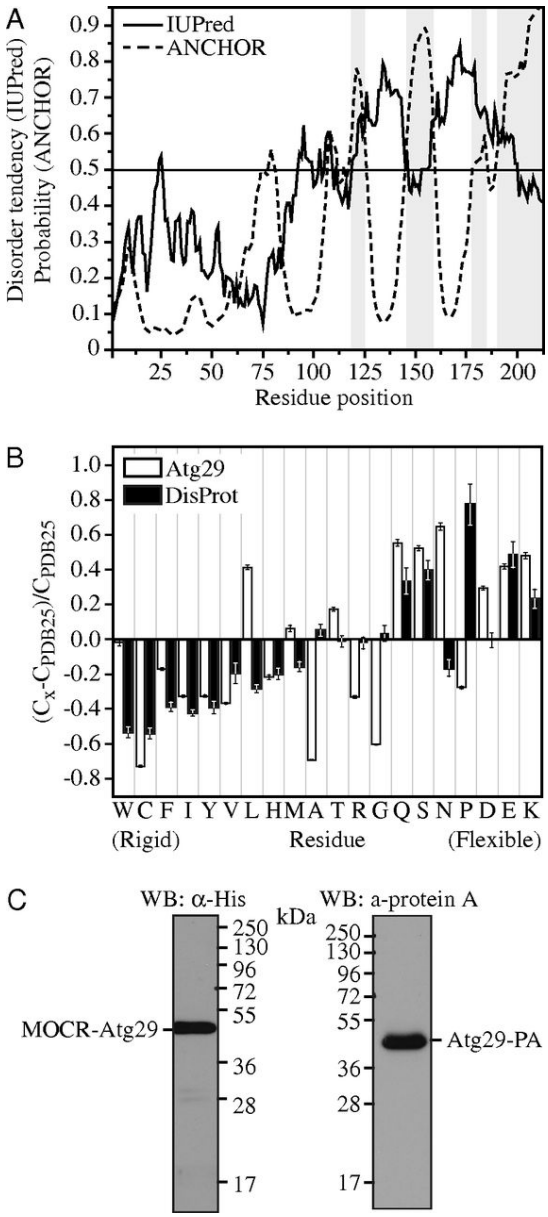

Figure 4.4 Atg29 is an intrinsically disordered protein.
(A) Tendency for intrinsic disorder and probability of an Atg29 residue being in a disordered binding site, as predicted by IUPred and ANCHOR, respectively. Gray areas, generated by ANCHOR, identify the disordered binding segments in Atg29 that are likely to be stabilized through binding to a globular protein partner. The Met residue at the Atg29 N terminus was not included in the calculations for this plot and the plots in panel B and Figure 4.S1B.
(B) Compositional profiling of Atg29. The gray and black bars show the fractional difference (calculated as $(C_X - C_{PDB25})/C_{PDB25}$) in amino acid composition of Atg29 and IDPs from the DisProt database, respectively, relative to a reference set of proteins in PDB database (149) that is biased towards the composition of proteins responsive to crystallization. C_X is the content of amino acids in Atg29 or IDPs in DisProt and C_{PDB25} is the corresponding value for proteins in the PDB protein set. A negative/positive

fractional difference indicates depletion/enrichment in the corresponding amino acid. Amino acids are arranged on the x-axis from the most rigid to the most flexible according to the Vihinen's flexibility scale (159).
(C) Migration of Atg29 fusion proteins following SDS-PAGE. (Left) Atg29 fused to the MOCR solubilization tag was visualized by immunoblotting the *E. coli* cell lysate with antiserum to polyHis and by Coomassie Blue staining of the purified protein. (Right) Atg29 fused to protein A was detected by immunoblotting the yeast cell extract with antiserum that detects PA.

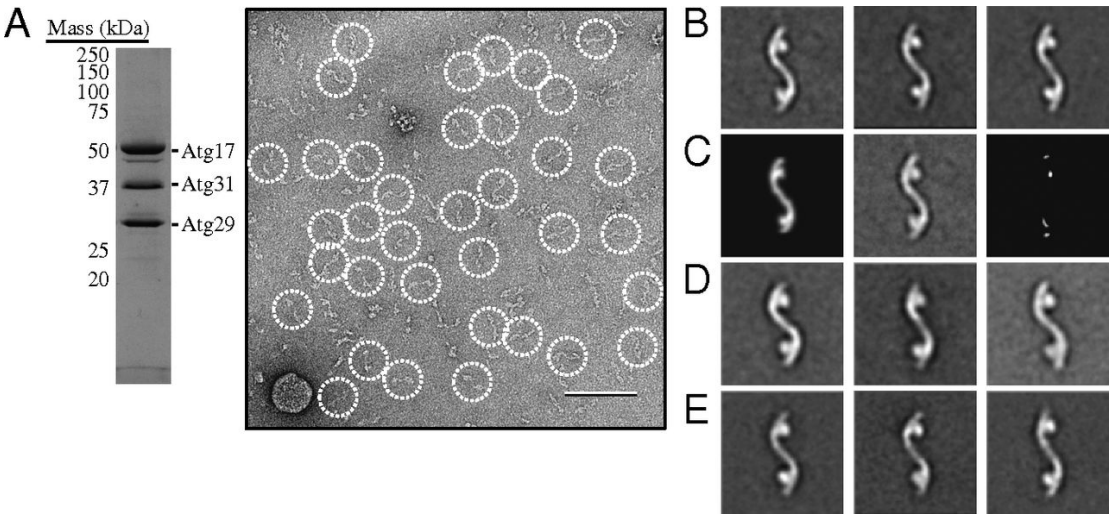

Figure 4.5 The Atg17-Atg31-Atg29 complex adopts an elongated S-shaped structure.

(A) Coomassie Blue-stained SDS-PAGE analysis of gel filtration-purified recombinant Atg17-Atg31-Atg29 (*left*). A raw image taken from a negatively stained recombinant Atg17-Atg31-Atg29 specimen (*right*). Particles are circled and the scale bar represents 100 nm.

(B) Representative class averages obtained from reference-free classification of 6,788 negatively stained Atg17-Atg31-Atg29 particles into 50 classes. Each of the three classes contains between 110 to 220 particles. The side length of each panel is 52 nm.

(C) Difference mapping between the high-resolution crystal structure projection (*left*) and the negative stained EM average of the full-length components from *S. cerevisiae* (*middle*). The difference image (*right*) indicates that the Atg29 C terminus is located in the globular domains.

(D) Representative class averages obtained from classification of 4,671 negatively stained Atg29[3SD]-containing particles into 50 classes. Each of the three classes contains between 100 to 190 particles.

(E) Representative class averages obtained from classification of 6,588 negatively stained Atg29[20STA/3SD]-containing particles into 50 classes. Each of the three classes contains between 150 to 170 particles.

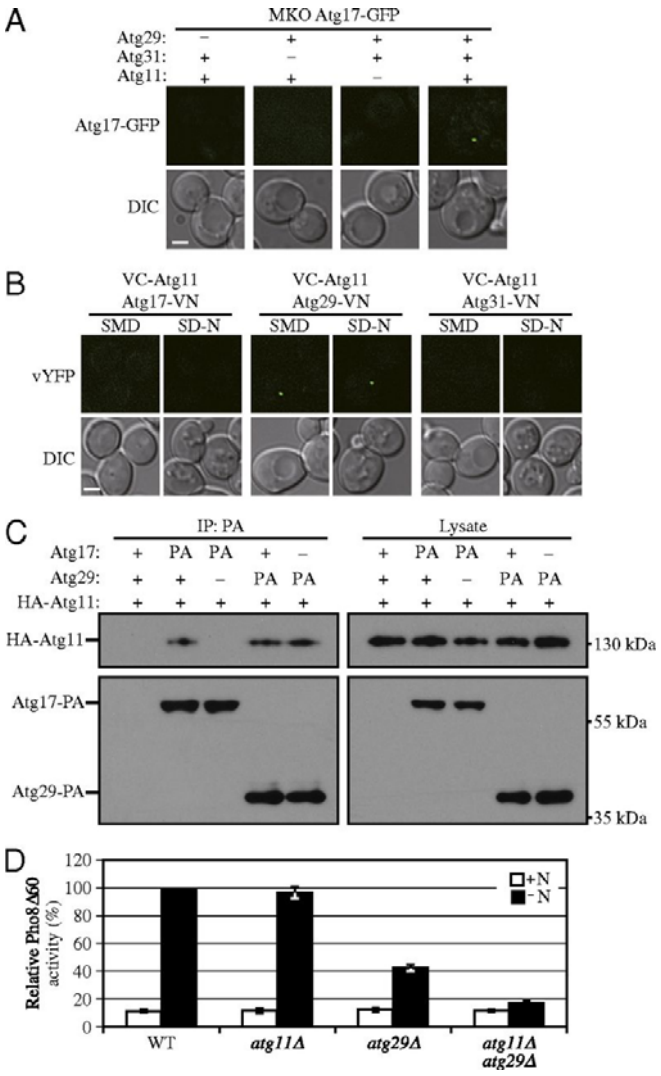

Figure 4.6 Atg11 is important for the PAS recruitment of the Atg17-Atg31-Atg29 Complex.

(A) An empty vector or a plasmid expressing Atg29-PA was co-expressed with empty vector or a plasmid encoding HA-Atg11 under the control of the *CUP1* promoter (pCuHA-Atg11) in MKO *ATG17-GFP* (HCY107) or MKO *ATG17-GFP atg31*Δ (HCY108) cells as indicated. Cells were cultured in SMD to early log phase.

(B) *VC-ATG11 ATG17-VN* (KDM1551), *VC-ATG11 ATG29-VN* (KDM1552), and *VC-ATG11 ATG31-VN* (KDM1553) cells were cultured in YPD and shifted to SD-N for 2 h. All of the cell samples in (A) and (B) were observed by fluorescence microscopy. The images are representative pictures from single Z-section images. DIC, differential interference contrast. Bars, 2 μm.

(C) The plasmid pCuHA-Atg11(416) was transformed into wild-type (SEY6210), *ATG17-PA* (KDM1234), *ATG17-PA atg29*Δ (KDM1235), *ATG29-PA* (HCY129), or *ATG29-PA atg17*Δ (HCY125) cells. Cells were cultured in SMD, and cell lysates were prepared and incubated with IgG-Sepharose for affinity isolation as described in Materials and Methods. The eluted proteins were separated by

SDS-PAGE and detected with monoclonal antibody that recognizes HA or PA. (D) Pho8Δ60 wild-type (TN124), *atg11*Δ (KDM1406), *atg29*Δ (YIY36), or *atg29*Δ *atg11*Δ (KDM1407) cells were cultured in YPD (+N) and shifted to SD-N for 4 h. The Pho8Δ60 assay was performed. Error bars correspond to the standard deviation (SD), and were obtained from three independent repeats.

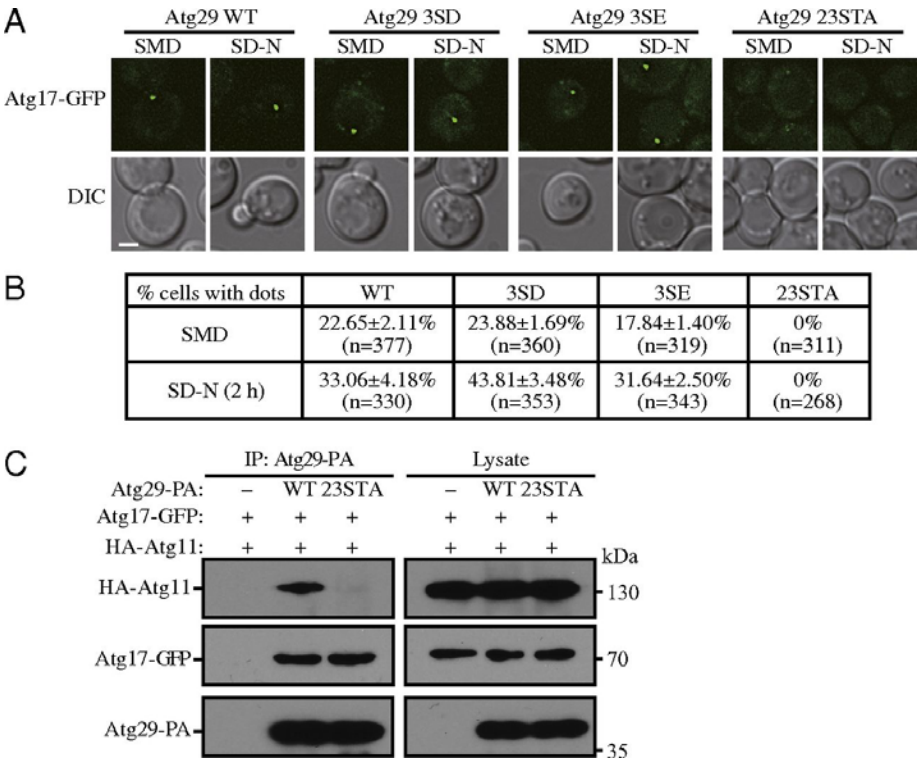

Figure 4.7 Phosphorylation of Atg29 is required for binding to Atg11.
(A) Plasmids encoding Atg29, Atg29[3SD], Atg29[3SE], or Atg29[23STA] were co-expressed with HA-Atg11 under the control of the *CUP1* promoter (pCuHA-Atg11) in MKO *ATG17-GFP* (HCY107) cells. Cells were cultured in SMD and shifted to SD-N for 2 h, and cell samples were observed by fluorescence microscopy. The images are representative pictures from single Z-section images. DIC, differential interference contrast. Bars, 2 μm.
(B) Quantification of Atg17-GFP dots. 12 Z-section images were projected and the percentage of cells containing the Atg17-GFP puncta was determined. The SD was calculated from three independent experiments.
(C) A plasmid encoding Atg29, or Atg29[23STA] was co-expressed with pCuHA-Atg11 in MKO *ATG17-GFP* (HCY107) cells. Cells were cultured in SMD, and cell lysates were prepared and incubated with IgG-Sepharose for affinity isolation.

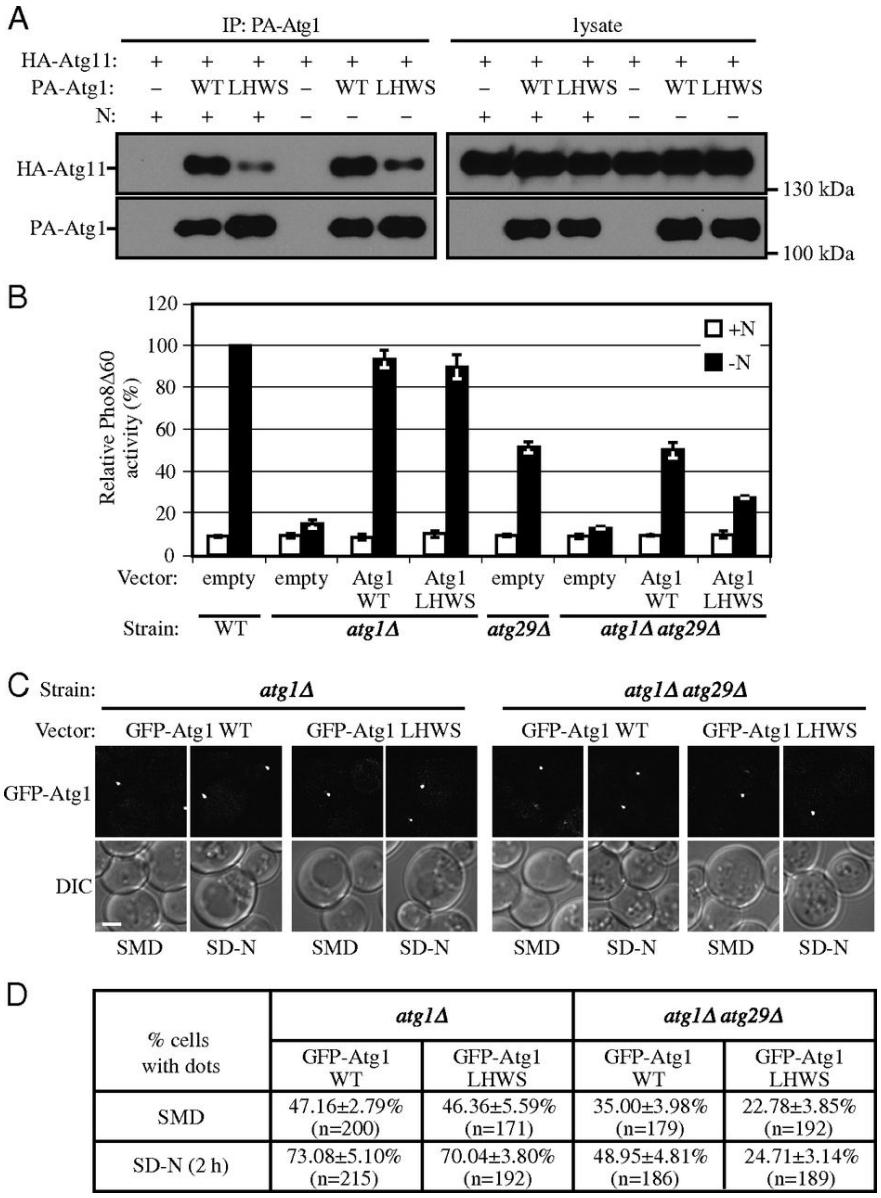

% cells with dots	*atg1Δ*		*atg1Δ atg29Δ*	
	GFP-Atg1 WT	GFP-Atg1 LHWS	GFP-Atg1 WT	GFP-Atg1 LHWS
SMD	47.16±2.79% (n=200)	46.36±5.59% (n=171)	35.00±3.98% (n=179)	22.78±3.85% (n=192)
SD-N (2 h)	73.08±5.10% (n=215)	70.04±3.80% (n=192)	48.95±4.81% (n=186)	24.71±3.14% (n=189)

Figure 4.8 Atg29 and Atg11 have redundant roles in the recruitment of Atg1 to the PAS.

(A) The plasmids pCuPA(416) or pCuPA-Atg1(416) and pCuHA-Atg11(414) were transformed into *atg1*Δ *atg11*Δ cells (KDM1270). Cells were cultured in SMD, and cell lysates were prepared and incubated with IgG-Sepharose for affinity isolation as described in Materials and Methods. The eluted proteins were separated by SDS-PAGE and detected with monoclonal antibody that recognizes HA or PA.

(B) The plasmid pRS414, pAtg1(414), or pAtg1(LHWS)(414) was transformed into either Pho8Δ60 wild-type (WLY176), *atg1*Δ (KDM1408), *atg29*Δ (KDM1409), or *atg11*Δ *atg29*Δ (KDM1410) cells. Cells were cultured in SMD (+N) and shifted to SD-N (-N) for 4 h. The Pho8Δ60 assay was performed as described in Materials and Methods. Error bars correspond to the standard deviation (SD), and were obtained from three independent repeats.

(C) The plasmid pGFP-Atg1(416) or pGFP-Atg1(LHWS)(416) was transformed into either *atg1*Δ (WHY1) or *atg1*Δ *atg29*Δ (TKY12) cells. Cells were cultured in SMD and shifted to SD-N for 2 h, and cell samples were observed by fluorescence microscopy. The images are representative pictures from single Z-sections. DIC, differential interference contrast. Bars, 2 μm.
(D) Quantificaiton of (C). 12 Z-section images were projected and the percentage of cells that contained GFP-Atg1 dots was determined. Standard deviation was calculated from three independent experiments.

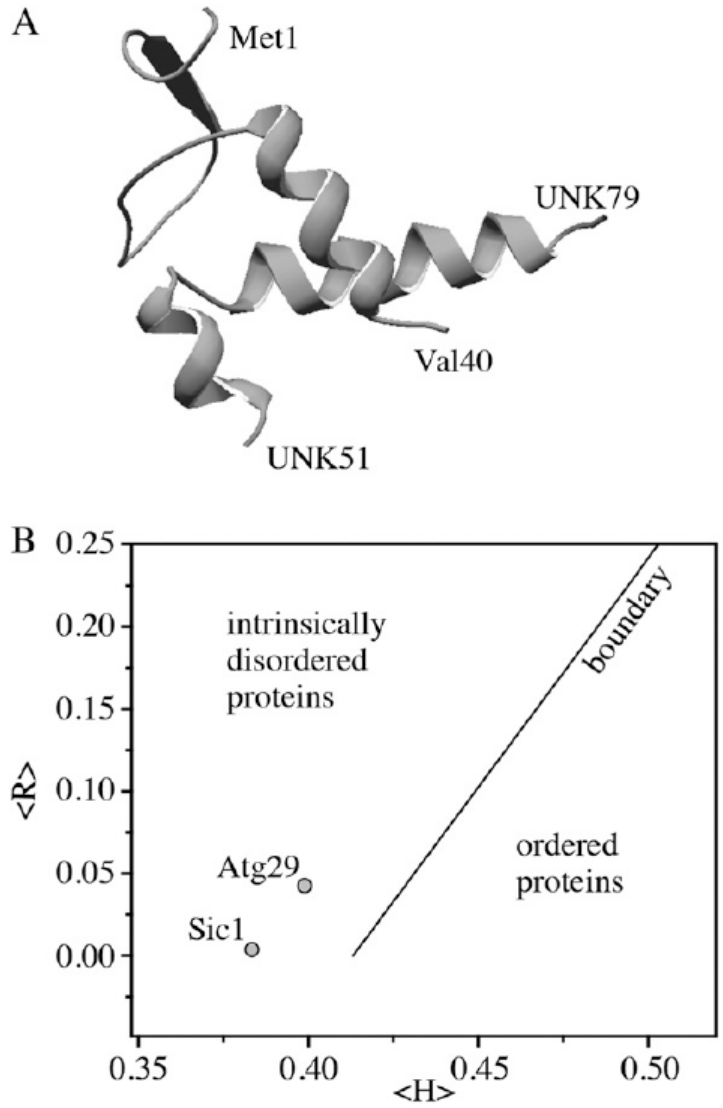

Figure 4.S1 Atg29 is an intrinsically disordered protein (IDP).
(A) Ribbon model of Atg29 [Protein Data Bank (PDB) ID code 4HPQ]. End residues on secondary structure elements are labeled. UNK, unknown.
(B) Charge-hydrophobicity (CH) plot shows the mean net charge <R> as a function of the mean hydrophobicity <H>. Solid line marks the boundary that separates ordered (globular) proteins from intrinsically disordered proteins. Plot shows the position of Atg29 relative to the boundary and the position of the recently characterized IDP Sic1 from *Saccharomyces cerevisiae* (147).

Chapter 5

The progression of peroxisomal degradation through autophagy requires peroxisomal division[4]

5.1 Abstract

Peroxisomes are highly dynamic organelles that have multiple functions in cellular metabolism. To adapt the intracellular conditions to the changing extracellular environment, peroxisomes undergo constitutive segregation and degradation. The segregation of peroxisomes are mediated by two dynamin-related GTPases, Dnm1 and Vps1, whereas, the degradation of peroxsisomes is accomplished through pexophagy, a selective type of autophagy. During pexophagy, the size of the organelle is always a challenging factor for the efficiency of engulfment by the sequestering compartment, the phagophore, which implies a potential role for peroxisomal fission in the degradation process, similar to the situation with selective mitochondria degradation. In this study, we report that peroxisomal fission is indeed critical for the efficient elimination of the organelle. When pexophagy is induced, both Dnm1 and Vps1 are recruited to the degrading peroxisomes through interactions with Atg11 and Atg36. In addition, we find that specific peroxisomal fission, which is only needed for pexophagy, occurs at mitochondria-peroxisome contact sites.

5.2 Introduction

In most eukaryotic cells, mitochondria and peroxisomes drive the catabolism of long chain fatty acids through β-oxidation, and convert the hydrogen peroxide into water and oxygen; in yeasts, this process is restricted

4 Submitted to *Autophagy* (under revision) with authors listed as Kai Mao*, Xu Liu*, Yuchen Feng and Daniel J. Klionsky (* denotes equal contribution).

to peroxisomes. One byproduct of β-oxidation is the production of reactive oxygen species that have the potential to damage cellular components. Therefore, it is essential that proper peroxisomal function is maintained, and that these organelles are removed if damaged or no longer needed. To adapt to the changing extracellular environment, peroxisomes undergo a remarkable remolding of their cellular pattern of expression, morphology, and abundance. Peroxisomes achieve this dynamic property through biogenesis, division, and degradation. Budding from the endoplasmic reticulum (ER) appears to be one source of the peroxisome membrane, which is generated in a Pex3- and Pex19-dependent manner; however, the organelle may be primarily generated through fission of a preexisting peroxisome followed by import of additional membrane and proteins (160). The proliferation and replication of peroxisomes that is achieved by division is under the control of two dynamin-related GTPases, Dnm1 and Vps1 (160, 161). Superfluous, or extensively damaged peroxisomes are targeted for vacuole-dependent degradation through selective autophagy, which is termed pexophagy (127, 162).

Autophagy is a conserved lysosome/vacuole-dependent catabolic pathway degrading cytosol, protein aggregates, and organelles. Depending on the extracellular stresses and the degrading targets, autophagy can occur in either nonselective or selective modes. Nonselective autophagy mediates bulk degradation and recycling of cytoplasm to support cell survival during nutrient deprivation (47, 48). Selective autophagy recognizes and targets specific cargos or organelles, such as peroxisomes (pexophagy) and mitochondria (mitophagy) (163).

After a decade of study, a general model has been established for selective autophagy. A ligand on the degrading target binds to a specific receptor; the receptor in turn recruits a scaffold protein, which links the cargo-receptor complex with the autophagy machinery (51). In yeast, Atg11 is the scaffold and its binding receptor varies depending on the degrading cargos. In the case of pexophagy, Atg36 serves as the receptor in *Saccharomyces cerevisiae*, and

PpAtg30 in *Pichia pastoris*; Pex3 functions as the ligand, binding to either Atg36 or ppAtg30 (65, 66). The receptor Atg36 binds to Atg11, a scaffold, which will promote the attachment of the degrading peroxisomes with Atg8–PE, and subsequent engulfment of the organelles by the phagophore, the initial sequestering compartment. We recently showed that when mitophagy is induced, the Atg11 scaffold is recruited by the mitophagy receptor Atg32, and in turn links the fission complex containing Dnm1 to those mitochondria that are destined for degradation to drive their division (164). Similar to mitochondria, the size of peroxisomes also makes it problematic to sequester this organelle by the phagophore, leading us to hypothesize that peroxisomal fission is necessary for pexophagy.

Here, we show that the two dynamin-related GTPases Dnm1 and Vps1 are important for pexophagy. The scaffold protein Atg11 interacts with both Dnm1 and Vps1 with the Atg11-Dnm1 interaction occurring on both mitochondria and peroxisomes, whereas the Atg11-Vps1 interaction takes place exclusively on peroxisomes. Unlike the mitophagy receptor Atg32, the pexophagy receptor Atg36 is able to interact directly with Dnm1 and Vps1, and these interactions occur on the peroxisomes. Importantly, these interactions represent the process of pexophagy-specific fission, which always occurs at mitochondria-peroxisome contact sites.

5.3 Results

5.3.1 Peroxisomal fission is a significant step during pexophagy.

In *Saccharomyces cerevisiae*, peroxisomes proliferate with increasing number and size when cells are cultured in growth medium containing oleic acid as the sole carbon source. When these cells are subjected to conditions of nitrogen starvation in the presence of glucose, this elevated population of peroxisomes is no longer necessary, and pexophagy is dramatically induced to degrade the excess organelles (127). To track the state and morphology of peroxisomes during pexophagy, we transformed a plasmid expressing the blue

fluorescent protein (BFP) fused with a C-terminal type I peroxisomal targeting signal, serine-lysine-leucine (BFP-SKL) (11). When yeast cells were cultured in nutrient rich medium with oleic acid (YTO), punctate peroxisomes appeared in the cytosol (Figure 5.1A, left). After we shifted the cells to nitrogen starvation medium with glucose (SD-N) for 2 h, which we have previously shown induces pexophagy (127), the morphology of some peroxisomes changed and displayed an elongated pattern (Figure 5.1A, right). The elongation of peroxisomal membrane precedes the division of these organelles, which is significant for their replication and proliferation (161). The occurrence of peroxisomal elongation under pexophagy-inducing conditions implied that the fission event also happened during the degradation of peroxisomes. Accordingly, we asked whether fission plays an important role for the progression of pexophagy.

The division of peroxisomes in budding yeast is mediated by two dynamin-related GTPases, Dnm1 and Vps1. Dnm1 is able to constrict membrane, and its proper function and localization on the peroxisomes requires a fission complex, which also includes Fis1, Mdv1, and Caf4 (129). Fis1 is a tail-anchored membrane receptor that interacts with the partially redundant proteins Mdv1 and Caf4, which in turn bind to Dnm1, to recruit the latter to the peroxisome. This fission complex is shared with mitochondria, and promotes mitochondrial fission through the same mechanism of Dnm1 recruitment (102, 161). Vps1 also controls the segregation of peroxisomes, and is recruited to the peroxisomes through interaction with Pex19 (165).

In order to detect and quantify the number of peroxisomes during pexophagy, we used a plasmid containing a green fluorescent protein with the C-terminal type I peroxisomal targeting signal (GFP-SKL) and CellTracker Blue CMAC dye to mark the peroxisomes and vacuole lumen, respectively. The *atg1*Δ mutant served as a control, since autophagy induction and peroxisomal degradation are completely absent in the *atg1*Δ mutant. When the yeast cells were grown in YTO medium, wild-type and *atg1*Δ mutant cells had

approximately 11.5 and 12.3 peroxisomes on average per cell, respectively (Figure 5.1C); however, there were fewer peroxisomes in *fis1*Δ (9.2/cell) and *dnm1*Δ (8.3/cell) mutants (Figure 5.2B and C), which is consistent with the previous report that the replication of peroxisomes is compromised in these mutants (128). In *vps1*Δ and *dnm1*Δ *vps1*Δ mutants, peroxisomes are highly clustered making it difficult to differentiate and quantify individual peroxisomes (Figure 5.1B). After the wild-type cells were starved in SD-N medium for 7 h, peroxisomes were degraded in the vacuole, however, the fluorescent signal from GFP-SKL was relatively stable and was diffuse in the vacuolar lumen; at the same time, the number of peroxisomes in the cytosol was largely decreased (corresponding to 56.4% turnover). In *fis1*Δ and *dnm1* mutants, a vacuolar GFP signal was also detected, but a reduced number of peroxisomes (39.1% and 35.3%, respectively) were degraded (Figure 5.1B and C), which indicated that pexophagy was partially blocked in these two mutants. In *atg1*Δ, *vps1*Δ and *dnm1*Δ *vps1*Δ mutants, no vacuolar GFP was detected, which implied that pexophagy was completely absent in these mutants (Figure 5.1B). However, as noted above, peroxisomes were largely clustered in the *vps1*Δ and *dnm1*Δ *vps1*Δ mutants (Figure 5.1B), making the quantification of peroxisomal degradation difficult.

To confirm the pexophagy defects in fission mutants, and to more precisely evaluate the pexophagy activities in *vps1*Δ and *dnm1*Δ *vps1*Δ mutants, we took advantage of a second method for monitoring pexophagy, the Pex14-GFP processing assay. *PEX14* encodes a peroxisomal integral membrane protein, and a chromosomally tagged version with GFP at the C terminus is correctly localized on this organelle. When pexophagy is induced, peroxisomes, along with Pex14-GFP, are delivered into the vacuole for degradation. Pex14 is proteolytically degraded, whereas the GFP moiety is relatively stable and accumulates in the vacuolar lumen. Thus, pexophagy can be monitored based on the amount of free GFP by immunoblot (118). After 1 or 2 h of nitrogen starvation with glucose, a considerable amount of free GFP was detected in

wild-type cells; however, the amount of free GFP was dramatically reduced in *fis1*Δ, *dnm1*Δ and *vps1*Δ mutants, and was almost completely absent in double *dnm1*Δ *vps1*Δ mutants (Figure 5.1D). In agreement with this observation, the decrease of intact (i.e., full-length) Pex14-GFP was apparent in wild-type, *fis1*Δ, and *dnm1*Δ mutant cells, but hardly detectable in the *vps1*Δ and *dnm1*Δ *vps1*Δ mutants (Figure 5.1D). These results suggested that both Dnm1-dependent and Vps1-dependent peroxisomal fission are important for pexophagy, with Vps1 playing a more significant role.

5.3.2 Atg11 interacts with Dnm1 and Fis1 on the degrading peroxisomes.

In growing yeast cells, Atg11 is mostly diffuse in the cytosol; its translocation to various organelles depends on the presence of different receptor proteins. Our recent studies showed that upon translocation to mitochondria through binding to Atg32, Atg11 recruits the Dnm1-containing fission complex to these mitochondria that are being targeted for degradation by mitophagy (164). The Atg11-bound population of Dnm1, which is specific for fission associated with mitophagy, is different from the previously characterized Atg11-free Dnm1, which controls homeostatic mitochondrial division. Pexophagy and mitophagy share the use of the Atg11 scaffold and the Dnm1-containing fission complex. Accordingly, we speculate that Atg11 is also able to recruit the Dnm1-containing fission complex to peroxisomes to facilitate their division prior to pexophagy.

To test this hypothesis, we used the bimolecular fluorescence complementation (BiFC) assay to determine where the Atg11-Dnm1 interaction occurs. Briefly, in the BiFC assay, the Venus yellow fluorescent protein (vYFP) is split into two fragments, VN (N terminus of vYFP) and VC (C terminus of vYFP) (119). We fused VN to Atg11 on the genome and transformed cells with a plasmid containing Dnm1-VC. Fluorescence from these two chimeras can only be detected when the two proteins interact and bring the two fragments of vYFP proximal to each other. Thus, for example,

when mitophagy is induced, VN-Atg11 and Dnm1-VC form vYFP puncta on the mitochondrial network (164). We carried out the same strategy and also introduced a C-terminal mCherry at the *PEX14* locus on the chromosome to be able to monitor peroxisomes. When we starved the yeast cells to induce pexophagy, the Atg11-Dnm1 interacting puncta colocalized with Pex14-mCherry (Figure 5.2A, arrowhead), which indicated that Atg11 recruited Dnm1 to the degrading peroxisomes when pexophagy was induced.

Atg11 and the Dnm1-containing fission complex are shared by peroxisomes and mitochondria. To carefully analyze the location of Atg11-Dnm1 interaction, we transformed a plasmid harboring BFP-SKL to display peroxisomes and stained the mitochondria with MitoTracker Red dye. After pexophagy was induced by nitrogen starvation with glucose, the localization of Atg11-Dnm1 interacting puncta could be classified into three different classes. The class I puncta appeared on the mitochondrial network (Figure 5.2B, arrow), and thus correspond to complexes that are involved in mitophagy-specific fission (164). Mitophagy is highly induced when yeast are grown solely in the presence of a non-fermentable carbon source and then switched to nitrogen starvation medium containing a fermentable carbon source (58). Because oleic acid is a non-fermentable carbon source, these culture conditions (i.e., switching from YTO to SD-N) likely induce mitophagy. Class II puncta were localized on peroxisomes (Figure 5.2B, arrowhead), and are presumed to represent the fission complexes that mediate pexophagy-specific fission. Unexpectedly, these puncta were found to be proximal to mitochondria. The class III puncta colocalized with both peroxisomes and mitochondria (Figure 5.2B, asterisk). The cellular pattern of both class II and class III puncta implied the Dnm1-mediated peroxisomal fission might occur at the mitochondria-peroxisome contact sites.

To test this hypothesis, we also examined the sites of the Atg11-Fis1 interaction. Based on our previous work, Atg11 interacts with Fis1 in addition to Dnm1 on the targeted mitochondria (164). We chromosomally tagged *ATG11*

and *FIS1* with VN and VC, respectively, and used BFP-SKL and MitoTracker Red to track peroxisomes and mitochondria, respectively. The distribution of Atg11-Fis1 puncta was extremely similar to that of Atg11-Dnm1 puncta, with the existence of distinct populations localized to mitochondria (Figure 5.2C, arrow), peroxisomes that were proximal to mitochondria (Figure 5.2C, arrowhead), and puncta localized on both organelles (Figure 5.2C, asterisks). Of note, the peroxisomes marked by the Atg11-Fis1 interaction were always close to or associated with mitochondria. After the analysis of both Atg11-Dnm1 and Atg11-Fis1 puncta, we concluded that Atg11 recruited Dnm1-containing fission complexes to peroxisomes being targeted for degradation, and this fission event happened at mitochondria-peroxisome contact sites. We propose that this distinct localization might be due to the fact that mitochondria and peroxisomes share the Dnm1-containing fission complex.

5.3.3 Atg11 interacts with Vps1 on peroxisomes.

We noticed that compared to Dnm1 inhibition of the Vps1-mediated peroxisomal fission had a stronger effect on pexophagy (Figure 5.1B and D). Therefore, we wondered if there is also an Atg11-bound form of Vps1, which localizes on the peroxisomes that will become targeted for sequestration and regulates pexophagy-specific division. We chromosomally tagged *ATG11* with VN and *PEX14* with mCherry, and transformed the cells with a plasmid expressing Vps1-VC. VN-Atg11 and Vps1-VC formed puncta in pexophagy-inducing conditions, and these puncta localized on the peroxisomes marked by Pex14-mCherry (Figure 5.3A, arrowhead).

To verify the interaction between Atg11 and Vps1, we carried out protein A affinity isolation with IgG-Sepharose. In our previous work, we showed that the Dnm1 mutant lacking the last 30 amino acids [Dnm1 (30Δ)] is unable to interact with Atg11. The C terminus of Vps1 has a high similarity at the amino acid sequence level compared to Dnm1. We suspected that the Vps1 mutant

lacking the last 30 amino acids [Vps1 (30Δ)] would also lose interaction with Atg11. Protein A (PA)-tagged wild-type Vps1 co-precipitated a substantial amount of the available HA-Atg11, whereas Dnm1 (30Δ) precipitated a very small amount of this protein (Figure 5.3B). In contrast to our expectation, Vps1 (30Δ) precipitated a similar level of HA-Atg11 relative to that affinity isolated by wild-type (i.e., full length) Vps1. Therefore, Vps1 interacts with Atg11 through a different mechanism from the one used by Dnm1.

We showed that the Dnm1-regulated peroxisomal division occurred extremely close to mitochondria (Figure 5.2B), which we propose may be due to the fact that the Dnm1-containing fission complex is shared by mitochondria and peroxisomes. Up until now, there have not been any published data indicating a role for Vps1 in mitochondria segregation. Accordingly, we decided to determine whether Vps1-mediated peroxisomal fission, in contrast to that driven by Dnm1, occurred at a site that was distal from mitochondria. We transformed cells with the BFP-SKL plasmid and used MitoTracker Red to allow us to monitor both peroxisomes and mitochondria, respectively. Puncta corresponding to the sites of Atg11-Vps1 interaction did not appear to localize directly on the mitochondrial network; however, the peroxisomes marked by these puncta were still closely associated with mitochondria (Figure 5.3C, arrowhead). This result suggested that pexophagy-specific fission, whether mediated by Dnm1 or Vps1, might require the participation of mitochondria.

5.3.4 Atg36 interacts with Dnm1 and Vps1.

Atg32 and Atg36 are receptors that bind to Atg11 during mitophagy and pexophagy, respectively; however, their properties vary in several respects. For example, overexpression of Atg36 results in a high level of basal pexophagy independent of nitrogen starvation, whereas overexpression of Atg32 does not induce mitophagy in nutrient-rich conditions (59, 66). Atg32 is localized on the mitochondrial outer membrane and interacts with the Dnm1-containing fission complex through Atg11. In contrast, Atg36 is a

cytosolic protein and is targeted to peroxisomes through binding to Pex3 (59, 66), which raises the possibility that Atg36 is also able to interact with Dnm1 or Vps1, which are also cytosolic proteins, to recruit the fission complex to peroxisomes; this would be in contrast to Atg32, which binds Dnm1 indirectly through Atg11.

To test this hypothesis, and to gain further insight into the mechanism of Vps1-mediated pexophagy, we generated a series of strains expressing VN-Atg36 combined with Dnm1-VC, VC-Fis1, Mdv1-VC, Caf4-VC, or Vps1-VC, and carried out the BiFC assay to search for the possible interactions of these chimeric pairs. VN-Atg36 formed vYFP puncta with Dnm1-VC, or Vps1-VC, but not with the other fusion proteins (Figure 5.4A). Therefore, unlike Atg32, Atg36 interacts with the two dynamin-related GTPases Dnm1 and Vps1.

To determine where Atg36 interacts with Dnm1 and Vps1, we used BFP-SKL and MitoTracker Red to track peroxisomes and mitochondria, respectively. Both Atg36-Dnm1 and Atg36-Vps1 interacting puncta were localized on peroxisomes extremely close to mitochondria (Figure 5.4B and C, arrowheads). This location was similar to that seen for Atg11-Dnm1, Atg11-Fis1, and Atg11-Vps1, which reinforced our finding that the pexophagy-specific fission happened at the mitochondrial periphery.

5.4 Discussion

The degradation of organelles is an energy and time consuming process in eukaryotic cells. In addition, the size of the organelle can present steric challenges, and smaller fragments of organelles are presumably easier for sequestering. Autophagy is the primary mechanism responsible for the bulk degradation of cytoplasmic components and the selective removal of organelles. In nonselective autophagy, the protein level of Atg8 controls the size of the autophagosomes (123). In contrast, during selective types of autophagy the phagophore membrane is closely apposed to the cargo, excluding bulk cytoplasm. Therefore, the factors that determine the curvature

of the phagophore and the ultimate size of the autophagsomes might be more somewhat distinct between these two modes of sequestration. The cytoplasm-to-vacuole targeting (Cvt) pathway is a biosynthetic route that delivers resident hydrolases to the vacuole. Overexpression of the primary cargo of the Cvt pathway, precursor aminopeptidase I, results in the formation of larger complexes, which are sequestered less efficiently (53). Mitochondria exist as a highly extended, reticular structure, which is even more difficult for sequestering within phagophores. Our recent work suggested that during mitophagy a selective and specific fission event occurs on the mitochondria that will become substrates for degradation (164). Although the peroxisomes may be dispersed in the cytosol as individual compartments, the size of this organelle appears to be close to the limit for sequestration by smaller phagophores, such as those generated in the absence of Atg17 (134). This may be a particular problem after these organelles proliferate following growth in an oleic acid-containing medium. Therefore, we hypothesized that peroxisomes have to divide prior to degradation, and that only the small fragments of the peroxisomes would be targeted by autophagy.

Here, we showed that deletion of the *DNM1* and *VPS1* genes, which encode two dynamin-related GTPases, resulted in substantially lower efficiency of peroxisomal degradation. Previous work indicated that even though the amino acid sequences of Dnm1 and Vps1 are quite similar, deletion of either individual gene has different effects on peroxisomal division. Deletion of *VPS1* dramatically abolishes peroxisomal fission when yeast cells are cultured in both glucose and oleic acid media. However, deletion of *DNM1* affects the division of peroxisomes only in oleic acid, and the defect is not as strong as that of the *vps1*Δ mutant (128). Consistent with these results, pexophagy is significantly blocked in a *vps1*Δ strain, whereas there was only an intermediate affect in the *dnm1*Δ mutant (Figure 5.1B and D). Overall, it is clear that peroxisomal fission, whether mediated by Dnm1 or Fis1, is important for pexophagy, which is in agreement with our hypothesis.

As a scaffold protein, Atg11 binds to a variety of cargo receptors to mediate different types of selective autophagy. For example, Atg11 binds to Atg19, to Atg32 and to Atg36 for cargo selection during the Cvt pathway, mitophagy and pexophagy, respectively (11, 56, 59, 66, 125). Atg11 also interacts with Atg1 and Atg17, which connects the step of cargo selection to the initiation of autophagosome formation (125). Here, and with our previous work, we add a new piece to the puzzle: during pexophagy and mitophagy, Atg11 recruits the fission machineries to the organelles and promotes their specific segregation, resulting in smaller fragments of these compartments that can be easily degraded.

It is surprising that the pexophagy-specific fission, mediated either by Dnm1 or Vps1, is always occurring in proximity to mitochondria. The division of mitochondria requires the participation of the ER (120), and the fission of peroxisomes apparently involves mitochondria. The crosstalk that occurs between organelles is attracting increasing attention. The peroxisome represents an interesting organelle to study in this regard, having connections with the ER, the mitochondria, and the vacuole.

5.5 Materials and methods

Strains, media, and growth conditions. Yeast strains used in this study are listed in Table 5.1. Yeast cells were grown in rich (YPD; 1% yeast extract, 2% peptone, and 2% glucose) or synthetic minimal (SMD; 0.67% yeast nitrogen base, 2% glucose, and auxotrophic amino acids and vitamins as needed) media. For peroxisomal proliferation, cells were grown in YPD to approximately 0.5 OD_{600} and shifted to glycerol medium (SGd; 0.67% yeast nitrogen base, 0.1% glucose, and 3% glycerol) for 16 h. The cells were then incubated for 4 h with the addition of yeast extract and peptone into the SGd medium. The cells were ultimately shifted to oleic acid medium (YTO; 0.67% yeast nitrogen base, 0.1% oleic acid, 0.1% Tween 40 and auxotrophic amino acids as needed) for 20 h. Pexophagy was induced by shifting the cells to

nitrogen starvation medium containing glucose (SD-N; 0.17% yeast nitrogen base without ammonium sulfate or amino acids, and 2% glucose).

Plasmids. pBFP-SKL(405), pCuGFP-SKL(416), pCuHA-Atg11(416) and pDnm1-VC(416) have been reported previously.(11, 59, 164) For constructing pVps1-VC(416), the *DNM1* promoter and ORF were removed by XbaI and XmaI from pDnm1-VC(416), the resulting linearized vector was ligated in the presence of the DNA fragment containing the *VPS1* promoter and ORF, which was amplified by PCR from the genome of the yeast strain SEY6210 and digested with XbaI and XmaI.

Fluorescence microscopy. For fluorescence microscopy, yeast cells were grown as described above to induce peroxisome proliferation and shifted to SD-N for nitrogen starvation. Samples were then examined by microscopy (Delta Vision, Applied Precision) using a 100x objective and pictures were captured with a CCD camera (CoolSnap HQ; Photometrics). For each microscopy picture, 12 Z-section images were captured with a 0.3-μm distance between two neighboring sections. MitoTracker Red CMXRos (Molecular Probes/Invitrogen, M7512) was used to stain the mitochondria.

Additional assay and reagents. Immunoprecipitation was performed as described previously (59). Immunoprecipitation was carried out with monoclonal anti-YFP antibody clone JL-8 (Clontech, 632381), monoclonal anti-HA antibody clone-HA7 (Sigma-Aldrich, H3663), and an antibody that binds to protein A with high affinity (no longer commercially available).

5.6 Acknowledgements

This work was supported by NIH grant GM053396 to DJK, and by a University of Michigan Rackham Predoctoral Fellowship to KM.

Table 5.1 Yeast strain list.

Name	Genotype	Reference
KDM1103	SEY6210 *PEX14-GFP::KAN dnm1Δ::LEU2*	This study
KDM1104	SEY6210 *PEX14-GFP::KAN fis1Δ::LEU2*	This study
KDM1105	SEY6210 *PEX14-GFP::KAN vps1Δ::HIS5*	This study
KDM1249	SEY6210 *atg11Δ::LEU2 DNM1(C30Δ)-PA::HIS3*	(164)
KDM1252	SEY6210 *dnm1Δ::LEU2*	(164)
KDM1269	SEY6210 *atg11Δ::LEU2 VPS1-PA::HIS3*	This study
KDM1545	SEY6210 *RPL7Bp-VN-ATG11::TRP1 RPL7Bp-VC-FIS1::HIS3*	(164)
KDM1535	SEY6210 *RPL7Bp-VN-ATG11::TRP1*	(164)
SEY6210	MATα *leu2-3,112 ura3-52 his3-Δ200 trp1-Δ901 suc2-Δ9 lys2-801; GAL*	(101)
TKYM67	SEY6210 *PEX14-GFP::KAN*	(118)
WHY1	SEY6210 *atg1Δ::HIS5*	(166)
XLY049	SEY6210 *pRS405-BFP-SKL::LEU2*	This study
XLY059	SEY6210 *PEX14-GFP::KAN dnm1Δ::LEU2 vps1Δ::HIS5*	This study
XLY060	SEY6210 *fis1Δ::LEU2*	This study
XLY061	SEY6210 *vps1Δ::LEU2*	This study
XLY062	SEY6210 *dnm1Δ::LEU2 vps1Δ::HIS5*	This study
XLY063	SEY6210 *RPL7Bp-VN-ATG36::TRP1*	This study
XLY064	SEY6210 *RPL7Bp-VN-ATG36::TRP1 RPL7Bp-VC-FIS1::KAN*	This study
XLY065	SEY6210 *RPL7Bp-VN-ATG36::TRP1 CAF4-VC::KAN*	This study
XLY066	SEY6210 *RPL7Bp-VN-ATG36::TRP1 MDV1-VC::KAN*	This study
XLY067	SEY6210 *RPL7Bp-VN-ATG11::TRP1 pRS405-BFP-SKL::LEU2*	This study
XLY068	SEY6210 *RPL7Bp-VN-ATG11::TRP1 RPL7Bp-VC-FIS1::KAN pRS405-BFP-SKL::LEU2*	This study
XLY069	SEY6210 *RPL7Bp-VN-ATG36::TRP1 pRS405-BFP-SKL::LEU2*	This study
XLY070	SEY6210 *RPL7Bp-VN-ATG11::TRP1 PEX14-mCherry::KAN*	This study
XLY072	SEY6210 *ATG36-VN::HIS3 pRS405-BFP-SKL::LEU2*	This study
XLY073	SEY6210 *atg11Δ::LEU2 VPS1(C30Δ)-PA::HIS3*	This study
YTS147	SEY6210 *atg11Δ::LEU2*	(58)

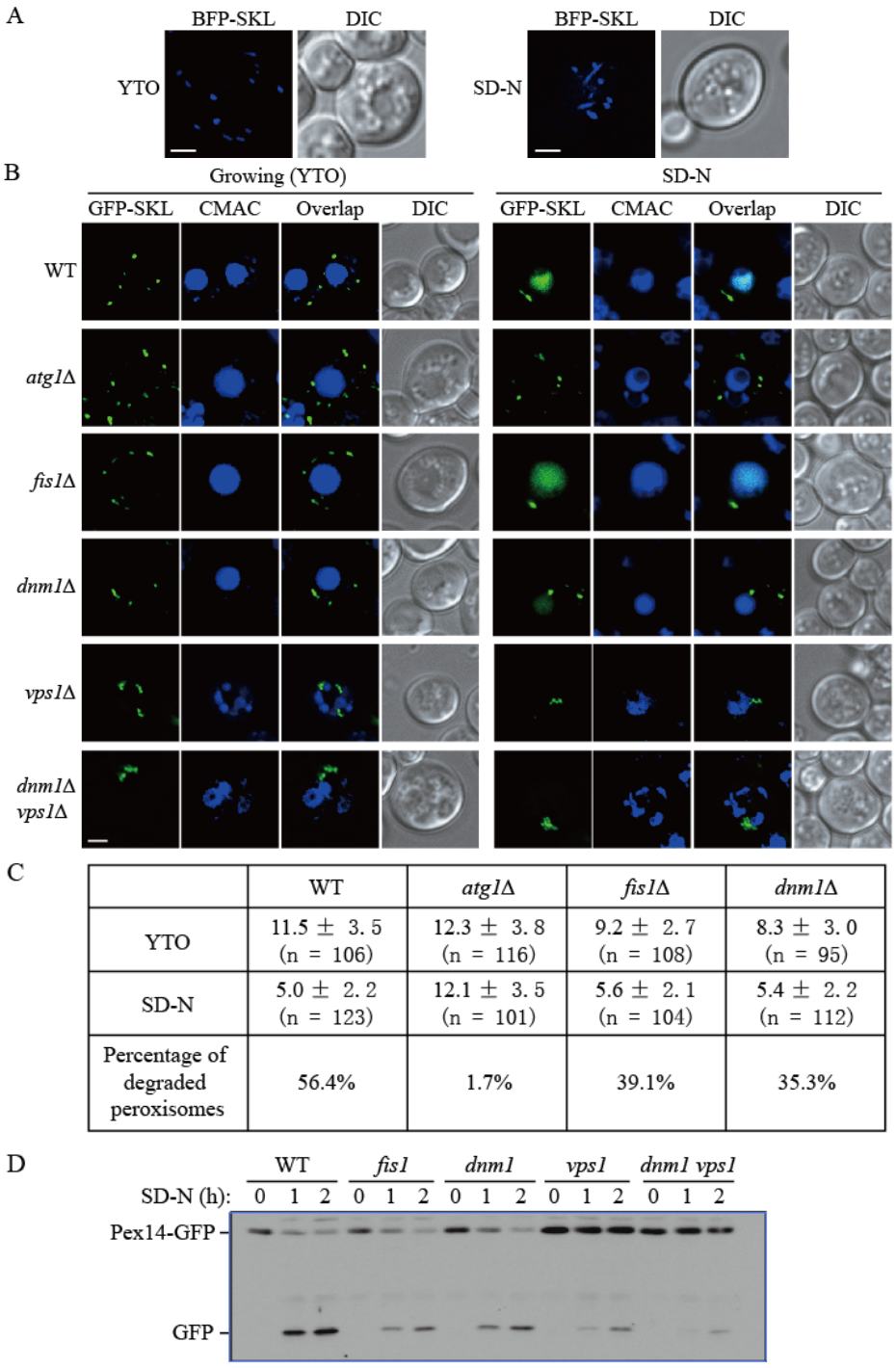

Figure 5.1 Peroxisomal fission is required for pexophagy.
(A) Wild-type yeast cells, transformed with pBFP-SKL (XLY049), were cultured in YTO as described in Materials and Methods to induce peroxisome proliferation, and shifted to SD-N for 2 h.
(B) Wild-type (SEY6210), *atg1*Δ (WHY1), *dnm1*Δ (KDM1252), *fis1*Δ (XLY060), *vps1*Δ (XLY061), and *dnm1*Δ *vps1*Δ (XLY062) cells, transformed with pGFP-SKL, were cultured in YTO to induce peroxisome proliferation and shifted to SD-N for 7 h. CellTracker Blue CMAC was used to stain the vacuolar

lumen.
(C) Quantification of the numbers of peroxisomes in (B). 12 Z-section images were projected and the number of peroxisomes per cell was determined. Standard deviation was calculated from 3 independent experiments.
In (A) and (C), all of the images are representative pictures from single Z-sections. DIC, differential interference contrast. Scale bar, 2 μm.
(D) GFP was tagged at the C terminus of *PEX14* gene on the genome of wild-type (TKYM67), *dnm1*Δ (KDM1103), *fis1*Δ (KDM1104), *vps1*Δ (KDM1105), and *dnm1*Δ *vps1*Δ (XLY059) cells. These cells were cultured in YTO to induce peroxisome proliferation and shifted to SD-N for 1 and 2 h. Immunoblotting was done with anti-YFP antibody.

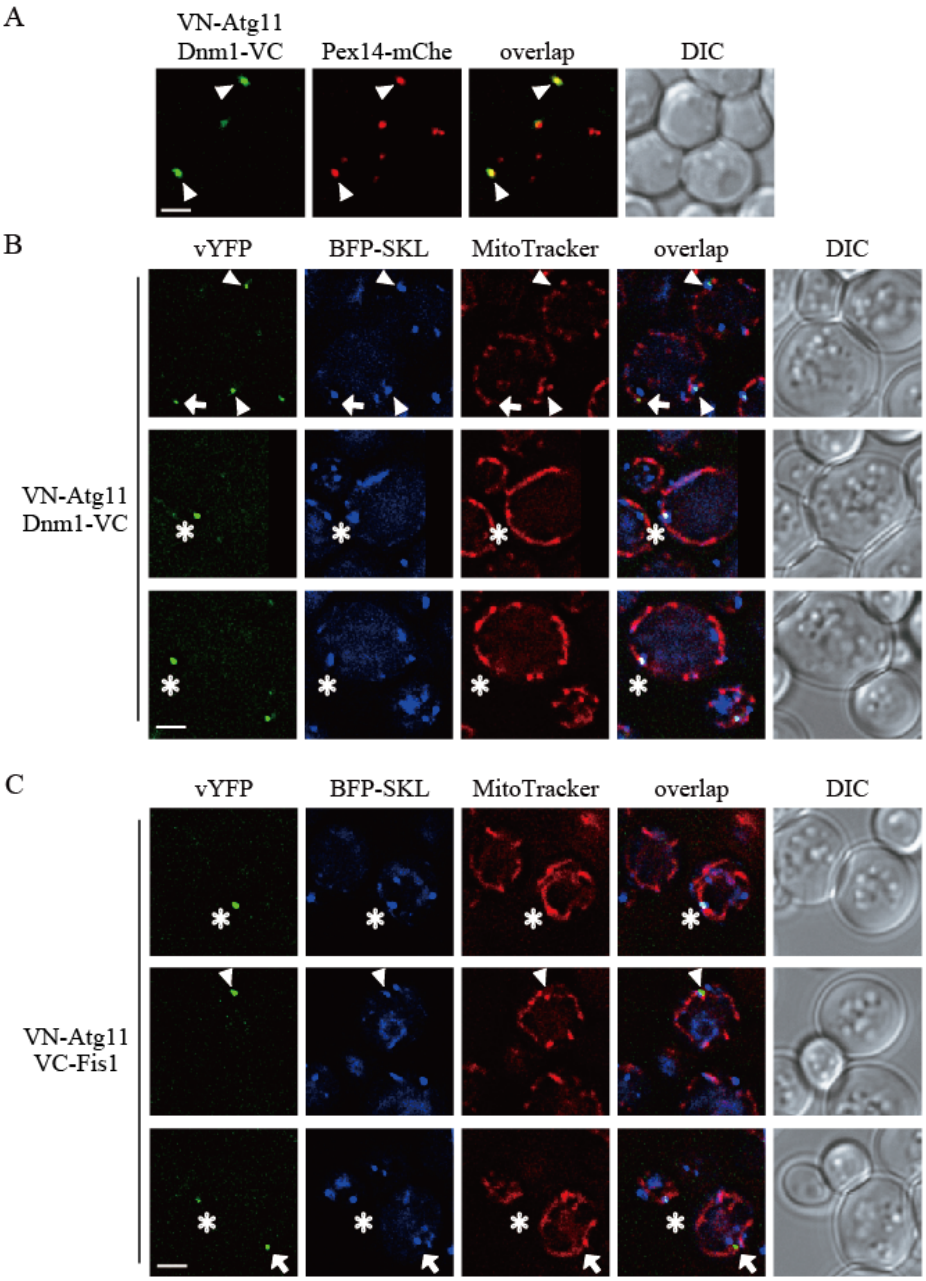

Figure 5.2 Atg11 recruits the Dnm1 fission complex to peroxisomes.
(A) *VN-ATG11 PEX14-mCherry* (Pex14-mChe; XLY070) cells, transformed with pDnm1-VC, were cultured in YTO to induce peroxisome proliferation and then shifted to SD-N for 1 h. The arrowheads mark colocalizing BiFC and mCherry puncta.
(B, C) The plasmids pBFP-SKL and pDnm1-VC were transformed into the *VN-ATG11* (KDM1535) cells used in (**B**). pBFP-SKL was transformed into *VN-ATG11 VC-FIS1* (KDM1545) cells in (**C**). The arrows mark BIFC puncta colocalizing with MitoTracker Red; arrowheads denote BiFC puncta colocalizing with peroxisomes that are proximal to mitochondria; asterisks indicate BiFC puncta colocalizing with both peroxisomes and mitochondria. Cells were cultured as described in the Materials and Methods to induce peroxisome proliferation and shifted to SD-N for 1 h. MitoTracker Red was

used to stain mitochondria.
In (A), (B) and (C), all of the images are representative pictures from single Z-sections. DIC, differential interference contrast. Scale bar, 2 μm.

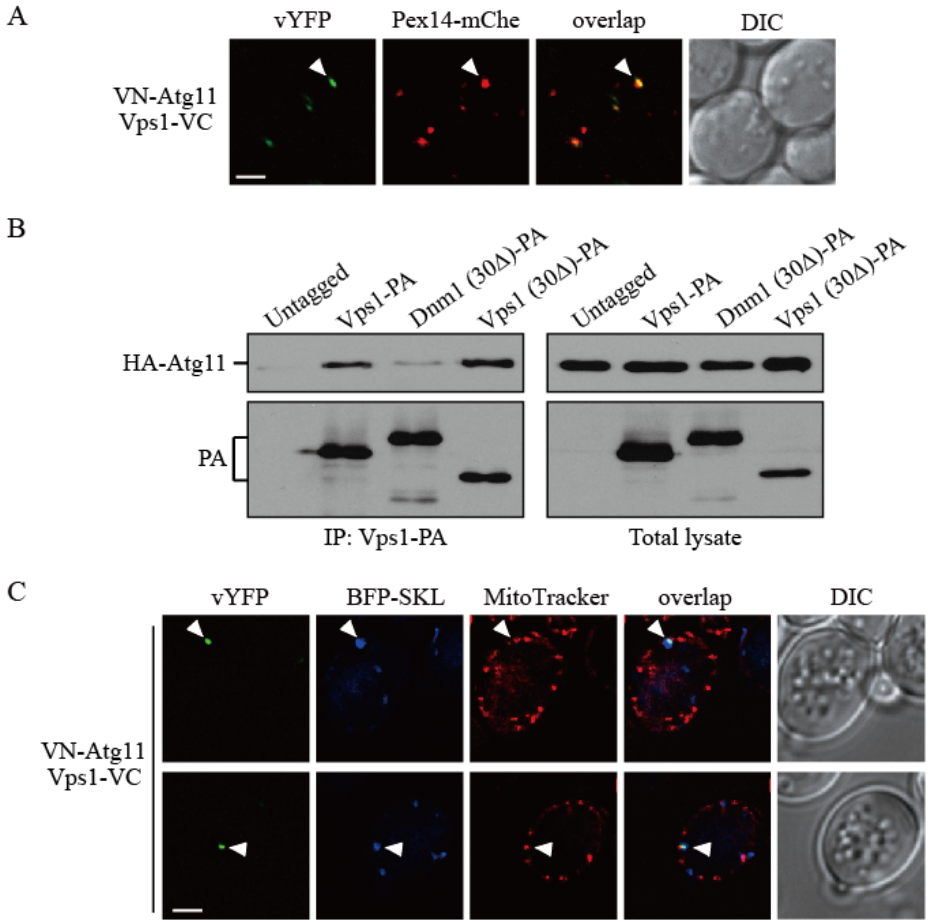

Figure 5.3 Atg11 recruits Vps1 to peroxisomes that are targeted for degradation.

(A) *VN-ATG11 PEX14-mCherry* (Pex14-mChe; XLY070) cells, transformed with pVps1-VC, were cultured in YTO to induce peroxisome proliferation and subsequently shifted to SD-N for 1 h.

(B) The plasmid pCuHA-Atg11 was transformed into *atg11*Δ (YTS147), *atg11*Δ *VPS1-PA* (KDM1269), *atg11*Δ *DNM1(C30*Δ*)* (KDM1249) cells, and *atg11*Δ *VPS1(C30*Δ*)* (XLY073). Cells were cultured in YTO to induce peroxisome proliferation and then shifted to SD-N for 2 h. Cell lysates were prepared and incubated with IgG-Sepharose for affinity isolation. The eluted proteins were separated by SDS-PAGE and detected with monoclonal anti-HA antibody and an antibody that binds to PA.

(C) The plasmids pBFP-SKL and pVps1-VC were transformed into *VN-ATG11* (KDM1535) cells. Cells were cultured in YTO to induce peroxisome proliferation and then shifted to SD-N for 1 h. MitoTracker Red was used to stain mitochondria.

In (A) and (C) all of the images are representative pictures from single Z-sections. DIC, differential interference contrast. Scale bar, 2 μm.

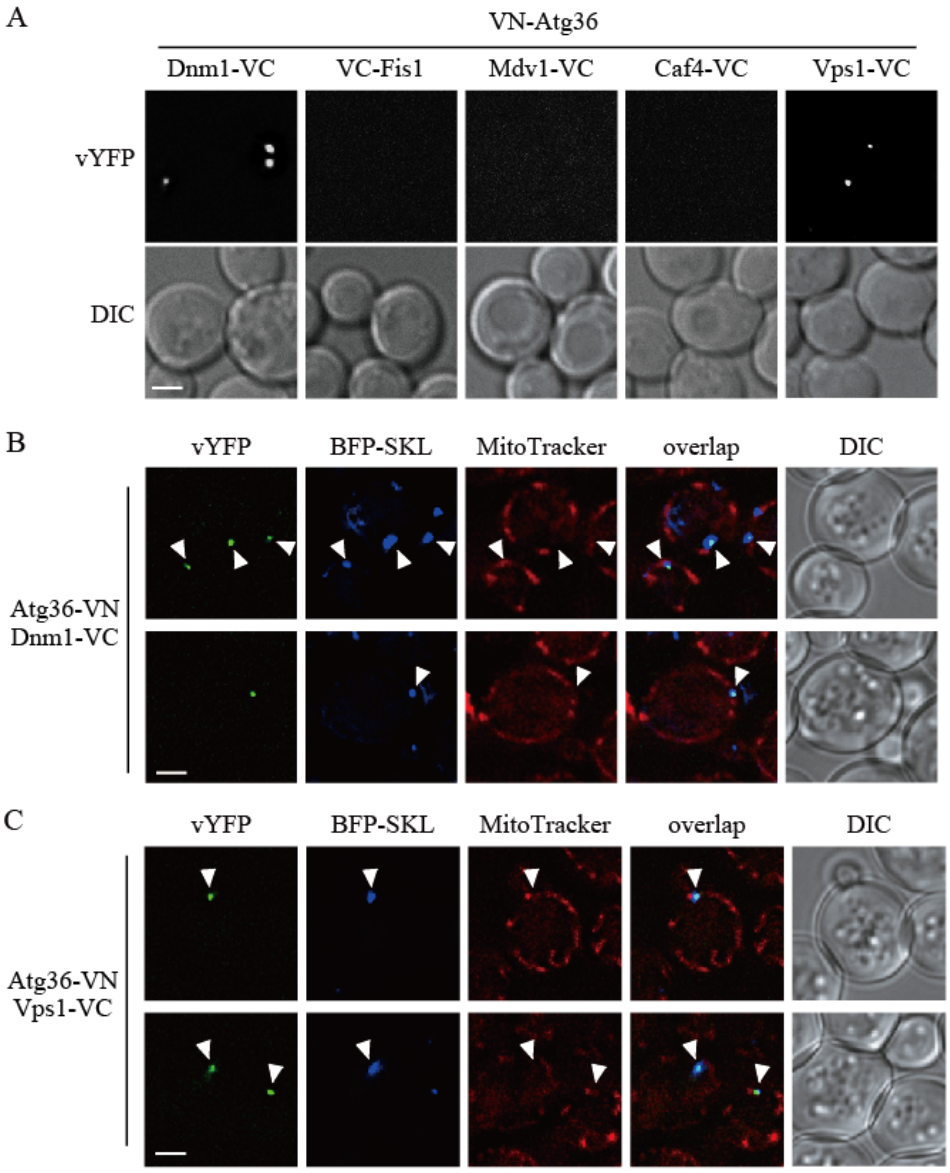

Figure 5.4 Atg36 interacts with both Dnm1 and Vps1 on the degrading peroxisomes.

(A) The plasmid pDnm1-VC or pVps1-VC was transformed into *VN-ATG36* (XLY063) cells. These cells together with cells from strains *VN-ATG36 VC-FIS1* (XLY064), *VN-ATG36 CAF4-VC* (XLY065), and *VN-ATG36 MDV1-VC* (XLY066) were cultured in YTO to induce peroxisome proliferation and then shifted to SD-N for 1 h.

(B, C) The plasmid pBFP-SKL and pDnm1-VC were transformed into *VN-ATG36* (XLY063) cells in (B), and pBFP-SKL and pVps1-VC were transformed into *VN-ATG36* (XLY063) cells in (C). Cells were cultured in YTO to induce peroxisome proliferation and then shifted to SD-N for 1 h. MitoTracker Red was used to stain mitochondria. In (A), (B), and (C), all of the images are representative pictures from single Z-sections. DIC, differential interference contrast. Scale bar, 2 μm.

Chapter 6
Conclusion and implications

Autophagy plays significant roles in a wide range of biological processes, including development, immune defense, programmed cell death, tumor suppression, and prevention of neuron degeneration. In this thesis, I describe several aspects of the molecular mechanisms of autophagy and mitophagy in *Saccharomyces cerevisiae*. In this chapter, I will summarize the key implications and discuss future directions.

6.1 Identification of the targets of MAPKs during mitophagy

Chapter 2 describes the roles of the MAPKs Slt2 and Hog1 during the process of mitophagy. In our study, even though both Slt2 and Hog1 are activated when cells are cultured in mitophagy-inducing conditions, the timing of activation is different; Slt2 is activated before Hog1, and plays a role in the recruitment of mitochondria destined for degradation to the phagophore assembly site. Thus, we suggest that Slt2 might be involved in an early stage of mitophagy, and Hog1 functions in a later stage.

Our further work reveals the origins of the two MAPK signaling pathways, which links the changes of extracellular environment to the intracellular adaption. The origins of the two signaling pathways are two plasma membrane-localized sensors, Wsc1 and Sln1. The involvement of proteins that are implicated in extracellular sensing is surprising to us, because mitophagy is likely to be induced by an intracellular signal. One explanation is that these plasma membrane sensors might also be able to respond to intracellular signals. For example, a previous report suggests that ER stress (i.e., an intracellular signal) activates the Slt2 signaling pathway through Wsc1 (plasma membrane-sensor), which is another example that supports our hypothesis

(94).

We were unable to identify the relevant targets of either Slt2 or Hog1 for mitophagy regulation. After we showed in Chapter 3 that the dynamin-related GTPase Dnm1 promotes mitophagy, I suspected that Slt2 might regulate mitophagy through phosphorylating and activating Dnm1 based on the following three reasons: First, the activities of the higer eukaryotic homologs of Dnm1 are mediated by several kinases, including mitogen-activated protein kinase 1/3 (MAPK1/3), protein kinase A (PKA), cyclin-dependent kinase 1 (CDK1), and calcium/calmodulin-dependent protein kinase I (CAMKI) (167-171). Of these kinases, MAPK1/3 shows high similarity with Slt2. Second, our results suggest that Slt2 regulates mitophagy through phosphorylating certain cytosolic protein(s) (Figure 2.3 A and B; Figure 2.5 C and D); and Dnm1 localizes in the cytosol and translocates to the mitochondria to promote this organelle's fission. Third, the timing of Dnm1's participation in mitophagy fits the timing of Slt2 activation (Figure 2.5 A and B; Figure 3.2C). Aside from this hypothesis, we also plan to screen the yeast genome to identify the targets of Slt2 and Hog1 based on stable isotope labeling by amino acids in cell culture (SILAC) combined with quantitative mass spectrometry (MS) (172).

6.2 Molecular and structural analysis of the Atg1 complex

Structural analysis is critical in obtaining detailed information about the molecular mechanisms in cellular events and the identification of potential drug targets. The structural information of Atg proteins is severely limited, and further study is necessary to obtain a comprehensive understanding of the Atg complexes.

Chapter 4 describes the function of Atg29 phosphorylation during autophagy induction and the structural information of the Atg17-Atg31-Atg29 protein complex. The Atg17-Atg31-Atg29 complex is a subcomplex of the Atg1 complex, which plays a key role in autophagy induction. Therefore, in order to gain more information about how the Atg1 complex mediates autophagy

initiation, the structure-function analysis of the intact Atg1 complex is necessary and will be one of our future aims.

The intact Atg1 complex consists of Atg1, Atg11, Atg13, Atg17, Atg29, and Atg31. We successfully purified the Atg17-Atg31-Atg29 complex and observed its structure by single particle electron microscopy. We plan to continue and purify the intact Atg1 complex.

The tandem affinity purification (TAP) tag consists of a calmodulin-binding peptide (CBP) and a protein A (ProtA) tag. When the TAP tag is chromosomally fused to the target gene, the expression of the gene will be controlled by its own promoter region and maintain the fusion protein at its native level. The fusion protein and its binding partners are recovered from cell extracts by affinity purification of ProtA with IgG beads (first step) and of CBP with calmodulin beads (second step). Our collaborator, Dr. Calvin K. Yip, recently generated the native At17-Atg31-Atg29 complex and analyzed its structure by single particle electron microscopy (173). We will continue the collaboration and purify the native Atg1 complex.

The most challenging part of TAP purification is to generate enough protein, especially considering that the expression levels of the corresponding genes are relatively low in yeast, as well as to maintain the intact complex without losing any of the subunits. Therefore, we also plan to purify each subunit separately from either yeast or *E. coli*, and rebuild the Atg1 complex *in vitro*.

Protein purification in *E. coli* is commonly used and known by most people; therefore, I will only introduce the method of protein purification in yeast. *GAL1* promoter-driven gene overexpression is a commonly used system in yeast. By integration of the *GAL1* promoter and a GST affinity tag into the target gene in the genome, the fusion protein will be highly overexpressed when yeast cells are grown in galactose-containing medium. Protein purification is conducted by the affinity of the GST tag for glutathione beads. In order to remove the GST tag after purification, a TEV protease recognition sequence will be introduced

between the target protein and the GST tag. Gel filtration will be applied to separate the final product. Other tags (polyHistidine, MBP, Myc) may also be used depending on the outcome.

Bibliography

1. Levine B & Klionsky DJ (2004) Development by self-digestion: molecular mechanisms and biological functions of autophagy. *Dev Cell* 6(4):463-477.
2. Shintani T & Klionsky DJ (2004) Autophagy in health and disease: a double-edged sword. *Science* 306(5698):990-995.
3. Munz C (2006) Autophagy and antigen presentation. *Cell Microbiol* 8(6):891-898.
4. Suzuki K*, et al.* (2001) The pre-autophagosomal structure organized by concerted functions of *APG* genes is essential for autophagosome formation. *EMBO J* 20(21):5971-5981.
5. Kim J, Huang W-P, Stromhaug PE, & Klionsky DJ (2002) Convergence of multiple autophagy and cytoplasm to vacuole targeting components to a perivacuolar membrane compartment prior to de novo vesicle formation. *J Biol Chem* 277(1):763-773.
6. Hamasaki M*, et al.* (2013) Autophagosomes form at ER-mitochondria contact sites. *Nature* 495(7441):389-393.
7. Reggiori F, Tucker KA, Stromhaug PE, & Klionsky DJ (2004) The Atg1-Atg13 complex regulates Atg9 and Atg23 retrieval transport from the pre-autophagosomal structure. *Dev Cell* 6(1):79-90.
8. Abeliovich H, Zhang C, Dunn WA, Jr., Shokat KM, & Klionsky DJ (2003) Chemical genetic analysis of Apg1 reveals a non-kinase role in the induction of autophagy. *Mol Biol Cell* 14(2):477-490.
9. Cheong H, Nair U, Geng J, & Klionsky DJ (2008) The Atg1 kinase complex is involved in the regulation of protein recruitment to initiate sequestering vesicle formation for nonspecific autophagy in *Saccharomyces cerevisiae*. *Mol Biol Cell* 19(2):668-681.
10. Kamada Y*, et al.* (2000) Tor-mediated induction of autophagy via an Apg1 protein kinase complex. *J Cell Biol* 150(6):1507-1513.
11. Kim J*, et al.* (2001) Cvt9/Gsa9 functions in sequestering selective cytosolic cargo destined for the vacuole. *J Cell Biol* 153(2):381-396.
12. Kabeya Y*, et al.* (2009) Characterization of the Atg17-Atg29-Atg31 complex specifically required for starvation-induced autophagy in *Saccharomyces cerevisiae*. *Biochem Biophys Res Commun* 389(4):612-615.
13. Cao Y, Nair U, Yasumura-Yorimitsu K, & Klionsky DJ (2009) A multiple ATG gene knockout strain for yeast two-hybrid analysis. *Autophagy* 5(5):699-705.
14. Kabeya Y*, et al.* (2005) Atg17 functions in cooperation with Atg1 and

Atg13 in yeast autophagy. *Mol Biol Cell* 16(5):2544-2553.
15. Suzuki K, Kubota Y, Sekito T, & Ohsumi Y (2007) Hierarchy of Atg proteins in pre-autophagosomal structure organization. *Genes Cells* 12(2):209-218.
16. Kawamata T, Kamada Y, Kabeya Y, Sekito T, & Ohsumi Y (2008) Organization of the pre-autophagosomal structure responsible for autophagosome formation. *Mol Biol Cell* 19(5):2039-2050.
17. Lindmo K & Stenmark H (2006) Regulation of membrane traffic by phosphoinositide 3-kinases. *J Cell Sci* 119(Pt 4):605-614.
18. Stack JH, Herman PK, Schu PV, & Emr SD (1993) A membrane-associated complex containing the Vps15 protein kinase and the Vps34 PI 3-kinase is essential for protein sorting to the yeast lysosome-like vacuole. *EMBO J* 12(5):2195-2204.
19. Panaretou C, Domin J, Cockcroft S, & Waterfield MD (1997) Characterization of p150, an adaptor protein for the human phosphatidylinositol (PtdIns) 3-kinase. Substrate presentation by phosphatidylinositol transfer protein to the p150.Ptdins 3-kinase complex. *J Biol Chem* 272(4):2477-2485.
20. Kihara A, Noda T, Ishihara N, & Ohsumi Y (2001) Two distinct Vps34 phosphatidylinositol 3-kinase complexes function in autophagy and carboxypeptidase Y sorting in *Saccharomyces cerevisiae*. *J Cell Biol* 152(3):519-530.
21. Obara K, Sekito T, & Ohsumi Y (2006) Assortment of phosphatidylinositol 3-kinase complexes--Atg14p directs association of complex I to the pre-autophagosomal structure in *Saccharomyces cerevisiae*. *Mol Biol Cell* 17(4):1527-1539.
22. Stromhaug PE, Reggiori F, Guan J, Wang C-W, & Klionsky DJ (2004) Atg21 is a phosphoinositide binding protein required for efficient lipidation and localization of Atg8 during uptake of aminopeptidase I by selective autophagy. *Mol Biol Cell* 15(8):3553-3566.
23. Liang XH*, et al.* (1999) Induction of autophagy and inhibition of tumorigenesis by *beclin 1*. *Nature* 402(6762):672-676.
24. Furuya N, Yu J, Byfield M, Pattingre S, & Levine B (2005) The evolutionarily conserved domain of Beclin 1 is required for Vps34 binding, autophagy and tumor suppressor function. *Autophagy* 1(1):46-52.
25. Zeng X, Overmeyer JH, & Maltese WA (2006) Functional specificity of the mammalian Beclin-Vps34 PI 3-kinase complex in macroautophagy versus endocytosis and lysosomal enzyme trafficking. *J Cell Sci* 119(Pt 2):259-270.
26. Mizushima N*, et al.* (1998) A protein conjugation system essential for autophagy. *Nature* 395(6700):395-398.
27. Ichimura Y*, et al.* (2000) A ubiquitin-like system mediates protein lipidation. *Nature* 408(6811):488-492.

28. Paz Y, Elazar Z, & Fass D (2000) Structure of GATE-16, membrane transport modulator and mammalian ortholog of autophagocytosis factor Aut7p. *J Biol Chem* 275(33):25445-25450.
29. Suzuki NN, Yoshimoto K, Fujioka Y, Ohsumi Y, & Inagaki F (2005) The crystal structure of plant ATG12 and its biological implication in autophagy. *Autophagy* 1(2):119-126.
30. Mizushima N, Sugita H, Yoshimori T, & Ohsumi Y (1998) A new protein conjugation system in human. The counterpart of the yeast Apg12p conjugation system essential for autophagy. *J Biol Chem* 273(51):33889-33892.
31. Sou YS, Tanida I, Komatsu M, Ueno T, & Kominami E (2006) Phosphatidylserine in addition to phosphatidylethanolamine is an in vitro target of the mammalian Atg8 modifiers, LC3, GABARAP, and GATE-16. *J Biol Chem* 281(6):3017-3024.
32. Kirisako T*, et al.* (2000) The reversible modification regulates the membrane-binding state of Apg8/Aut7 essential for autophagy and the cytoplasm to vacuole targeting pathway. *J Cell Biol* 151(2):263-276.
33. Hemelaar J, Lelyveld VS, Kessler BM, & Ploegh HL (2003) A single protease, Apg4B, is specific for the autophagy-related ubiquitin-like proteins GATE-16, MAP1-LC3, GABARAP, and Apg8L. *J Biol Chem* 278(51):51841-51850.
34. Tanida I, Tanida-Miyake E, Ueno T, & Kominami E (2001) The human homolog of *Saccharomyces cerevisiae* Apg7p is a Protein-activating enzyme for multiple substrates including human Apg12p, GATE-16, GABARAP, and MAP-LC3. *J Biol Chem* 276(3):1701-1706.
35. Tanida I*, et al.* (1999) Apg7p/Cvt2p: A novel protein-activating enzyme essential for autophagy. *Mol Biol Cell* 10(5):1367-1379.
36. Tanida I, Tanida-Miyake E, Komatsu M, Ueno T, & Kominami E (2002) Human Apg3p/Aut1p homologue is an authentic E2 enzyme for multiple substrates, GATE-16, GABARAP, and MAP-LC3, and facilitates the conjugation of hApg12p to hApg5p. *J Biol Chem* 277(16):13739-13744.
37. Shintani T*, et al.* (1999) Apg10p, a novel protein-conjugating enzyme essential for autophagy in yeast. *EMBO J* 18(19):5234-5241.
38. Nemoto T*, et al.* (2003) The mouse APG10 homologue, an E2-like enzyme for Apg12p conjugation, facilitates MAP-LC3 modification. *J Biol Chem* 278(41):39517-39526.
39. Yamada T*, et al.* (2005) Endothelial nitric-oxide synthase antisense (NOS3AS) gene encodes an autophagy-related protein (APG9-like2) highly expressed in trophoblast. *J Biol Chem* 280(18):18283-18290.
40. Young AR*, et al.* (2006) Starvation and ULK1-dependent cycling of mammalian Atg9 between the TGN and endosomes. *J Cell Sci* 119(Pt 18):3888-3900.
41. Reggiori F, Shintani T, Nair U, & Klionsky DJ (2005) Atg9 cycles between mitochondria and the pre-autophagosomal structure in yeasts.

Autophagy 1(2):101-109.
42. Yen WL, Legakis JE, Nair U, & Klionsky DJ (2007) Atg27 is required for autophagy-dependent cycling of Atg9. *Mol Biol Cell* 18(2):581-593.
43. Legakis JE, Yen W-L, & Klionsky DJ (2007) A cycling protein complex required for selective autophagy. *Autophagy* 3(5):422-432.
44. Guan J*, et al.* (2001) Cvt18/Gsa12 is required for cytoplasm-to-vacuole transport, pexophagy, and autophagy in *Saccharomyces cerevisiae* and Pichia pastoris. *Mol Biol Cell* 12(12):3821-3838.
45. Shintani T, Suzuki K, Kamada Y, Noda T, & Ohsumi Y (2001) Apg2p functions in autophagosome formation on the perivacuolar structure. *J Biol Chem* 276(32):30452-30460.
46. Wang CW*, et al.* (2001) Apg2 is a novel protein required for the cytoplasm to vacuole targeting, autophagy, and pexophagy pathways. *J Biol Chem* 276(32):30442-30451.
47. Xie Z & Klionsky DJ (2007) Autophagosome formation: core machinery and adaptations. *Nat Cell Biol* 9(10):1102-1109.
48. Mizushima N, Levine B, Cuervo AM, & Klionsky DJ (2008) Autophagy fights disease through cellular self-digestion. *Nature* 451(7182):1069-1075.
49. Zheng YT*, et al.* (2009) The adaptor protein p62/SQSTM1 targets invading bacteria to the autophagy pathway. *J Immunol* 183(9):5909-5916.
50. Orvedahl A*, et al.* (2010) Autophagy protects against Sindbis virus infection of the central nervous system. *Cell Host Microbe* 7(2):115-127.
51. Mijaljica D*, et al.* (2012) Receptor protein complexes are in control of autophagy. *Autophagy* 8(11):1701-1705.
52. Klionsky DJ, Cueva R, & Yaver DS (1992) Aminopeptidase I of *Saccharomyces cerevisiae* is localized to the vacuole independent of the secretory pathway. *J Cell Biol* 119(2):287-299.
53. Baba M, Osumi M, Scott SV, Klionsky DJ, & Ohsumi Y (1997) Two distinct pathways for targeting proteins from the cytoplasm to the vacuole/lysosome. *J Cell Biol* 139(7):1687-1695.
54. Scott SV, Baba M, Ohsumi Y, & Klionsky DJ (1997) Aminopeptidase I is targeted to the vacuole by a nonclassical vesicular mechanism. *J Cell Biol* 138(1):37-44.
55. Scott SV, Guan J, Hutchins MU, Kim J, & Klionsky DJ (2001) Cvt19 is a receptor for the cytoplasm-to-vacuole targeting pathway. *Mol Cell* 7(6):1131-1141.
56. Shintani T, Huang W-P, Stromhaug PE, & Klionsky DJ (2002) Mechanism of cargo selection in the cytoplasm to vacuole targeting pathway. *Dev Cell* 3(6):825-837.
57. Campanella M & Klionsky DJ (2013) Keeping the engine clean: A mitophagy task for cellular physiology. *Autophagy* 9(11):1647.
58. Kanki T & Klionsky DJ (2008) Mitophagy in yeast occurs through a

selective mechanism. *J Biol Chem* 283(47):32386-32393.
59. Kanki T, Wang K, Cao Y, Baba M, & Klionsky DJ (2009) Atg32 is a mitochondrial protein that confers selectivity during mitophagy. *Dev Cell* 17(1):98-109.
60. Okamoto K, Kondo-Okamoto N, & Ohsumi Y (2009) Mitochondria-anchored receptor Atg32 mediates degradation of mitochondria via selective autophagy. *Dev Cell* 17(1):87-97.
61. Schweers RL*, et al.* (2007) NIX is required for programmed mitochondrial clearance during reticulocyte maturation. *Proc Natl Acad Sci U S A* 104(49):19500-19505.
62. Sandoval H*, et al.* (2008) Essential role for Nix in autophagic maturation of erythroid cells. *Nature* 454(7201):232-235.
63. Matsuda N*, et al.* (2010) PINK1 stabilized by mitochondrial depolarization recruits Parkin to damaged mitochondria and activates latent Parkin for mitophagy. *J Cell Biol* 189(2):211-221.
64. Tanaka A*, et al.* (2010) Proteasome and p97 mediate mitophagy and degradation of mitofusins induced by Parkin. *J Cell Biol* 191(7):1367-1380.
65. Farre JC, Manjithaya R, Mathewson RD, & Subramani S (2008) PpAtg30 tags peroxisomes for turnover by selective autophagy. *Dev Cell* 14(3):365-376.
66. Motley AM, Nuttall JM, & Hettema EH (2012) Pex3-anchored Atg36 tags peroxisomes for degradation in *Saccharomyces cerevisiae*. *EMBO J* 31(13):2852-2868.
67. Bernales S, McDonald KL, & Walter P (2006) Autophagy counterbalances endoplasmic reticulum expansion during the unfolded protein response. *PLoS Biol* 4(12):e423.
68. Reggiori F, Monastyrska I, Shintani T, & Klionsky DJ (2005) The actin cytoskeleton is required for selective types of autophagy, but not nonspecific autophagy, in the yeast *Saccharomyces cerevisiae*. *Mol Biol Cell* 16(12):5843-5856.
69. Kraft C, Deplazes A, Sohrmann M, & Peter M (2008) Mature ribosomes are selectively degraded upon starvation by an autophagy pathway requiring the Ubp3p/Bre5p ubiquitin protease. *Nat Cell Biol* 10(5):602-610.
70. Geng J, Nair U, Yasumura-Yorimitsu K, & Klionsky DJ (2010) Post-Golgi Sec proteins are required for autophagy in *Saccharomyces cerevisiae*. *Mol Biol Cell* 21(13):2257-2269.
71. Wallace DC (2005) A mitochondrial paradigm of metabolic and degenerative diseases, aging, and cancer: a dawn for evolutionary medicine. *Annu Rev Genet* 39:359-407.
72. Yen WL & Klionsky DJ (2008) How to live long and prosper: autophagy, mitochondria, and aging. *Physiology* 23:248-262.
73. Budovskaya YV, Stephan JS, Reggiori F, Klionsky DJ, & Herman PK

(2004) The Ras/cAMP-dependent protein kinase signaling pathway regulates an early step of the autophagy process in *Saccharomyces cerevisiae*. *J Biol Chem* 279(20):20663-20671.
74. Yorimitsu T, Zaman S, Broach JR, & Klionsky DJ (2007) Protein kinase A and Sch9 cooperatively regulate induction of autophagy in *Saccharomyces cerevisiae*. *Mol Biol Cell* 18(10):4180-4189.
75. Yang Z, Geng J, Yen W-L, Wang K, & Klionsky DJ (2010) Positive or negative roles of different cyclin-dependent kinase Pho85-cyclin complexes orchestrate induction of autophagy in *Saccharomyces cerevisiae*. *Mol Cell* 38(2):250-264.
76. Levin DE (2005) Cell wall integrity signaling in *Saccharomyces cerevisiae*. *Microbiol Mol Biol Rev* 69(2):262-291.
77. Westfall PJ, Ballon DR, & Thorner J (2004) When the stress of your environment makes you go HOG wild. *Science* 306(5701):1511-1512.
78. Kanki T*, et al.* (2009) A genomic screen for yeast mutants defective in selective mitochondria autophagy. *Mol Biol Cell* 20(22):4730-4738.
79. Heinisch JJ, Lorberg A, Schmitz HP, & Jacoby JJ (1999) The protein kinase C-mediated MAP kinase pathway involved in the maintenance of cellular integrity in *Saccharomyces cerevisiae*. *Mol Microbiol* 32(4):671-680.
80. Klionsky DJ & Emr SD (1989) Membrane protein sorting: biosynthesis, transport and processing of yeast vacuolar alkaline phosphatase. *EMBO J* 8(8):2241-2250.
81. Noda T, Matsuura A, Wada Y, & Ohsumi Y (1995) Novel system for monitoring autophagy in the yeast *Saccharomyces cerevisiae*. *Biochem Biophys Res Commun* 210(1):126-132.
82. Campbell CL & Thorsness PE (1998) Escape of mitochondrial DNA to the nucleus in yme1 yeast is mediated by vacuolar-dependent turnover of abnormal mitochondrial compartments. *J Cell Sci* 111(16):2455-2464.
83. Alonso-Monge R, Carvaihlo S, Nombela C, Rial E, & Pla J (2009) The Hog1 MAP kinase controls respiratory metabolism in the fungal pathogen Candida albicans. *Microbiology* 155(2):413-423.
84. Brewster JL, de Valoir T, Dwyer ND, Winter E, & Gustin MC (1993) An osmosensing signal transduction pathway in yeast. *Science* 259(5102):1760-1763.
85. Saito H & Tatebayashi K (2004) Regulation of the osmoregulatory HOG MAPK cascade in yeast. *J Biochem* 136(3):267-272.
86. Hahn JS & Thiele DJ (2002) Regulation of the *Saccharomyces cerevisiae* Slt2 kinase pathway by the stress-inducible Sdp1 dual specificity phosphatase. *J Biol Chem* 277(24):21278-21284.
87. Bicknell AA, Tourtellotte J, & Niwa M (2010) Late phase of the endoplasmic reticulum stress response pathway is regulated by Hog1 MAP kinase. *J Biol Chem* 285(23):17545-17555.
88. Reggiori F*, et al.* (2004) Early stages of the secretory pathway, but not

endosomes, are required for Cvt vesicle and autophagosome assembly in *Saccharomyces cerevisiae*. *Mol Biol Cell* 15(5):2189-2204.
89. Webber JL & Tooze SA (2010) New insights into the function of Atg9. *FEBS Lett* 584(7):1319-1326.
90. Shintani T & Klionsky DJ (2004) Cargo proteins facilitate the formation of transport vesicles in the cytoplasm to vacuole targeting pathway. *J Biol Chem* 279(29):29889-29894.
91. Yeh YY, Wrasman K, & Herman PK (2010) Autophosphorylation within the Atg1 activation loop is required for both kinase activity and the induction of autophagy in *Saccharomyces cerevisiae*. *Genetics* 185(3):871-882.
92. Scott SV*, et al.* (2000) Apg13p and Vac8p are part of a complex of phosphoproteins that are required for cytoplasm to vacuole targeting. *J Biol Chem* 275(33):25840-25849.
93. Scrimale T, Didone L, de Mesy Bentley KL, & Krysan DJ (2009) The unfolded protein response is induced by the cell wall integrity mitogen-activated protein kinase signaling cascade and is required for cell wall integrity in *Saccharomyces cerevisiae*. *Mol Biol Cell* 20(1):164-175.
94. Babour A, Bicknell AA, Tourtellotte J, & Niwa M (2010) A surveillance pathway monitors the fitness of the endoplasmic reticulum to control its inheritance. *Cell* 142(2):256-269.
95. Manjithaya R, Jain S, Farre JC, & Subramani S (2010) A yeast MAPK cascade regulates pexophagy but not other autophagy pathways. *J Cell Biol* 189(2):303-310.
96. Ozpolat B, Akar U, Mehta K, & Lopez-Berestein G (2007) PKC delta and tissue transglutaminase are novel inhibitors of autophagy in pancreatic cancer cells. *Autophagy* 3(5):480-483.
97. Chen JL*, et al.* (2008) Novel roles for protein kinase Cdelta-dependent signaling pathways in acute hypoxic stress-induced autophagy. *J Biol Chem* 283(49):34432-34444.
98. Wei Y, Pattingre S, Sinha S, Bassik M, & Levine B (2008) JNK1-mediated phosphorylation of Bcl-2 regulates starvation-induced autophagy. *Mol Cell* 30(6):678-688.
99. Shahnazari S*, et al.* (2010) A diacylglycerol-dependent signaling pathway contributes to regulation of antibacterial autophagy. *Cell Host Microbe* 8(2):137-146.
100. Ma J*, et al.* (2008) Localization of autophagy-related proteins in yeast using a versatile plasmid-based resource of fluorescent protein fusions. *Autophagy* 4(6):792-800.
101. Robinson JS, Klionsky DJ, Banta LM, & Emr SD (1988) Protein sorting in *Saccharomyces cerevisiae*: isolation of mutants defective in the delivery and processing of multiple vacuolar hydrolases. *Mol Cell Biol* 8(11):4936-4948.

102. Okamoto K & Shaw JM (2005) Mitochondrial morphology and dynamics in yeast and multicellular eukaryotes. *Annu Rev Genet* 39:503-536.
103. Narendra D, Tanaka A, Suen DF, & Youle RJ (2008) Parkin is recruited selectively to impaired mitochondria and promotes their autophagy. *J Cell Biol* 183(5):795-803.
104. Kanki T & Klionsky DJ (2009) Mitochondrial abnormalities drive cell death in Wolfram syndrome 2. *Cell Res* 19(8):922-923.
105. Narendra DP*, et al.* (2010) PINK1 is selectively stabilized on impaired mitochondria to activate Parkin. *PLoS Biol* 8(1):e1000298.
106. Vives-Bauza C*, et al.* (2010) PINK1-dependent recruitment of Parkin to mitochondria in mitophagy. *Proc Natl Acad Sci U S A* 107(1):378-383.
107. Mijaljica D*, et al.* (2012) Receptor protein complexes are in control of autophagy. *Autophagy* 8(11).
108. Twig G*, et al.* (2008) Fission and selective fusion govern mitochondrial segregation and elimination by autophagy. *EMBO J* 27(2):433-446.
109. Tieu Q & Nunnari J (2000) Mdv1p is a WD repeat protein that interacts with the dynamin-related GTPase, Dnm1p, to trigger mitochondrial division. *J Cell Biol* 151(2):353-366.
110. Mozdy AD, McCaffery JM, & Shaw JM (2000) Dnm1p GTPase-mediated mitochondrial fission is a multi-step process requiring the novel integral membrane component Fis1p. *J Cell Biol* 151(2):367-380.
111. Karren MA, Coonrod EM, Anderson TK, & Shaw JM (2005) The role of Fis1p-Mdv1p interactions in mitochondrial fission complex assembly. *J Cell Biol* 171(2):291-301.
112. Bleazard W*, et al.* (1999) The dynamin-related GTPase Dnm1 regulates mitochondrial fission in yeast. *Nat Cell Biol* 1(5):298-304.
113. Griffin EE, Graumann J, & Chan DC (2005) The WD40 protein Caf4p is a component of the mitochondrial fission machinery and recruits Dnm1p to mitochondria. *J Cell Biol* 170(2):237-248.
114. Naylor K*, et al.* (2006) Mdv1 interacts with assembled dnm1 to promote mitochondrial division. *J Biol Chem* 281(4):2177-2183.
115. Mendl N*, et al.* (2011) Mitophagy in yeast is independent of mitochondrial fission and requires the stress response gene WHI2. *J Cell Sci* 124(8):1339-1350.
116. Aoki Y*, et al.* (2011) Phosphorylation of Serine 114 on Atg32 mediates mitophagy. *Mol Biol Cell* 22(17):3206-3217.
117. Kondo-Okamoto N*, et al.* (2012) Autophagy-related protein 32 acts as autophagic degron and directly initiates mitophagy. *J Biol Chem* 287(13):10631-10638.
118. Mao K, Wang K, Zhao M, Xu T, & Klionsky DJ (2011) Two MAPK-signaling pathways are required for mitophagy in *Saccharomyces cerevisiae*. *J Cell Biol* 193(4):755-767.
119. Sung MK & Huh WK (2007) Bimolecular fluorescence complementation

analysis system for in vivo detection of protein-protein interaction in *Saccharomyces cerevisiae*. *Yeast* 24(9):767-775.
120. Friedman JR*, et al.* (2011) ER tubules mark sites of mitochondrial division. *Science* 334(6054):358-362.
121. Kornmann B*, et al.* (2009) An ER-mitochondria tethering complex revealed by a synthetic biology screen. *Science* 325(5939):477-481.
122. Fukushima NH, Brisch E, Keegan BR, Bleazard W, & Shaw JM (2001) The GTPase effector domain sequence of the Dnm1p GTPase regulates self-assembly and controls a rate-limiting step in mitochondrial fission. *Mol Biol Cell* 12(9):2756-2766.
123. Xie Z, Nair U, & Klionsky DJ (2008) Atg8 controls phagophore expansion during autophagosome formation. *Mol Biol Cell* 19(8):3290-3298.
124. Baba M, Osumi M, Scott SV, Klionsky DJ, & Ohsumi Y (1997) Two distinct pathways for targeting proteins from the cytoplasm to the vacuole/lysosome. *J Cell Biol* 139(7):1687-1695.
125. Yorimitsu T & Klionsky DJ (2005) Atg11 links cargo to the vesicle-forming machinery in the cytoplasm to vacuole targeting pathway. *Mol Biol Cell* 16(4):1593-1605.
126. Wada S*, et al.* (2009) Autophagy plays a role in chloroplast degradation during senescence in individually darkened leaves. *Plant Physiol* 149(2):885-893.
127. Hutchins MU, Veenhuis M, & Klionsky DJ (1999) Peroxisome degradation in *Saccharomyces cerevisiae* is dependent on machinery of macroautophagy and the Cvt pathway. *J Cell Sci* 112(22):4079-4087.
128. Kuravi K*, et al.* (2006) Dynamin-related proteins Vps1p and Dnm1p control peroxisome abundance in *Saccharomyces cerevisiae*. *J Cell Sci* 119(19):3994-4001.
129. Motley AM, Ward GP, & Hettema EH (2008) Dnm1p-dependent peroxisome fission requires Caf4p, Mdv1p and Fis1p. *J Cell Sci* 121(10):1633-1640.
130. Zhang X & Hu J (2010) The Arabidopsis chloroplast division protein DYNAMIN-RELATED PROTEIN5B also mediates peroxisome division. *Plant Cell* 22(2):431-442.
131. Labbe S & Thiele DJ (1999) Copper ion inducible and repressible promoter systems in yeast. *Methods Enzymol* 306:145-153.
132. Rubinsztein DC, Shpilka T, & Elazar Z (2012) Mechanisms of autophagosome biogenesis. *Curr Biol* 22(1):R29-34.
133. Mizushima N, Yoshimori T, & Ohsumi Y (2011) The role of Atg proteins in autophagosome formation. *Annu Rev Cell Dev Biol* 27:107-132.
134. Cheong H*, et al.* (2005) Atg17 regulates the magnitude of the autophagic response. *Mol Biol Cell* 16(7):3438-3453.
135. Kawamata T*, et al.* (2005) Characterization of a novel autophagy-specific gene, ATG29. *Biochem Biophys Res Commun*

338(4):1884-1889.
136. Kabeya Y, Kawamata T, Suzuki K, & Ohsumi Y (2007) Cis1/Atg31 is required for autophagosome formation in *Saccharomyces cerevisiae*. *Biochem Biophys Res Commun* 356(2):405-410.
137. Nair U & Klionsky DJ (2005) Molecular mechanisms and regulation of specific and nonspecific autophagy pathways in yeast. *J Biol Chem* 280(51):41785-41788.
138. Abeliovich H, Dunn WA, Jr., Kim J, & Klionsky DJ (2000) Dissection of autophagosome biogenesis into distinct nucleation and expansion steps. *J Cell Biol* 151(5):1025-1034.
139. Kamada Y*, et al.* (2010) Tor directly controls the Atg1 kinase complex to regulate autophagy. *Mol Cell Biol* 30(4):1049-1058.
140. Uversky VN, Gillespie JR, & Fink AL (2000) Why are "natively unfolded" proteins unstructured under physiologic conditions? *Proteins* 41(3):415-427.
141. Uversky VN (2002) Natively unfolded proteins: a point where biology waits for physics. *Protein Sci* 11(4):739-756.
142. Dunker AK*, et al.* (2001) Intrinsically disordered protein. *J Mol Graph Model* 19(1):26-59.
143. Turoverov KK, Kuznetsova IM, & Uversky VN (2010) The protein kingdom extended: ordered and intrinsically disordered proteins, their folding, supramolecular complex formation, and aggregation. *Prog Biophys Mol Biol* 102(2-3):73-84.
144. Ragusa MJ, Stanley RE, & Hurley JH (2012) Architecture of the Atg17 Complex as a Scaffold for Autophagosome Biogenesis. *Cell*. 151(7):1501-12
145. Dosztanyi Z, Csizmok V, Tompa P, & Simon I (2005) IUPred: web server for the prediction of intrinsically unstructured regions of proteins based on estimated energy content. *Bioinformatics* 21(16):3433-3434.
146. Dosztanyi Z, Meszaros B, & Simon I (2009) ANCHOR: web server for predicting protein binding regions in disordered proteins. *Bioinformatics* 25(20):2745-2746.
147. Brocca S*, et al.* (2009) Order propensity of an intrinsically disordered protein, the cyclin-dependent-kinase inhibitor Sic1. *Proteins* 76(3):731-746.
148. Sickmeier M*, et al.* (2007) DisProt: the Database of Disordered Proteins. *Nucleic Acids Res* 35(Database issue):D786-793.
149. Vacic V, Uversky VN, Dunker AK, & Lonardi S (2007) Composition Profiler: a tool for discovery and visualization of amino acid composition differences. *BMC Bioinformatics* 8:211.
150. Tompa P (2002) Intrinsically unstructured proteins. *Trends Biochem Sci* 27(10):527-533.
151. Cao Y, Cheong H, Song H, & Klionsky DJ (2008) In vivo reconstitution of autophagy in *Saccharomyces cerevisiae*. *J Cell Biol* 182(4):703-713.

152. Tompa P (2005) The interplay between structure and function in intrinsically unstructured proteins. *FEBS Lett* 579(15):3346-3354.
153. Uversky VN (2013) A decade and a half of protein intrinsic disorder: Biology still waits for physics. *Protein science: a publication of the Protein Society* 22(6):693-724.
154. He C*, et al.* (2006) Recruitment of Atg9 to the preautophagosomal structure by Atg11 is essential for selective autophagy in budding yeast. *J Cell Biol* 175(6):925-935.
155. Stols L*, et al.* (2002) A new vector for high-throughput, ligation-independent cloning encoding a tobacco etch virus protease cleavage site. *Protein Expr Purif* 25(1):8-15.
156. DelProposto J, Majmudar CY, Smith JL, & Brown WC (2009) Mocr: a novel fusion tag for enhancing solubility that is compatible with structural biology applications. *Protein Expr Purif* 63(1):40-49.
157. Ohi M, Li Y, Cheng Y, & Walz T (2004) Negative staining and image classification – powerful tools in modern electron microscopy. *Biol Proced Online* 6:23-34.
158. Ludtke SJ, Baldwin PR, & Chiu W (1999) EMAN: semiautomated software for high-resolution single-particle reconstructions. *J Struct Biol* 128(1):82-97.
159. Vihinen M (1987) Relationship of protein flexibility to thermostability. *Protein Eng* 1(6):477-480.
160. Motley AM & Hettema EH (2007) Yeast peroxisomes multiply by growth and division. *J Cell Biol* 178(3):399-410.
161. Schrader M, Bonekamp NA, & Islinger M (2012) Fission and proliferation of peroxisomes. *Biochim Biophys Acta* 1822(9):1343-1357.
162. Sakai Y, Oku M, van der Klei IJ, & Kiel JAKW (2006) Pexophagy: autophagic degradation of peroxisomes. *Biochim Biophys Acta* 1763(12):1767-1775.
163. Reggiori F & Klionsky DJ (2013) Autophagic processes in yeast: mechanism, machinery and regulation. *Genetics* 194(2):341-361.
164. Mao K, Wang K, Liu X, & Klionsky DJ (2013) The scaffold protein atg11 recruits fission machinery to drive selective mitochondria degradation by autophagy. *Dev Cell* 26(1):9-18.
165. Vizeacoumar FJ*, et al.* (2006) The dynamin-like protein Vps1p of the yeast *Saccharomyces cerevisiae* associates with peroxisomes in a Pex19p-dependent manner. *J Biol Chem* 281(18):12817-12823.
166. Mao K*, et al.* (2013) Atg29 phosphorylation regulates coordination of the Atg17-Atg31-Atg29 complex with the Atg11 scaffold during autophagy initiation. *Proc Natl Acad Sci U S A* 110(31):E2875-2884.
167. Yu T, Jhun BS, & Yoon Y (2011) High-glucose stimulation increases reactive oxygen species production through the calcium and mitogen-activated protein kinase-mediated activation of mitochondrial fission. *Antioxid Redox Signal* 14(3):425-437.

168. Gomes LC, Di Benedetto G, & Scorrano L (2011) During autophagy mitochondria elongate, are spared from degradation and sustain cell viability. *Nat Cell Biol* 13(5):589-598.
169. Merrill RA*, et al.* (2011) Mechanism of neuroprotective mitochondrial remodeling by PKA/AKAP1. *PLoS Biol* 9(4):e1000612.
170. Taguchi N, Ishihara N, Jofuku A, Oka T, & Mihara K (2007) Mitotic phosphorylation of dynamin-related GTPase Drp1 participates in mitochondrial fission. *J Biol Chem* 282(15):11521-11529.
171. Han XJ*, et al.* (2008) CaM kinase I alpha-induced phosphorylation of Drp1 regulates mitochondrial morphology. *J Cell Biol* 182(3):573-585.
172. Everley PA, Krijgsveld J, Zetter BR, & Gygi SP (2004) Quantitative cancer proteomics: stable isotope labeling with amino acids in cell culture (SILAC) as a tool for prostate cancer research. *Mol Cell Proteomics* 3(7):729-735.
173. Chew LH, Setiaputra D, Klionsky DJ, & Yip CK (2013) Structural characterization of the Saccharomyces cerevisiae autophagy regulatory complex Atg17-Atg31-Atg29. *Autophagy* 9(10).